TAMPEREEN TEKNILLINEN YLIOPISTO
TAMPERE UNIVERSITY OF TECHNOLOGY

ILARI SAARINEN

SIMULATION STUDY OF A DUAL FUEL INJECTOR

Master's Thesis

Tarkastaja: professori Kalevi Huhtala
Tarkastaja ja aihe hyväksytty
Teknisten tieteiden tiedekuntaneuvoston kokouksessa 26. syyskuuta 2017

ABSTRACT

ILARI SAARINEN: Simulation Study of a Dual Fuel Injector
Tampere University of Technology
Master's Thesis, 112 pages, 1 appendix pages
September 2017
Master's degree program in mechanical engineering
Major: Hydraulics
Examiner: Professor Kalevi Huhtala

Key words: Fuel injection, common rail, injector, dual-fuel injector, simulation

The need for this thesis comes from the timely objective to minimize emissions and maximize efficiency in combustion engines. The latest trend in the marine industry is to utilize dual fuel engines as the power source for vessels, allowing the engine to be run on both diesel and gas. In the gas mode, the gas is ignited by injecting a small amount of diesel, in a so-called pilot injection, into the combustion chamber. The pilot injection event, and the fuel injector creating it, is the topic of this thesis.

To be able to understand the operation of a fuel injector, mechanic, hydraulic and electromagnetic theory is presented. Next, fuel injector operation is descripted. Then, a simulation model of the fuel injector is built and verified. Sensitivity analyses are made for both the pilot injection and the full injection event, for the purpose of understanding which parameters affect the injector outputs. Finally, both the pilot injection and the full injection event are optimized in order to reach the emission and efficiency targets.

The sensitivity analysis clearly shows that the most important parameters affecting the injector performance are the inlet, outlet and filling orifices. Naturally, also the number of nozzle holes and the hole diameters play a crucial role, a smaller flow area resulting in a faster pilot injection but less injected quantity in a full injection. The pressure step and the needle spring have a lesser impact. The geometry of the needle tip is also important but hard to model accurately. In the studied injector, the control valve was so fast that it did not restrict the pilot injection speed. After optimizing the model, it was clear that the size of the outlet orifice needs to be increased, and that the sizes of the inlet and filling orifice can be kept roughly the same.

TIIVISTELMÄ

ILARI SAARINEN: Simulation Study of a Dual Fuel Injector
Tampereen teknillinen yliopisto
Diplomityö, 112 sivua, 1 liitesivua
Syyskuu 2017
Konetekniikan diplomi-insinöörin tutkinto-ohjelma
Pääaine: Hydrauliikka
Tarkastaja: professori Kalevi Huhtala

Avainsanat: Polttoaineen ruiskutus, yhteispaineruiskutusjärjestelmä, kaksoispolttoaineruisku, simulointi

Tarve tämän työn tekemiseen tulee nykyajan polttomoottorien kehityksestä, jossa moottoreita kehitetään tehokkaammiksi ja vähäpäästöisemmiksi. Viimeisin trendi meriteollisuudessa ovat ns. dual-fuel moottorit, joissa polttoaineena käytetään sekä kaasua että nestemäistä polttoainetta. Ajettaessa moottoria kaasulla, kaasun sytytys tapahtuu ruiskuttamalla palokammioon ns. esiruiskutuksella pieni määrä nestemäistä polttoainetta, joka sytyttää kaasun. Tässä työssä tarkastellaan tätä esiruiskutusta ja sen aikaansaavaa komponenttia, ruiskutusventtiiliä.

Tämän ymmärtämiseksi työssä käydään lävitse mekaniikan, hydrauliikan ja sähkömagnetismin teoriaa. Ruiskutusventtiilin toiminta käydään yksityiskohtaisesti lävitse, ja siitä tehdään simulointimalli, joka verifioidaan. Herkkyysanalyysi tehdään sekä esiruiskutukselle että pääruiskutukselle, ja siitä nähdään miten mikäkin parametri vaikuttaa kussakin tilanteessa. Lopulta sekä esiruiskutus ja pääruiskutus optimoidaan tehokkuus ja päästötavoitteiden saavuttamiseksi.

Herkkyysanalyysista nähdään että kaikista eniten ruiskutukseen vaikuttavat inlet-, outlet- ja filling-rakojen koot. Tietysti sekä suutin rakojen koko että lukumäärä ovat erittäin tärkeitä, ja pienempi virtauspinta-ala parantaakin esiruiskutusta. Nk. ”Pressure step” ja neulassa oleva jousi vaikuttavat vähemmän. Neulan kärjen koko ja muoto ovat myös tärkeitä, mutta hankala mallintaa tarkasti. Tässä tarkastellussa polttoaineruiskussa solenoidi ja sen ohjaama esiventtiili eivät rajoittaneet esiruiskutuksen nopeutta. Optimoinnin jälkeen oli selvää, että outlet –kuristutuksen kokoa pitää kasvattaa, ja että sekä filling että inlet –kuristuksia ei tarvitse muuttaa paljoa.

ACKNOWLEDGEMENTS

I would first like to thank my thesis advisor professor Kalevi Huhtala of the department of Intelligent Hydraulics and Automation at Tampere University of Technology. He provided me with the initial information needed to begin the thesis, and gave a lot of good advice during the journey. Furthermore, I want to thank my supervisor Niclas Liljenfeldt and project coordinator Rainer Lorenz for the time, interest and passion they have given for this thesis. Having a team with high hopes for me and my thesis richly fueled my ambitions, giving me power to reach even distant goals. In the end, even a thesis work turned out to be teamwork with discussions varying from the thesis objects to figure formatting. Also, I want to thank all the Wärtsilä staff that helped me during the thesis progress, for instance in learning to use GT-suite, taking measurements from an injector, advising on solenoid behavior, spray atomization, reporting, etc.

Finally, I want to express my profound gratitude to my family, friends and loved ones. During the thesis work, I received a significant amount of support and encouragement, which greatly motivated me. Thank you.

In Vaasa, 6.9.2017

Ilari Saarinen

TABLE OF CONTENTS

1. INTRODUCTION 1
1.1 Common rail system 1
1.2 Fuel injector types 2
1.3 Goals of the Thesis 3
2. THEORY 4
2.1 Mechanical 4
2.1.1 Kelvin-Voigt model 4
2.1.2 Dynamic friction 5
2.2 Fluid properties 6
2.2.1 Bulk modulus 6
2.2.2 Viscosity 7
2.2.3 Density 9
2.2.4 Speed of sound 9
2.2.5 Reynolds number 10
2.3 Flow 11
2.3.1 Fluid continuity 11
2.3.2 Orifice flow 11
2.3.3 Flow forces 12
2.3.4 Leakage 12
2.3.5 Cavitation 13
2.4 Electro-magnetism 18
2.5 Optimization 19
2.5.1 Genetic algorithm 19
3. INJECTOR 21
3.1 Operation 21
3.2 Force equation 23
3.3 Pressure step 24
3.4 Sac hole flow 26
3.5 Solenoid 26
4. SIMULATION MODEL 28
4.1 Solenoid 29
4.2 Control Valve 31
4.3 Nozzle 32
4.4 Flow fuse 33
5. MODEL VERIFICATION 34
5.1 Verification data 35
5.2 Verification set-up 36
5.3 Optimization runs 40
5.4 Model fit 42
6. SENSITIVITY ANALYSIS 48

6.1 Solenoid 48
6.1.1 Number of windings 48
6.1.2 Control valve mass 50
6.1.3 Control valve discharge coefficient 52
6.1.4 Air gap length 54
6.2 Control chamber 56
6.2.1 Inlet orifice 57
6.2.2 Outlet orifice 58
6.2.3 Inlet and outlet orifice 59
6.2.4 Filling orifice 63
6.2.5 Inlet, outlet and filling orifice 65
6.3 Needle 66
6.3.1 Spring 67
6.3.2 Pressure step 69
6.3.3 Weight 73
6.3.4 Tip geometry 75
6.4 Nozzle sac 79
6.4.1 Volume 79
6.4.2 Number of holes 81
6.4.3 Hole diameter 82
6.4.4 Hole rounding 84
6.4.5 Hole thickness 86
7. OPTIMIZATION 89
7.1 Boundary conditions 89
7.2 Targets 90
7.3 Results 91
7.3.1 Pilot injection with 4 variables 92
7.3.2 Full and pilot injection with 8 variables 94
7.3.3 Full and pilot injection with nozzle parameters 97
7.4 Arising problems 99
8. DISCUSSION 100
8.1 Criticism 100
8.2 Future research 101
8.2.1 Co-simulations 102
8.2.2 Optimization double loop 103
8.2.3 Dual control valve 104
9. CONCLUSION 106

SYMBOLS

CC	Control chamber
DF	Dual fuel
FEM	Finite Element Method
GT-Suite	The simulation software used in this thesis
GT-ISE	Integrated simulation environment, meaning the user interface of the simulation tool
GT-POST	User interface used for the post processing of the simulation results
GA	Genetic algorithm
PSR	Pressure step ratio

A	Opening area [m^2]
A_{cc}	Needle area in the control chamber [m^2]
A_{eff}	Effective flow area [m^2]
A_p	Effective area of the needle causing the upwards force [m^2]
A_s	Area of the needle tip [Pa]
a	A needle tip dimension [m]
B_{eff}	Effective bulk modulus [N/m^2]
b	A needle tip dimension
C_c	Contraction coefficient [-]
C_d	Discharge coefficient [-]
c	A needle tip dimension
c_s	Speed of sound [m/s]
D	Diameter of a hole [m]

d	Inner diameter of a cylinder [m]
dv	Derivative of velocity [m/s/m]
dy	Derivative of distance from the solid body [m/m]
E_0	Young's modulus [N/ m^2]
e	Eccentricity of the cylinder [m]
$\bar{F}_{acc}$	Inertial force [N]
$\bar{F}_{cc}$	Pressure force [N]
$\bar{F}_{flow}$	Flow force [N]
$\bar{F}_p$	Lower pressure force [N]
$\bar{F}_{pre}$	Precompression of the spring [N]
$F_{support}$	Support force of the lower contact of the needle [N]
F_μ	Friction force [N]
f	Friction factor [-]
f_{opt}	Optimization function
h	Gap between the cylinder and the hole [m]
I	Current [A]
K	Cavitation number [-]
K_{crit}	Critical cavitation number [-]
K_e	Effective bulk modulus [N/m^2]
K_f	Bulk modulus [N/m^2]
K_{inlet}	Orifice inlet loss coefficients [-]
K_{part}	Bulk modulus of a part [N/m^2]
k_{spring}	Spring stiffness [N/m]
l	Length of the hole [m]

m	Mass [kg]
m_{needle}	Needle mass [kg]
$\dot{m}$	Mass flow [kg/s]
p_1	Pressure before object [Pa]
p_2	Pressure after object [Pa]
p_{cc}	Control chamber pressure [Pa]
p_p	Pressure around the needle [Pa]
p_s	Sac hole pressure [Pa]
p_v	Vapour pressure [Pa]
$\dot{p}$	Derivative of pressure over time [Pa/s]
R	Rounding diameter of a hole [m]
R_e	Resistance [Ω]
Re	Reynolds number []
r_{lower}	Radius of the circle at the needle seat which is at 90 degree angle to the cone diameter [m]
r_{upper}	Radius of the cone of the needle tip [m]
SMD	Sauter Mean Diameter [m]
$SMD\_normalize$	Normalization value for the SMD
s	Wall thickness [m]
$t_{closing}$	Closing time of the needle [s]
$t_{closing}$	Normalization value for the closing time of the needle [s]
U	Voltage [V]
V	Volume [m^3]
v	Velocity [m/s]

v_{flow}	Maximum flow velocity in the optimization function [m/s]
$v_{flow\_normalize}$	Normalization value for flow velocity [m/s]
V_{part}	Volume of the fluid within the individual part [m^3]
v_s	Stribeck velocity
V_t	Volume of the fluid of the whole system [m^3]
V_0	Original volume size [m^3]
$\dot{V}$	Derivative of volume over time [m^3/s]
x_{needle}	Needle lift from the resting position [m]
$\ddot{x}_{needle}$	Needle acceleration [m/s^2]
$y_{data}(t)$	A value from the data in relation to time
$y_{sim}(t)$	A simulated value in relation to time
z	Average deflection of the bristles
Q	Volumetric flow through the orifice [m^3/s]
η	Dynamic viscosity [Pa·s]
η_{damper}	Viscosity of the damper [Ns/m^2]
μ_k	Kinetic friction coefficient, [-]
μ_s	Static friction coefficient [-]
ν	Kinematic viscosity [m^2/s]
ρ	Density [kg/m^3]
$\sum$	Sum
σ_E	Stress of the spring [N/m^2]
σ_η	Stress of the damper [N/m]
σ_0	Bristle stiffness

σ_1	Bristle damping coefficient
σ_2	Linear viscous friction coefficient
τ	Shear stress [N/m^2]
γ	A final model parameter

1. INTRODUCTION

Hydraulic system means a configuration that uses fluids to transfer energy. In fuel injection systems, the purpose is to transfer the fluid itself to the combustion chamber, and a hydraulic system is designed to fulfil this purpose. Atomization means the break-up of the spray and formation of drops, and in fuel injection systems it is done by spraying high-pressure fluid through small orifices to the combustion chamber. There are several design requirements for a fuel injection system. First, the fluid transferred needs to be highly pressurized in order to reach good atomization. Second, the injection event must begin and end at the right time for the engine to perform properly; the timing is very important, and the injection duration needs to be adjustable. Third, the fluid used in the system must be clean so that no clogs nor erosion appears; and it must not contain air because the air is highly compressible, and the system behaviour would therefore alter rapidly with different amounts of dissolved air.

In this introductory chapter, I briefly cover the common rail fuel injection system, general fuel injector operation and engine dual fuel operation. The work related theory is handled in chapter two and then applied in chapter three in which injectors are covered. The simulation model is built in chapter four, verified in chapter five and finally optimized in chapter seven. Before the optimization, a sensitivity analysis is made. In chapter eight, Discussion, possible future development and thesis criticism are discussed. The conclusions of the thesis are presented in chapter nine.

1.1 Common rail system

The main purpose of the common rail system is to deliver high-pressure fuel into the combustion chamber. Its main advantage is in varying injection pressure and timing, which is achieved by separating the injector from the fuel supply line. This means that the injector operation is controlled electrically, allowing different kinds of injection events at identical engine operation points. This kind of control results in higher power output, lower fuel consumption, reduced noise emission and decreased pollutant emissions. The main components of the common rail system can be seen in Figure 1.

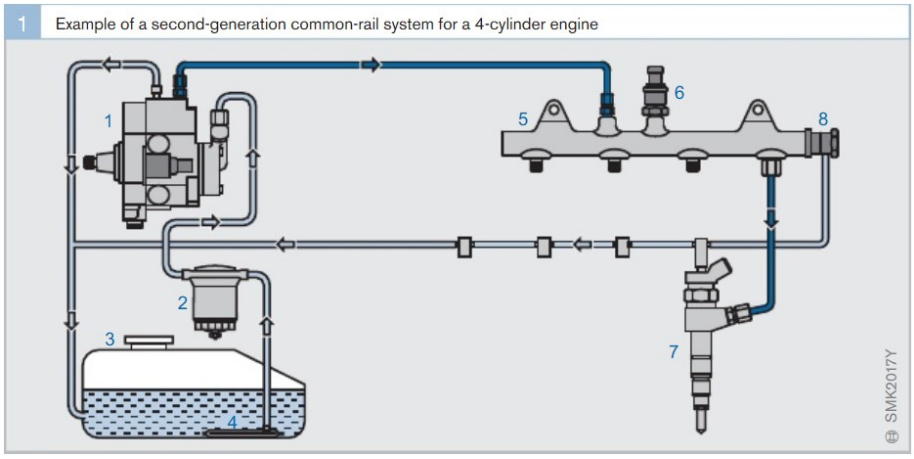

Figure 1. *Overview of a common rail system [1]*

The high-pressure pump (1) generates a high pressure which is transferred via a high-pressure line to the fuel rail (5). A presupply pump, which is located within the high-pressure pump, sucks the fuel from the fuel tank (4) via fuel filter (2). A pressure relief valve (8) is fitted in the fuel rail, to limit the maximum pressure. The injector (7) receives fuel from the fuel rail and injects it into the combustion chamber. During each injection period, a small amount of fuel is used for needle control and returned to the fuel tank via a fuel return line. [1]

1.2 Fuel injector types

A fuel injector is the component that controls the fuel passage to the combustion chamber. It is typically an electro-hydraulically controlled on/off needle valve where the needle moves up and down, thus controlling the opening area. Due to the extremely high pressures on the fuel supply line, the needle cannot be directly electrically controlled but needs to have a hydraulic servo. Hence, the needle movement is controlled with a control chamber, of which pressure is controlled electrically. In Figure 2, a simplified image of the needle can be seen with forces acting on it.

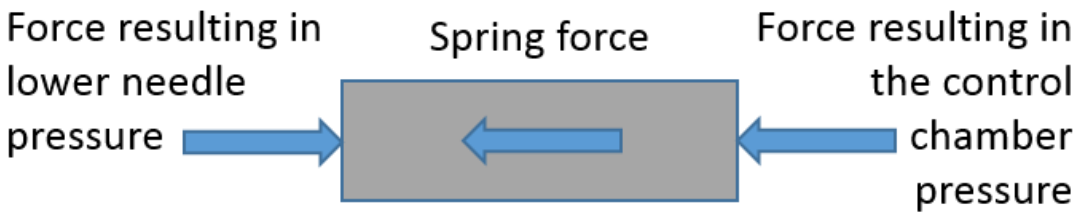

Figure 2. *Forces impacting the needle during needle movement*

The physics of an injector is more accurately described in chapter 3.2.

The two types of common rail fuel injectors are solenoid injectors and piezo injectors. The difference between the two is in the electrical system. The first one uses a solenoid for valve opening and the second one a piezo-electric actuator. These electrical components are used to control the control chamber pressure, which influences the force on the nozzle needle. The injectors scrutinized in this thesis are solenoid-operated. [1]

1.3 Goals of the Thesis

Nowadays engines may run with not only on diesel but also on natural gas. These engines are able to switch from the gas operation mode to diesel operation mode without considerable disruption in the power output. In addition, a combination of these two is possible: in the fuel sharing mode, the engine will run on a mixture of gas and liquid fuel.

While operating in the gas mode, low-pressure gas is mixed with air already before the inlet valve in the cylinder head. For the ignition to take place, a small amount of diesel fuel is injected into the gas mixture in the combustion chamber. The problem there is the minimal amount of the pilot diesel injection, resulting in bad spray quality, deficient atomization, and high emissions. The explanation for this effect might presumably be in a low sac hole pressure and needle movement speed. Hence, the main research question is, which injector parameters have the highest impact on the spray quality. Another question is, which are the optimal parameter values for the highest level of atomization

In order to find these parameters, a simulation model of the injector will be built. This will be verified to meet the measurement data so that we can see the validity of the model. Sensitivity analyses will be made in order to discover the most influential parameters. Finally, the model will be optimized to reach its optimal performance. [2]

2. THEORY

In this chapter, the work-related theory is explained. There are five main chapters: mechanical theory, flow theory, fluid properties theory, electro-magnetic theory and optimization theory.

2.1 Mechanical

Though mechanical design does not play a key role in this thesis, it is important to understand a few mechanical theories used in the thesis. These are the Kelvin-Voigt material model that is introduced in chapter 2.1.1 and dynamic friction that is introduced in chapter 2.1.2.

2.1.1 Kelvin-Voigt model

The Kelvin-Voigt material model is a viscoelastic model, where material stiffness is dependent on the rate of change of load or deformation. The model consists of two parts, a spring and a damper, and they are connected in parallel.

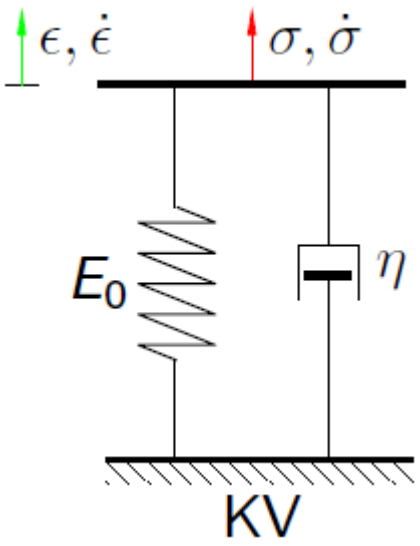

Figure 3. *Schematic of the Kelvin-Voigt material model [3]*

In the spring element, the stress is directly proportional to deformation

$$\sigma_E = E_0 \epsilon_E \tag{1}$$

where

σ_E Stress of the spring [N/m^2]

E_0 Young's modulus [N/ m^2]

In the damper element, the stress is directly proportional to deformation speed

$$\sigma_\eta = \eta \, \dot{\epsilon}_\eta \tag{2}$$

where

σ_η Stress of the damper [N/m]

η_{damper} Viscosity of the damper [Ns/m^2]

From the two equations above, a constitutive formula can be formed

$$\sigma_{total} = E_0 \epsilon_E + \eta \, \dot{\epsilon}_\eta \tag{3}$$

in which the total stress is the sum of the spring stress and the damper stress.

2.1.2 Dynamic friction

The friction of the needle is modelled with the dynamic friction model according to the equation below

$$F_\mu = \sigma_0 z + \sigma_1 \frac{dz}{dt} + \sigma_2 v \tag{4}$$

where

F_μ Resulting friction force

σ_0 Bristle stiffness

z Average deflection of the bristles

σ_1 Bristle damping coefficient

σ_2 Linear viscous friction coefficient

According to the theory of Canudas de Wit et al. [4], there are small bristles that bend before the actual movement begins. This makes the model to take account the static friction transforming into kinetic friction, the stick-slip phenomena and hysteresis. The kinetic friction does not transform to static friction when the object quickly changes direction. The time derivative of average bristle deflection z can be seen below

$$\frac{dz}{dt} = v - \frac{\sigma_0|v|}{\mu_k+(\mu_s-\mu_k)e^{-\left|v/v_s\right|^\gamma}} \quad (5)$$

where

μ_k	Kinetic friction coefficient,
μ_s	Static friction coefficient,
v_s	Stribeck velocity, and
γ	a final model parameter.

The model is quite complex, and it is not needed to understand thoroughly for this thesis.

2.2 Fluid properties

One important subject of interest in system design are the properties of the fluid used. These properties include the bulk modulus, viscosity, density, speed of sound and surface tension. Each of these are individually presented in the following chapters, and their behaviour with increasing temperature and pressure is briefly discussed as well.

2.2.1 Bulk modulus

As pressure is applied to a certain fluid, it gets compressed, which can be observed as system flexibility. Before the pressure reaches the level needed for system component movement, fluid deformations occur due to compressibility. This volume deformation is characterized by bulk modulus

$$\Delta V = \frac{1}{K_f} \cdot V_0 \cdot \Delta p \quad (6)$$

in which

ΔV	Volume difference [m^3]
V_0	Original volume size [m^3]
Δp	Pressure difference [Pa]
K_f	Bulk modulus [N/m^2]

From the equation above we can see that as the bulk modulus increases, the volume difference decreases. The bulk modulus is similar to Young's modulus of metals, but much smaller, and therefore fluids get compressed more than metals.

The bulk modulus is temperature- and pressure-dependent: as the temperature increases, the bulk modulus decreases, but as the pressure increases, the bulk modulus decreases. With normal pressure differences (0-30MPa), the pressure effect on bulk modulus is insignificant, but the temperature effect is 10-15% with 20°C-60°C. However, according to Karjalainen [5], a high pressure of 1500 bars approximately doubles the value of the bulk modulus for several fluids.

The deformation of the solid components of the hydraulic system affects the performance of the system as well. To take these component deformations into account too, the effective bulk modulus is used

$$\frac{1}{K_e} = \frac{1}{K_f} + \sum_{i=1}^{N1} \left(\frac{V_{part}}{V_t} \cdot \frac{1}{K_{part}} \right) \tag{7}$$

in which

K_e	Effective bulk modulus of the whole system [N/m^2]
V_t	Volume of the fluid of the whole system [m^3]
V_{part}	Volume of the fluid within the individual part [m^3]
K_{part}	Bulk modulus of the corresponding part [N/m^2]

The bulk modulus for a particular part is affected by its material properties, shape and dimensions, and a simplification for hollow cylindrical objects produces

$$K = \frac{E \cdot s}{d} \tag{8}$$

in which

E	Young's modulus of the material [N/m^2]
s	Wall thickness and [m]
d	Inner diameter of the cylinder [m]

which is how pipe deformation can be modelled. [6]

2.2.2 Viscosity

Friction between fluid particles resists the fluid deformation caused by fluid flow. When external forces are removed, this leads to a stagnation of the flow, and with different types of fluid, the amount of friction varies. This results in different kinds of flow behaviour

for different fluids, and the behaviour is characterised by viscosity, also known as the fluid stiffness. Among fluid properties, also temperature and pressure affect viscosity.

When studying a fluid flow adjacent to a solid body, the particles most close to the solid are not moving. This behaviour is due to adhesion forces. Moving away from the solid, the fluid speed increases, and the velocity distribution is at its highest when most far away from the solid. The velocity distribution is caused by the friction forces, each fluid particle slowing down the relative speed of the adjacent particles. The common form of the viscosity is

$$\tau = \eta \cdot \frac{dv}{dy} \tag{9}$$

in which

τ	Shear stress [N/m^2]
η	Dynamic viscosity [Pa·s]
dv	Derivative of velocity [m/s/m]
dy	Derivative of distance from the solid body [m/m]

Dynamic viscosity describes the friction resisting the movement of the fluid.

Fluids that comply with this law are called Newtonian fluids, and it means that even a small shear stress results in flow and correspondingly, at rest, there are no shear stresses. Dividing the above presented dynamic viscosity with fluid density, we get kinematic viscosity

$$\nu = \frac{\eta}{\rho} \tag{10}$$

in which

ρ	Fluid density [kg/m^3]
η	Dynamic viscosity [Pa·s]
ν	Kinematic viscosity [m^2/s]

Kinematic viscosity is more often used in theoretical examinations. The unit in the SI-system for dynamic viscosity is [Pa·s] and for kinematic viscosity [m^2/s].

When the fluid temperature decreases, fluid viscosity increases, making the fluid less stiff. Even a small transition in temperature makes a considerable difference in viscosity. Also pressure affects the viscosity, but not as much as temperature. An increase in the

pressure increases viscosity as well. This affects, for example, the fluid flow through orifices and clearances. A summary of the viscosity values can be seen in Table 1. [6]

Table 1. *Viscosity summary*

Name:	Formula:	Unit:	Temperature up:	Pressure up:
Dynamic viscosity	$\tau = \eta \cdot \frac{dv}{dy}$	[Pa·s]	decreases	increases
Kinematic viscosity	$\nu = \frac{\eta}{\rho}$	[m^2/s]	decreases	increases

2.2.3 Density

Density of a fluid is the amount of mass in a certain volume

$$\rho = \frac{m}{V} \tag{11}$$

where

ρ Density [kg/m^3]

m Mass [kg]

V Volume [m^3]

As the fluid mass m increases in a constant volume V, the fluid density grows higher. This has a connection to fluid compression, and a high compressibility of a fluid also means big differences in fluid density. Also, as the pressure increases and the fluid gets compressed, the density increases. With the pressure of 1500 bars, the density increases from 790 kg/m^3 to 860 kg/m^3 for Shell Calibration fluid S-9365. The density also affects the speed of sound: as the fluid density increases, the speed of sound decreases. Also with a higher density, the moment of inertia grows larger. [5]

2.2.4 Speed of sound

The speed of sound in a fluid equals the speed of the pressure propagation and therefore sets a limit to the maximum hydraulic response speed. Pressure waves are harmful to the hydraulic system as they increase wearing of parts, and therefore should be avoided. The propagation speed is calculated with

$$c_s = \sqrt{\frac{K_e}{\rho}} \tag{12}$$

where

c_s	Speed of sound [m/s]
K_e	Effective bulk modulus [m^2/s]
ρ	Density [kg/m^3]

The effective bulk modulus of the system K_e is divided by the fluid density ρ, and then squared. In reality, the speed of sound is a bit lower because the formula doesn't consider losses. As pressure increases, the speed of sound increases as well, but at increasing temperature, the speed of sound decreases. As pressure increases from 100 bars to 1500 bars, the speed of sound grows from approximately 1350 m/s to 1850 m/s for Shell Calibration fluid S-9365, a standard calibration fluid used in fuel injection systems [5]. The unit for the speed of sound is [m/s]. [6]

2.2.5 Reynolds number

Reynolds number is a dimensionless parameter used for describing flow turbulence. With high Reynolds number values the flow is more turbulent, and with low values, it's more laminar. Turbulent flow means that there are a lot of vortexes in the flow, and laminar flow means that the fluid particles move straightforward with less whirling. The Reynolds number is calculated with

$$Re = \frac{v \cdot D_h}{\nu} \tag{13}$$

where

Re	Reynolds number []
v	Fluid velocity [m/s]
ν	Fluid viscosity []

This means that as the flow velocity increases, so do the Reynolds number and turbulence as well. But when the viscosity increases, the Reynolds number decreases, and the flow turns less turbulent. [6]

2.3 Flow

In this chapter, the flow behaviour in different kind of conditions is explained. The fluid properties affect these flow behaviours, and in some cases it can be seen from the equations how they affect the flow.

2.3.1 Fluid continuity

The continuity of fluid is modelled with the following equation

$$\dot{p} = \frac{B_{eff}}{V}\left(\sum Q - \dot{V}\right) \tag{14}$$

where

$\dot{p}$	Derivative of pressure over time [Pa/s]
B_{eff}	Effective bulk modulus [N/m^2]
V	Volume [m^3]
$\dot{V}$	Derivative of volume over time [m^3/s]
$\sum Q$	Sum of incoming flows into the volume [m^3/s]

This equation is used to evaluate the pressure level of a changing volume. This means that the volume can have inlet and outlet flows and displacing areas, which form the derivative of pressure. This formula is often used to model a start or end of movement of an actuator, having a different flow into an actuator or changing level of temperature. [6]

2.3.2 Orifice flow

Flow through orifices has been modelled with the following equation

$$Q = C_d A \sqrt{\frac{2\Delta p}{\rho}} \tag{15}$$

where

Q	Volumetric flow through the orifice [m^3/s]
C_d	Discharge coefficient [-]
A	Opening area [m^2]
Δp	Pressure difference over the orifice [Pa]

ρ Fluid density [kg/m^3]

The value of the discharge coefficient is usually estimated to be a constant, and defined in a single state of pressure difference for a single orifice. This is done by multiplying the equation by density and solving the discharge coefficient.

$$C_d = \frac{\dot{m}}{\rho A\sqrt{2\Delta p}} \quad (16)$$

In this form, the mass flow and pressure difference can be measured, and by entering the values we get the calculated discharge coefficient. However, in applications where the pressure difference varies significantly, there is a need for determining the discharge coefficient in multiple states. That said, no flow measurement tests were made for this thesis, but the different flow conditions were taken into account, and they are thoroughly explained in chapter 2.3.5 Cavitation. [6]

2.3.3 Flow forces

When a fluid flows in a way that it shifts its direction of flow, it results in a force pushing the contacting surface. To calculate this force, the amount of flow and flow velocity need to be known

$$F = \dot{m} \cdot v \cdot cos(\theta) \quad (17)$$

where

$\dot{m}$ Mass flow [kg/s]

v Velocity of the flow [m/s]

$\cos(\theta)$ Cosine of the angle of the flow directions [-]

The resulting force is the product of mass flow, flow velocity and cosine of the angle. The direction of the force is always positive because the product of negative mass flow and flow speed is always positive. [6]

2.3.4 Leakage

In order to have movement between different parts, there needs to be some space between those parts. Otherwise, these parts would be in contact and their movement would be restricted by friction, which would result in wearing. These spaces are called clearances, and they are filled with a hydraulic fluid. If the clearance is too large, there will be too much fluid flowing through, and if the clearance is too small, the fluid doesn't enter the clearance space, which leads to erosion. Also, the temperature deformations of the parts

need to be taken into account to prevent unfavourable clearances. Laminar leakage flow in an annular pipe is calculated by

$$Q = \frac{\pi \cdot d \cdot h^3}{12 \cdot \eta \cdot l}\left[1 + 1.5 \cdot \left(\frac{e}{h}\right)^2\right] \cdot (p_1 - p_2) \quad (18)$$

in which

d	Diameter of the inner cylinder [m]
h	Gap between the cylinder and the hole [m]
η	Dynamic viscosity of the fluid [Pa·s]
l	Length of the hole [m]
p_1	Pressure before the annular clearance [Pa]
p_2	Pressure after the annular clearance [Pa]
e	Eccentricity of the cylinder [m]

The eccentricity *e* of the cylinder can make the flow 2.5 times higher in a non-eccentric cylinder. Therefore this means that the flow is highly dependent on the gap size and that the cylinder diameter has as much effect as does the clearance length, but inverse proportionally. Also, the higher the viscosity is, the lower is the resulting clearance flow. [6]

2.3.5 Cavitation

Cavitation is the phenomenon of liquid fluid transforming fast into vapour and back to liquid. The difference between cavitation and boiling is that, in the boiling process the pressure is kept constant while the temperature is increased, whereas in cavitation, the temperature is kept constant while the pressure is decreased. Also, the speed of phase transformation is much faster in cavitation which is also described as a reverse explosion, implosion.

Often there is air mixed within the hydraulic fluid, and the amount of dissolved air depends also on the system pressure and temperature. As air is much more compressible than oil, even a small amount of air mixed within the fluid causes a significant rise on the compressibility. When air bubbles emerge and implode within a fluid, the phenomena is called air buble cavitation.

Powerful local pressure peaks emerge from the implosions of cavitation, and their intensity is dependent on the bubble collapse speed, which depends on the fluid pressure transition speed. If the cavitation implosion occurs close to a solid surface, it has an erosive

effect on the surface, and it is then called cavitation erosion. This wearing leads to a change in the components operation and finally into malfunction. Cavitation also can be observed as a rise in the system noise. [6]

Some of the most important places in terms of cavitation effects are orifices. In Figure 4, five different flow types through orifice nozzles can be seen. The hole is considered as axisymmetric, and the walls are considered perfectly smooth. Point 1 is the position in which no orifice losses have occurred, point *c* is the *vena contracta*, meaning the point at which the flow area is the lowest. Point *r* is the reattachment point, in which the flow attaches to the orifice walls, and point 2 is the position at the end of the orifice.

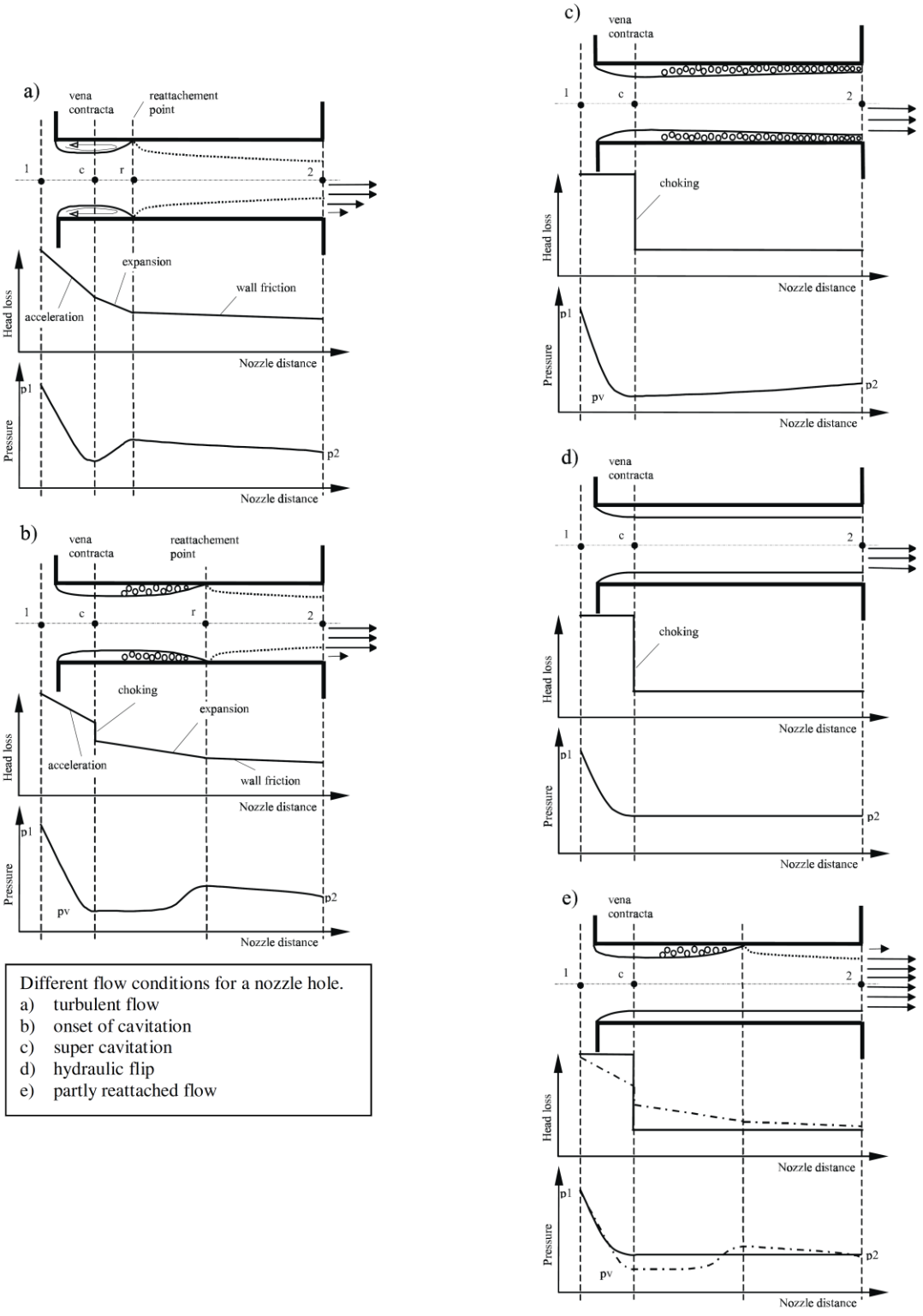

Different flow conditions for a nozzle hole.
a) turbulent flow
b) onset of cavitation
c) super cavitation
d) hydraulic flip
e) partly reattached flow

Figure 4. *Different flow conditions in a nozzle flow [7]*

In section *a,* we can see a normal, non-cavitating turbulent flow through an orifice. The effective area of the flow from point 1 to c decreases, and therefore the speed of the flow

increases, transferring the static pressure into dynamic pressure. Losses occur due to acceleration and formation of the velocity profile. After the *vena contracta*, an expansion of the flow area occurs until the flow touches the orifice walls again at the reattachment point. This flow behaviour causes expansion losses. After the reattachment point, the velocity profile increases from the orifice wall to the dotted line, after which the velocity profile remains flat, leaving a core slug of velocity profile to the centre of the orifice walls. The losses here are due to wall friction.

In section *b,* we can see a cavitating orifice flow, in which the cavitation does not reach the end of the hole. This type of flow occurs only in a very brief pressure section. The choking of the flow means that as the inlet pressure increases, there is no increase in the flow through the orifice. This saturation is due to the static pressure of the flow decreasing so low that a fluid phase change occurs, creating cavitation bubbles next to the orifice walls. If the inlet pressure continues to increase, the losses due to choking increase. However, the other losses at the inlet are smaller than in the previous case, and this is due to cavitation bubbles not transferring shear stress. After the reattachment point, the flow behaves like in the previous figure.

In section *c,* we can see a fully cavitating orifice. The cavitation begins at the start of the hole and ends at the end of the hole. Therefore there are no losses due to the wall friction. After the vena contracta, the flow spreads, and its speed decreases, recovering some of its static pressure. Most of the flow losses are due to the cavitation in the same way as in the previous case.

In section *d,* we can see a hydraulic flip. In this case, the pressure at the exit of the hole reaches back into the hole up until the vena contracta point. This is more likely to happen with shorter nozzles, higher injection velocities and large scale geometries. The discharge coefficient has the lowest value at this section, and the difference of the discharge coefficient, compared to the super cavitating flow, depends only on the back pressure. The mass flow is always lower in the case of hydraulic flip because the vena contracta is smaller in the case of back pressure suppressing it, compared to the case in which the *vena contracta* is suppressed by the vapour pressure. The losses are due to the choking, just like in the super cavitating flow. Random imperfections and asymmetrical flow fields make the hydraulic flip unlikely to occur in reality.

In section *e,* we can see a hydraulic flip which is partly attached to the orifice wall. This type of flow is a combination of the sections d and b. It occurs in long nozzles and in situations where the flow velocity distribution before the inlet is not even. Due to asymmetry, a one-dimensional analysis is impossible.

In Figure 5, we can see an example of how the discharge coefficient behaves at different flow regions. The value of the discharge coefficient is on the y-axis, and injection flow velocity is on the x-axis.

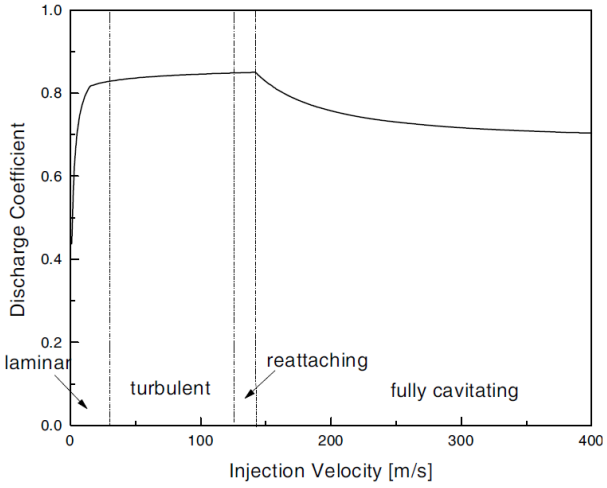

Figure 5. *Discharge coefficient at different flow regions [7]*

The vertical dotted lines in the figure represent the transition point from one flow region to another. In the laminar flow phase the discharge coefficient increases steeply, and then it increases tardily in the turbulent and reattaching flow, after which it begins to decrease in the fully cavitating region.

When a non-cavitating flow region is considered, the discharge coefficient is calculated by

$$C_d = \frac{1}{\sqrt{K_{inlet} + f \cdot \frac{L}{D} + 1}}, \qquad (19)$$

where K_{inlet} determines the inlet loss coefficients presented in Figure 6.

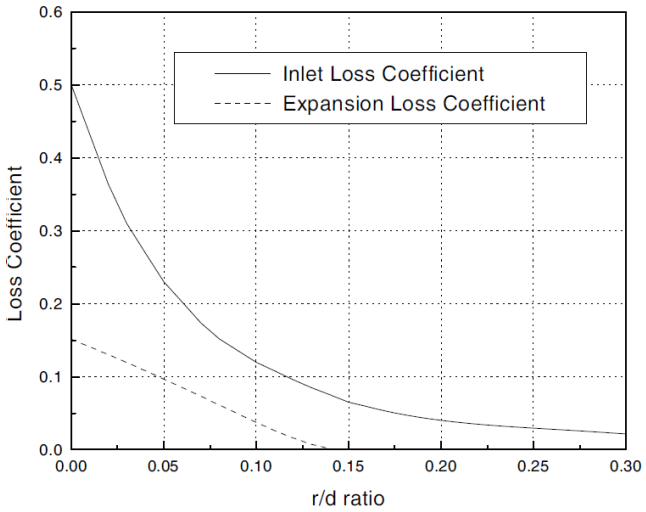

Figure 6. *Inlet and expansion loss coefficients [8]*

As the r/d ratio increases, the loss coefficients seem to decrease. Friction factor is denoted as *f* and calculated by

$$f = max\left(0.316 \cdot Re^{-0.25}, \frac{64}{Re}\right) \quad (20)$$

which means that the friction factor is calculated by either a laminar equation or Blasius equation for wall friction. When the flow is cavitating, the discharge coefficient is estimated by

$$C_d = C_c\sqrt{K} \quad (21)$$

where C_c is the contraction coefficient and K is the cavitation number which is

$$K = \frac{p_1 - p_v}{p_1 - p_2} \quad (22)$$

where p_1 is the pressure before the orifice and p_2 is the pressure after the orifice. The pressure at which cavitation bubbles appear is p_v, and it is also called the vapour pressure. The contraction coefficient C_c is estimated by

$$C_c = \left[\left(\frac{1}{0.61}\right)^2 - 11.4 \cdot \frac{R}{D}\right]^{-0.5} \quad (23)$$

where R is the diameter of the rounding of the orifice and D is the diameter of the hole. The contraction coefficient is saturated at the maximum value of 1.

By setting the discharge coefficient of the turbulent flow equal to the discharge coefficient of the cavitating flow, we can solve the value of the critical cavitation number which signals when the flow transforms from turbulent to cavitating flow.

$$K_{crit} = \frac{1}{C_c^2\left(K_{inlet} + f \cdot \frac{L}{D} + 1\right)} \quad (24)$$

The critical cavitation number is individual for each orifice.

2.4 Electro-magnetism

Regarding the electromagnetic theory, only the Ohm's law and Induction voltage formulas are presented. A complete understanding of the electromagnetics would require a comprehensive look to the theory.

Ohm's Law	$R_e = \frac{U}{I}$	U I R_e	Voltage [V] Current [A] Resistance [Ω]	With a certain amount of voltage, resistance defines how much current flows through
Induction voltage	$e = -N\frac{\Delta\varphi}{\Delta t}$	φ N t	Magnetic flux [Wb] Number of windings [-] time [s]	The change of magnetic flux determines the induction voltage. [9]

2.5 Optimization

Optimization is the process of finding the best possible solution to a problem. This solution usually means either maximizing, minimizing or targeting a certain value. That is why in optimization, it is the most essential to know what the optimization target is, and to be able to give a scalar value it. Some values, however, are not reachable due to various reasons, and this is why a set of boundary conditions needs to be implemented to limit chosen variables. For example in transportation problems, one wants to be able to move from one place to another in a minimal amount of time and costs, and the optimum solution could be moving by walking, by a bike or by a car – depending on the costs and distance. Also, it should be evaluated, how much one appreciates time over money, or vice versa. The implementation of this kind of preferences is called weighting. If there is some kind of a limit to this problem, for example if one has small budget, it would be called a boundary condition.

A problem that is present many times in the optimization processes is being stuck to a local optimum, and not reaching the global optimum. The difficulty of reaching the global optimum depends on how many local optimums there are, and how narrow the global optimum is. The only way to fully solve this problem, is to search the search space (i.e. all the possible values for the variables) thoroughly. Some algorithms, however, are more prone to being stuck in the local optimums than others.

2.5.1 Genetic algorithm

The genetic algorithm is inspired by the evolution process of the nature. The "survival of the fittest" is applied in parameter sets in a way that always the best sets get to pass their parameter values forward to new parameter sets. Before the optimization begins, the algorithm user must define the size of the population that is the number of the parameter

sets, and the number of generations that is how many times the parameter values are passed forward to the new generation.

For the first generation, the values for the parameter sets are randomly chosen from the user-defined parameter range and the amount of parameter sets are defined by the user with the name of population size. After the parameter sets in the first generation have been run, their fitness is evaluated. Usually this evaluation means that the parameter sets closer to the optimization target get a higher fitness value.

From the fittest parameter sets, a mating pool is formed. In the pool, new parameter sets are formed by using the crossover and mutation operations. In the crossover operation, two parent parameter sets are combined to form new parameter sets by randomly taking parts from the parent parameter sets. For example, if the parent parameter set consists of values of height and width, the new generation set could get the height from the other parent and the width from the other. The parameters chosen for the crossover operation are randomly selected, and the amount of crossover is random as well. For example, a new parameter set could be formed mostly from the other parent's parameter values, and only a few parameter values would come from the other parent. The mutation operation does small random changes in the parameters. For example, if a parent forwards a value for the new parameter set, the actual value in the new parameter set could be bigger or smaller.

While the generations progress, the boundary level for accepting the parameter sets increases and so does the average fitness of the population. The simulation stops when it has completed the predefined amount of iterations which is the population size multiplied by the number of generations. The genetic algorithm settings can be tuned by setting the crossover rate, the mutation rate, and the distribution indexes of their values. [10]

3. INJECTOR

In this chapter, injector operation and basic physics are covered. The operation is described in chapter 3.1, and in chapter 3.2 the force equation describing the needle movement is introduced. The pressure step is derived from it in chapter 3.3. Solenoid operation is described in chapter 3.4 and flow fuse operation in chapter 3.5.

3.1 Operation

The operation principle of an injector can be seen alongside its most important parts in Figure 7. Three types of movement are presented: injector at resting position, injector opening and injector closing.

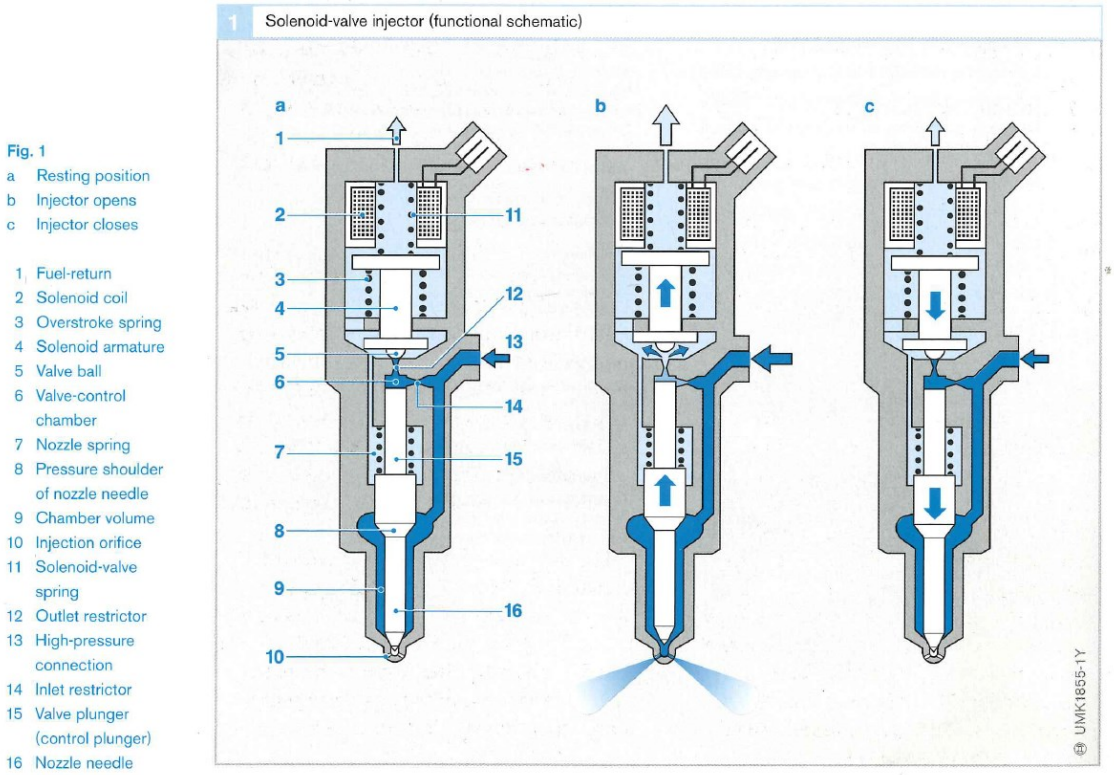

Figure 7. *Injector operation principle [1]*

The injector on the left side is in a resting position. The high pressure is marked with a dark blue colour and the low pressure with a light blue. The needle is closed, and there is no flow through the injector.

The injector in the middle illustrates an opening movement. First, the solenoid is turned on, and the solenoid armature moves upwards, thus opening the outlet orifice. This event leads to a decreasing pressure in the control chamber, which in turn results in needle

movement. Before the needle hits its seat, it comes to a stop. This is caused by a cushion of fuel flowing through the control chamber and known as the hydraulic stop. Some injectors, however, do physically hit the end of the control chamber, including the injector scrutinized in this thesis. The injector to the right shows a closing movement. The solenoid is turned off, and the solenoid armature moves downwards, closing the outlet orifice. The pressure in the control chamber rises, and the needle moves downwards, physically hitting its end position and thus closing the fluid path. A hydraulic diagram of the scrutinized injector can be seen in Figure 8.

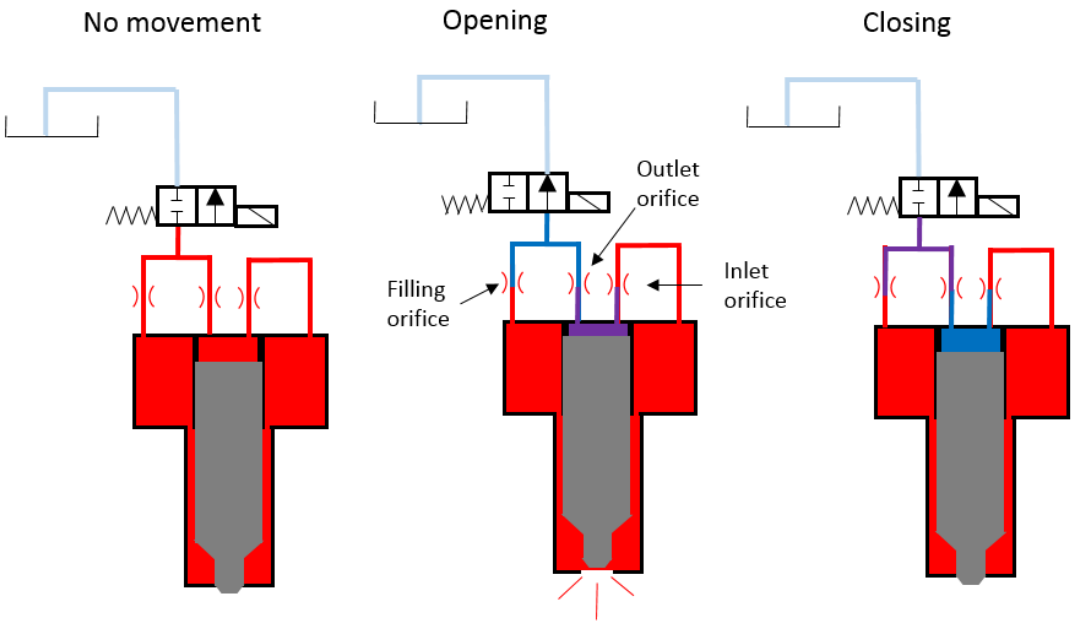

Figure 8. *Hydraulic diagram of the injector*

Again, three types of movement can be seen: the injector on the left, the needle and the control valve are closed and no fluid flow occurs. In the injector in the middle, an opening movement takes place. The control valve is open, and the needle moves upwards. In the injector on the right, a closing movement can be seen. The control valve is closed, and the needle moves downwards. The difference between the figure 8 and 9 is the filling orifice, an additional orifice, planned to make the closing of the injector needle faster. The red colour means high pressure, and the light blue is low pressure. Violet and blue are pressure levels between the high-pressure red and low-pressure light blue, and of these the violet one is a higher pressure than the blue one. Important to realize is that, between the opening and the closing movement, the higher violet pressure and the lower blue pressure switch places and that, in addition to the control chamber pressure, the pressure level in the space before the control valve plays a crucial role in the formation of the needle movement.

3.2 Force equation

The one-dimensional injector movement is modelled with the following force equation, which is also depicted in the forthcoming Figure 9.

$$\bar{F}_{acc} = \bar{F}_{cc} + \bar{F}_{p} + \bar{F}_{spring} + \bar{F}_{flow} \quad (25)$$

where

$\bar{F}_{acc}$	Inertial force [N]
$\bar{F}_{cc}$	Pressure force [N]
$\bar{F}_{p}$	Lower pressure force [N]
$\bar{F}_{flow}$	Flow force [N]

The upwards affecting forces have been selected as negative and downwards affecting forces as positive. With the equations presented in chapter 2, Theory, the equation can be rewritten as

$$m_{needle} \cdot \ddot{x}_{needle} = -p_{ctrl} \cdot A_{ctrl} + p_p \cdot A_p - x_{needle} \cdot k_{spring} - \bar{F}_{pre} + \dot{m} \cdot \dot{x} \quad (26)$$

where

m_{needle}	Needle mass [kg]
$\ddot{x}_{needle}$	Needle acceleration [m/s^2]
p_{cc}	Control chamber pressure [Pa]
A_{cc}	Needle area in the control chamber [m^2]
p_p	Pressure around the needle [Pa]
A_p	Effective area of the needle causing the upwards force [m^2]
x_{needle}	Needle lift from the resting position [m]
k_{spring}	Spring stiffness [N/m]
$\bar{F}_{pre}$	Precompression of the spring [N]

Notable is that, the value of the needle downward part area, parameter A_p, changes significantly during the opening movement, due to the pressure step effect explained in the following chapter.

By applying the theory presented in chapter 2, it would be possible to open the force equation even further. However, it is not essential for understanding the basic theory influencing the needle movement, and therefore it is not purposeful to expand any further. More important is to understand the physical phenomena affecting the control chamber pressure.

3.3 Pressure step

A pressure step is the effective force increase in the early phase of the needle opening. A force diagram of the pressure step can be seen in Figure 9 where only vertical forces are scrutinized in order to understand the resulting vertical acceleration of the needle.

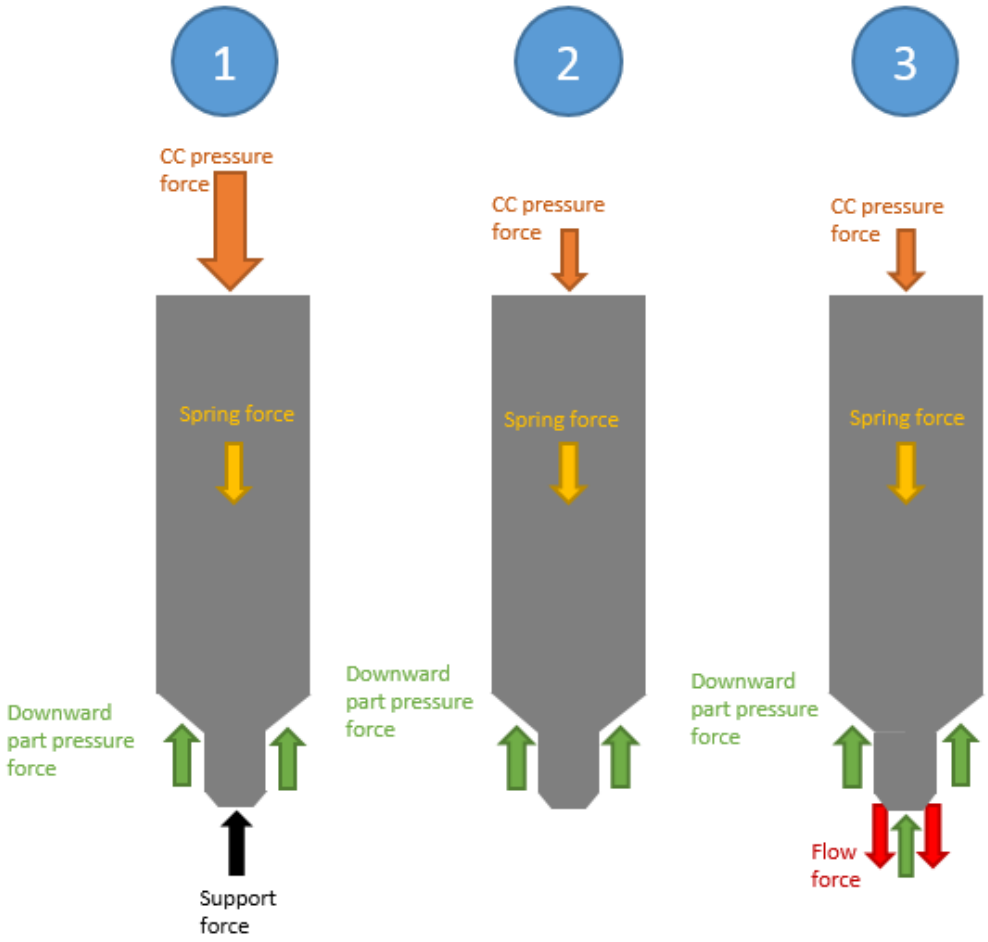

Figure 9. *Force diagram of the pressure step*

There are three different sub phases during the needle opening phase, which have been numbered from one to three in the picture. During the first phase when the nozzle is closed, the control chamber pressure force begins to drop due to the outlet orifice opening, and therefore the support force of the nozzle body begins to decrease as well. Yet, no needle movement occurs. In the second phase, the control chamber pressure has decreased

so far that the support force has vanished completely. The continuing control chamber pressure decrease leads to a slow upward movement of the needle, thereby opening a flow channel into the sac hole. As the flow through the needle tip grows, the pressure in the sac hole increases as well. This is phase three of the pressure step. The resulting forces are the flow force and the new pressure force affecting the needle tip.

Even though we can distinctly see that there are three clearly distinguishable phases during the pressure step, we should understand that the transition between the stages is smooth. The forces do not suddenly vanish nor appear but rather tardily diminish and inflate. Next, we examine how the previously introduced needle force equation looks like during the three different phases of the pressure step. In equation 34, we can see the force equation at phase one when the nozzle is closed, and the control valve is closed as well.

$$F_{support} = -p_{cc} \cdot A_{cc} + p_g \cdot A_g - F_{spring} \tag{27}$$

where

$F_{support}$ Support force of the lower contact of the needle [N]

Now the control chamber pressure and the needle gallery pressures are equal, and the equation reduces to

$$F_{support} = -p_{cc} \cdot (A_{cc} - A_g) - F_{spring} \tag{28}$$

from which the maximum support force can be calculated. The force equation at phase two, the start of nozzle opening, is

$$m_{needle} \cdot \ddot{x}_{needle} = -p_{cc} \cdot A_{cc} + p_g \cdot A_g - F_{spring} \tag{29}$$

in which we assume that the pressure in the sac volume is so small that it can be left unconsidered. Finally, in the third phase of the pressure step, the inflating sac hole pressure influencing the needle tip is considered as well.

$$m_{needle} \cdot \ddot{x}_{needle} = -p_{cc} \cdot A_{cc} + p_g \cdot A_g + p_s \cdot A_s - F_{spring} + \dot{m} \cdot \dot{x} \tag{30}$$

where

p_s Sac hole pressure [Pa]

A_s Area of the needle tip [Pa]

From these equations, we notice that the areas affected by the pressure have a key role in the formation of the needle acceleration. Now, if we look at the equation 34 at the time just before needle movement starts

$$0 = -p_{cc} \cdot A_{cc} + p_g \cdot A_g - F_{spring} \tag{31}$$

And by solving the control chamber pressure, we get

$$p_{cc} = p_g \cdot \frac{A_g}{A_{cc}} - \frac{F_{spring}}{A_{cc}} \tag{32}$$

where the ratio of areas $\frac{A_g}{A_{cc}}$ mainly defines how low the control chamber pressure needs to decrease in relation to the lower gallery pressure to cause movement if the spring force is considered small. Therefore, we name a new parameter for describing the area ratios and call it pressure step ratio (PSR).

$$PSR = \frac{A_g}{A_{cc}} \tag{33}$$

In the pressure step ratio, the control chamber area of the needle has been divided by the needle lower gallery area. We assume that it affects the needle movement somehow, and we study it later during the sensitivity analyses in chapter 6. Furthermore, if the spring force increases significantly, it will also have a high impact on how low the control chamber pressure needs to decrease in order to cause movement, which will affect the needle movement in the same fashion as increasing the lower gallery area does.

3.4 Sac hole flow

In the simulations, the pressure in the sac hole is modelled to be constant throughout the volume but time transient. In reality, though, the pressures within the sac are varying depending on the fluid dynamics, and this affects cavitation and the discharge coefficient of the nozzle holes. Even more important is to understand the behaviour of flow in the nozzle holes since it affects the pressure build-up in the sac volume.

According to Ohrn et al. [11], as cited in Ganippa et al. [12], the orifice inlet edge affects the flow discharge coefficient the most. Other, smaller affecting parameters are the orifice length to diameter (L/D) ratio and Reynolds number. In the study of Blessing et al. [13], it was found out that the conicity of the nozzle holes also has a crucial effect on the formation of cavitation which highly impacts the flow rate through the orifices, which in turn, leads to the discharge coefficient decreasing. In chapter 6, the effect of inlet orifice rounding is studied.

3.5 Solenoid

The solenoid is the component that controls the control chamber pressure. This control is achieved by solenoid armature movement which, in result, opens and closes the control valve. The solenoid armature has the shape of a pin with a plate at the other end, and the purpose of the plate is to act as a conduit through which the magnetic flux may flow. The

pin on the other hand functions as a valve, opening and closing the flow path after the outlet orifice. The pin part of the solenoid is also referred to as the control valve.

In the solenoid, there is a coil wrapped around a magnetic core. A current flows through the coil producing a magnetic field. This field circulates through the coil and generates a magnetic force, proportional to the current, into the armature. Also the force of the solenoid increases as the air gap decreases. The solenoid of the injector studied in this thesis has been cut half, and it can be seen in Figure 10.

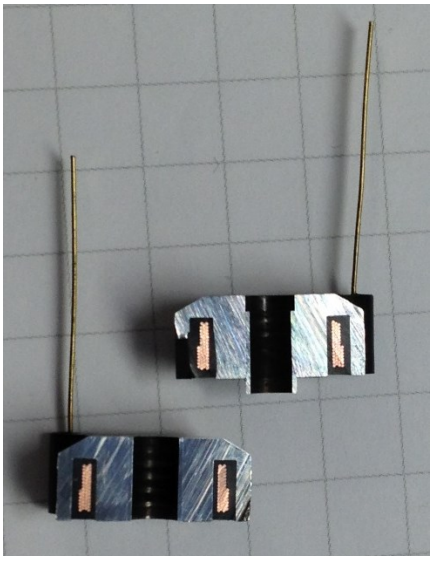

Figure 10. *A cut through of the solenoid*

When the voltage is connected to the electric circuit of the solenoid, the current begins to linearly increase, resisted by the inductance of the solenoid. In order to fasten the current rise of the solenoid, a boosting voltage is used. After the required force is reached, the solenoid voltage is reduced to its normal value which is required to hold the valve open. When the solenoid is turned off, its current flow direction changes, as its connection is changed. [14]

4. SIMULATION MODEL

In this chapter, the simulation model of the injector is introduced. In chapter 4.1 the solenoid model is explained, and the injector model is presented in the following chapters. The simulations were commenced using *GT-suite* simulation software.

In *GT-Suite*, templates are pre-defined components with certain attributes. By filling the attribute values in the template, we create an object. And by dragging the object into the model map, we create a part. From one template we can create multiple objects and, consequently, from one object, we can create multiple parts. A case means one single simulation run with certain parameters, and in the case setup, we can define multiple cases with different parameter values.

We can see the whole simulation model in Figure 11. The simulation model is divided into four submodels: fuel inlet, flow fuse, nozzle, control valve and solenoid. The rest seen in the model are smaller entities, mostly pipes and orifices, for which no separate submodels have been made.

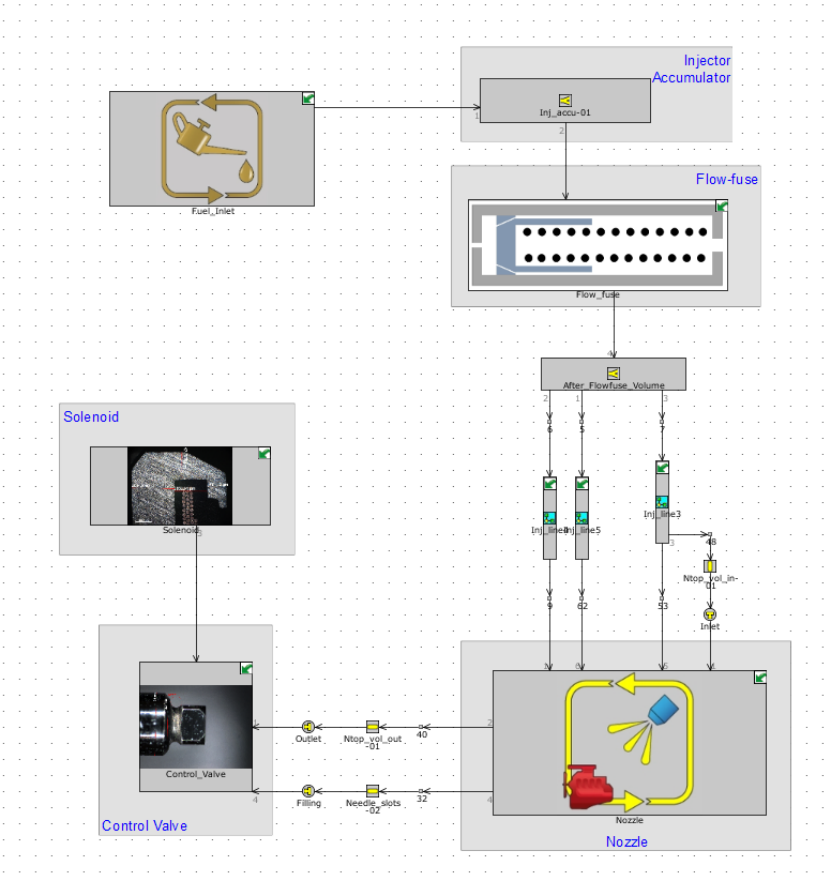

Figure 11. *Simulation model*

Initiating in the fuel inlet submodel, the flow travels through the high-pressure line into the injector and enters the nozzle from four different lines. Inside the nozzle, there is the end of the flow, the combustion chamber, modelled with a constant 50 bars. From the nozzle, fuel flows to the control valve via the inlet and outlet orifices. Between the solenoid and the control valve, there is no fluid flow but only the generated force and air gap length are exchanged.

4.1 Solenoid

A simplified solenoid simulation model can be seen in Figure 12. Instead of modelling the electro-magnetic phenomena, the generated force is determined by using a *ForceElectroMagnetic* template. A solenoid force map is defined by using an *XYZMap* template. The inputs of the force map are the air gap of the solenoid and the current in the solenoid windings.

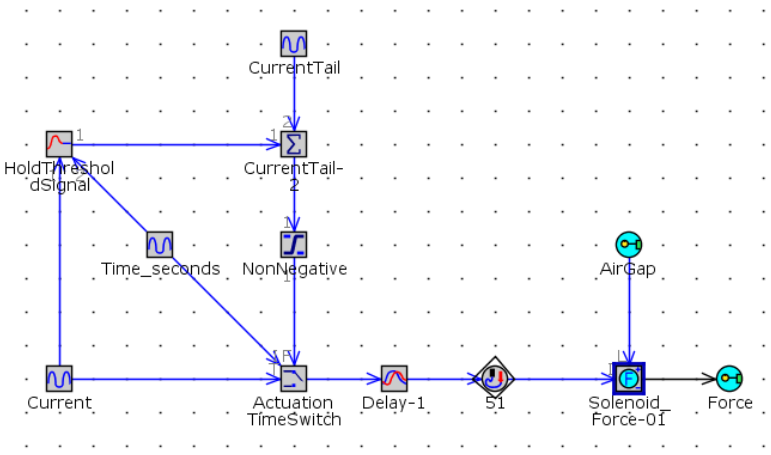

Figure 12. *Simplified solenoid*

First, the input current is defined in a signal generator template to match the time-current graph in the measurement data. The current graph can be seen in Figure 13. Second, the input current goes through a *Switch* template which has the simulation time and another input as inputs too. The simulation time is compared with the switch threshold to determine how long the actuation time is. The switch threshold is defined in the case setup as *[t_actuation],* and it is altered on a case by case basis.

When the simulation time meets the previously discussed actuation time, both the *HoldThresholdSignal* and *ActuationTimeSwitch* parts activate. The *HoldThresholdSignal* holds on to the last input value before the threshold condition was met and keeps sending it forward as a constant. In the *CurrentTail* part, a steep ramp signal is subtracted from the *HoldThresholdSignal* signal and sent forward into the switch. The resulting current is

steeply descending from the last current value before threshold time. This way it is possible to emit different lengths of actuation currents by changing only one parameter in the case setup.

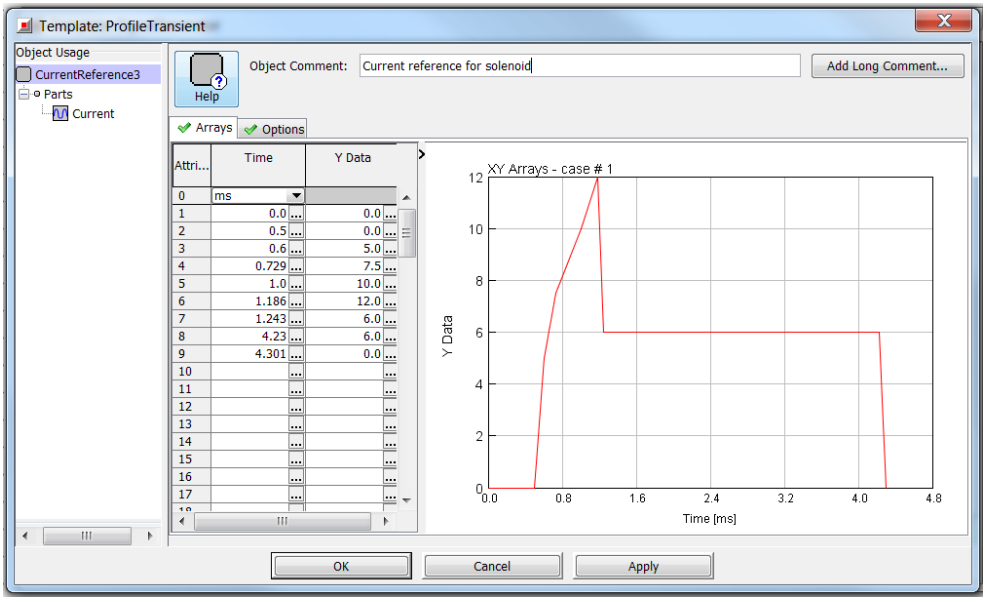

Figure 13. *The solenoid input current*

We are using a *ProfileTransient* template to input current values and the corresponding time. The values are rough estimates taken from the measurement data. In some measurement cases the start of injection was slightly different, and therefore a short delay part is inserted after the current switch.

A more detailed solenoid model is made by using magnetic simulation blocks, and its simulation model can be seen in the Figure 14.

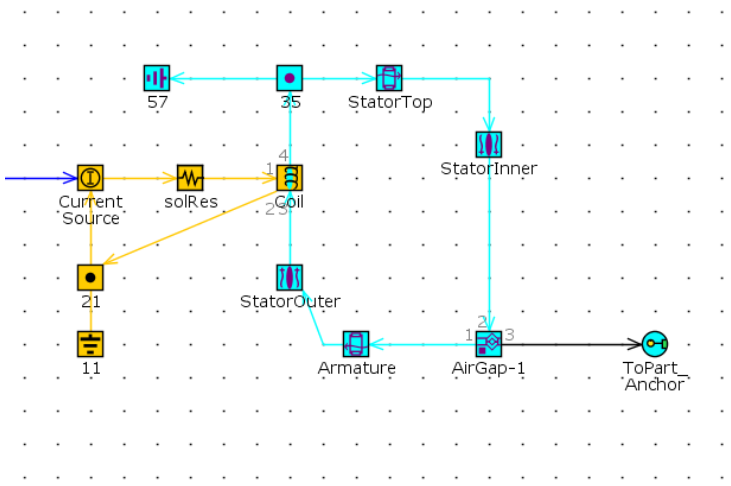

Figure 14. *Detailed solenoid model*

The current comes predefined, just like in the simple solenoid model. The coil generates a magnetic field which flows through the magnetic parts. In the *Airgap-1* part, a mechanical force is calculated depending on the length of the air gap and the magnetic flux flowing through it.

4.2 Control Valve

The control valve means the solenoid armature and the fluid flow path it controls. Here the armature receives the force from the solenoid model discussed in the previous section and sends the calculated armature position back to the solenoid. We can see the control valve model in Figure 12.

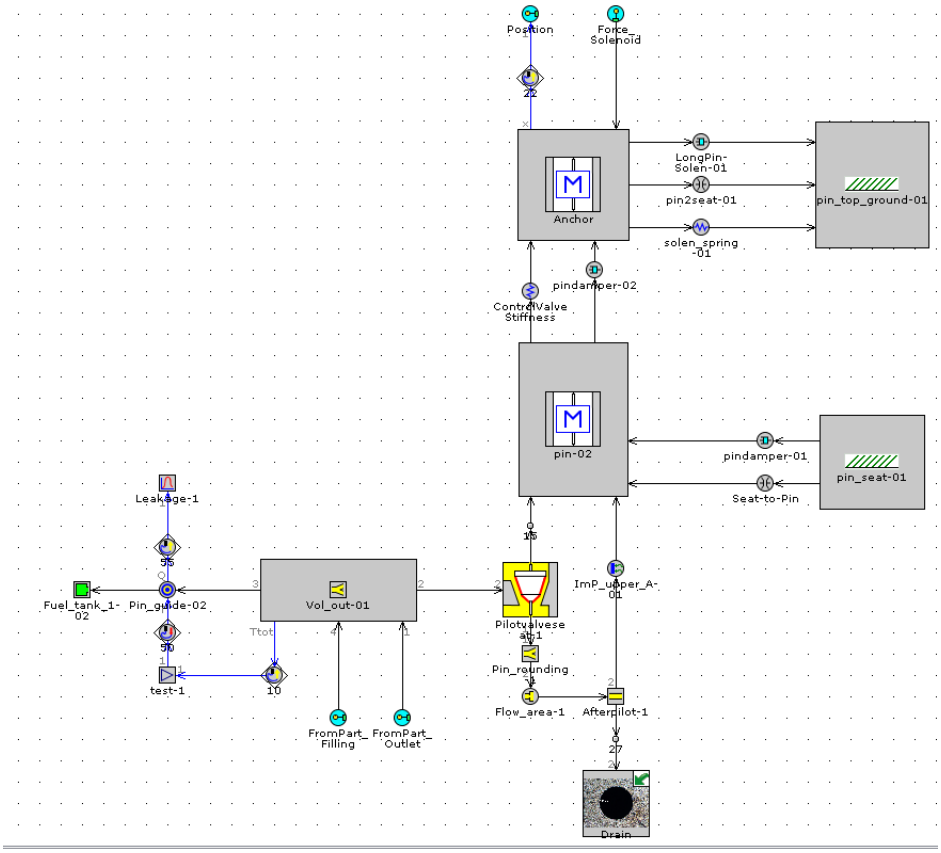

Figure 15. *Control valve*

Here the armature is modelled with two mass parts, an anchor and a pin. The parts are modelled to be connected by a spring and a damper, and their values are set the same as the injector needles. The force affecting on the lower mass part is generated by the *Pilotvalveseat* part and the area on the armature head. This is due to modelling the *Pilotvalveseat* with a rod that continues into the opening hole. The undercut (a round machining in the armature pin head) is modelled with a small volume and the flow paths around the pin head with a single orifice. Before the *Pilotvalveseat*, there is a volume where the filling orifice and outlet orifice feed in their flows.

4.3 Nozzle

In Figure 16, we can see the simulation model of the injector nozzle. The blue lines lead into the *ModelVerification, Scalarperformance and Stress* submodels, which are later discussed in chapter 5.

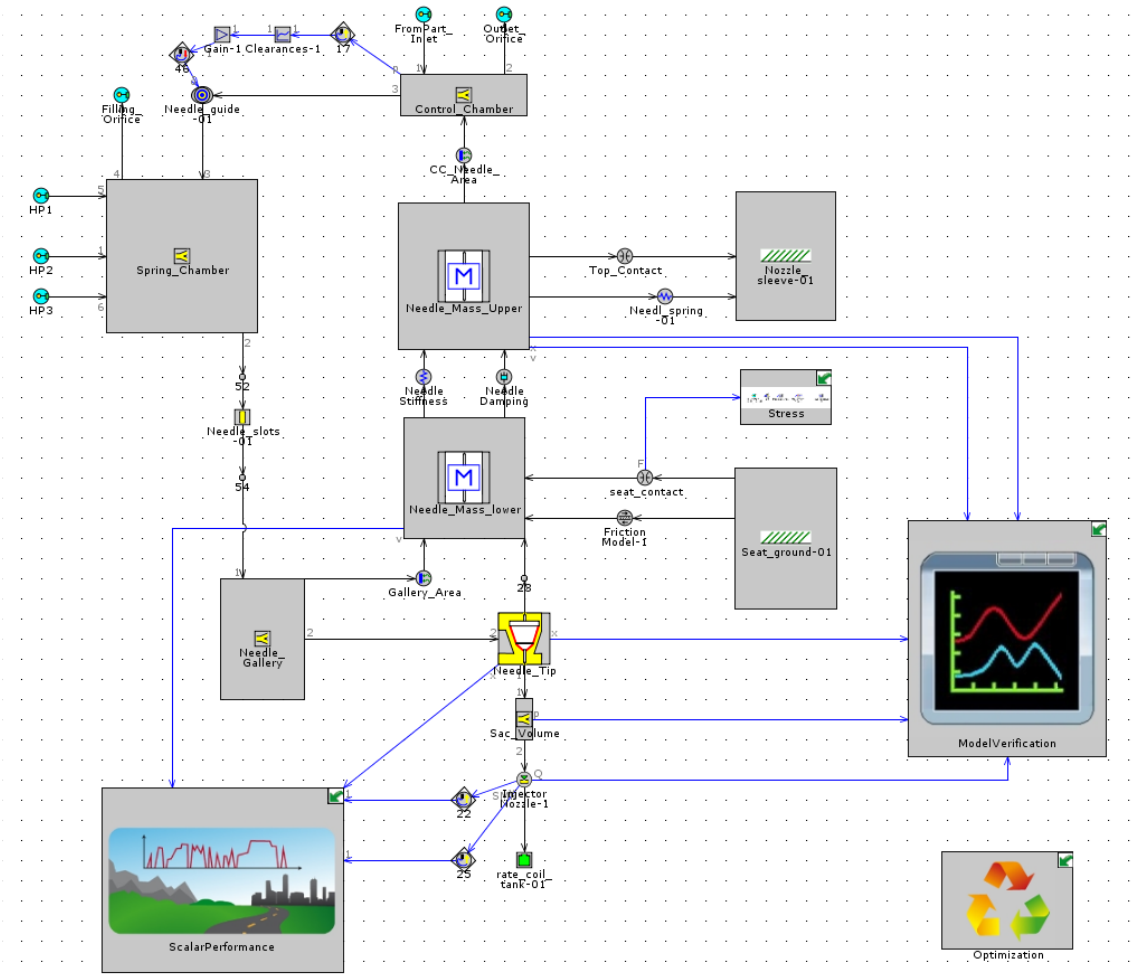

Figure 16. *Nozzle and additional submodels*

In the figure, high pressure enters the nozzle spring chamber from three different inlets, and we can see them named as *High_Pressure*. From the spring chamber, the flow continues into the *Needle_Gallery*, the volume at the bottom of the needle. Through the needle tip, the flow reaches the sac volume and, via the injector nozzle, enters the combustion chamber. From the spring chamber, there is also a leakage flow into the control chamber. The clearances alter depending on the pressure level due to the needle deformations. These deformations have been modelled with a finite element method (FEM), and the deformations as a function of pressure have been input into the *Clearances* look-up table.

The injector needle is modelled here with two identical mass objects, connected by a damper and a spring. This is the model for needle compression. The approximate needle stiffness attribute value has been discovered by a FEM–analysis of the needle and the

damping coefficient by an iteration. The needle spring influences the upper part of the needle although, in reality, the spring affects quite close to the midpoint of the needle. The control chamber pressure creates a force on the upper part of the needle, whereas the pressures on the lower gallery area and on the needle tip create a force to the lower part of the needle. Friction is considered to affect only the lower part of the injector masses on the basis of heuristic testing of the model.

4.4 Flow fuse

In Figure 17, we can see a simulation model of the flow fuse. The fuse comes after the injector accumulator and, after the fuse, there are the high-pressure inlet channels to the spring chamber.

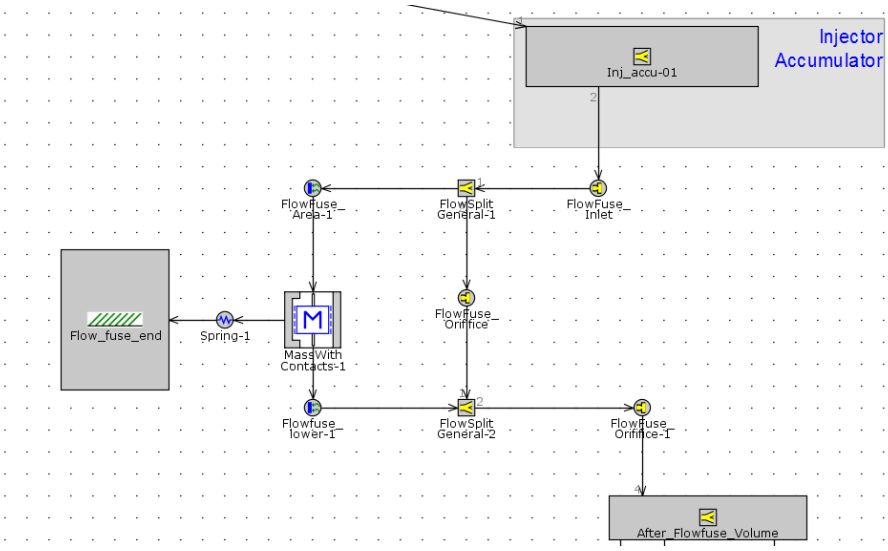

Figure 17. *Flow fuse*

The piston of the fuse is modelled with the *masswithcontacts* template, having only viscous friction determined within the object. The ends of the piston are the *flowfuseareas* connected to their corresponding volumes. Leakage flow has been assumed to be a part of the flow flowing through the *flowfuse_orifice* part.

5. MODEL VERIFICATION

In this chapter, the verification of the simulation model is described step by step. The verification data was compared to the simulation outputs within the simulation software, meaning that the verification data was input directly into the GT-ISE (integrated simulation environment) and then matched with the simulation outputs at the GT-Post. In this manner, it was also possible to calculate a total cumulative error in GT-ISE and minimize it by using the optimization tool of GT. We can see an example of the visualization of the error area in Figure 18.

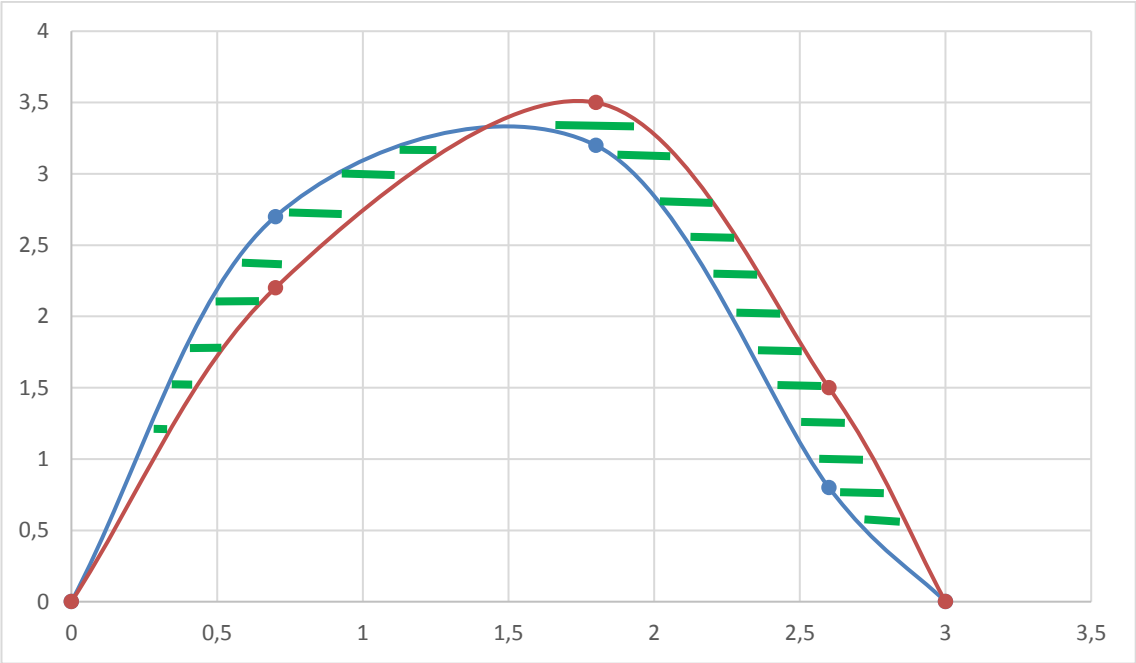

Figure 18. *Example of the minimization area*

The curves present the data values and the simulated values, and the area between them represents the cumulative error. First, the error in a single point is defined and then integrated to calculate the cumulative value

$$Cumulative\ error = \int_0^t |y_{simulated}(t) - y_{measured}(t)|\ dt$$

The error is not raised to the power of two because there are several errors which are later compared with other errors. Since a function for the cumulative error is defined, it is possible to send the total error of a single simulation run to the optimizer to be minimized.

In practice, it means that the optimizer runs the simulation model several times on different parameters and then chooses the parameters, with the smallest cumulative error. With this intention, the simulation outputs are made to match with the verification data.

The input of the verification data into the simulation model and the simulation calculation of the cumulative error are presented in chapter 5.2. This method of minimizing the error for verification purposes can be applied to any other GT simulation model as well.

5.1 Verification data

The observed quantities were the sac hole pressure, needle top velocity and needle lifts measured from the tip and the top of the needle. The data is presented in Figure 19 below, and it is depicted with two different cases of injection events.

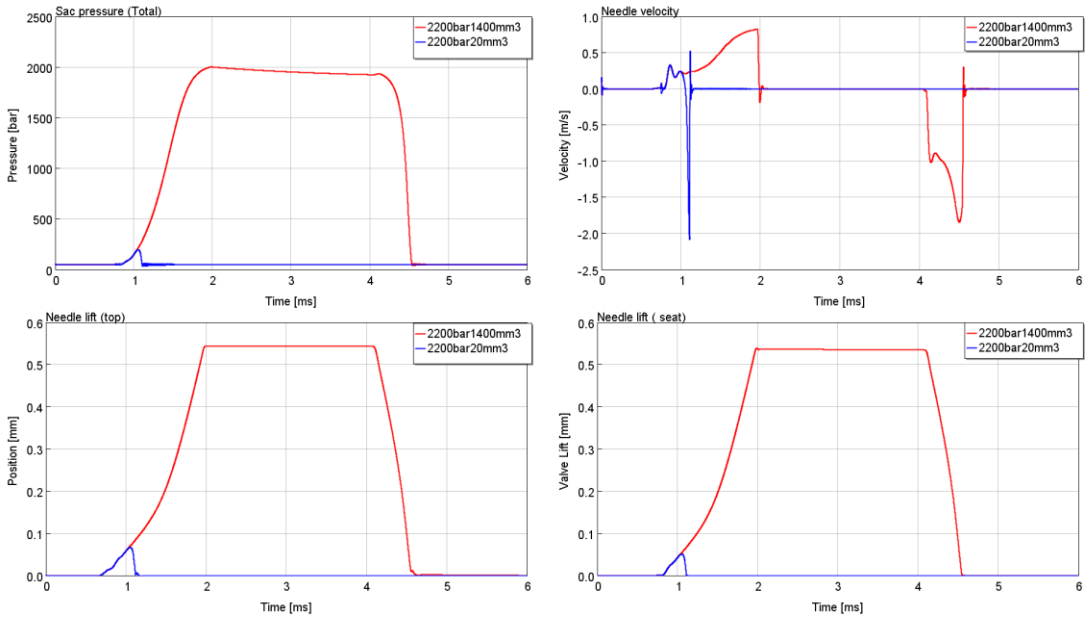

Figure 19. *Verification data of the first two injection cases*

In the ascending and descending parts of the pressure curve, we notice a sinusoidal curve, though the descending is much faster than the ascending. When the needle is fully opened, there is a discontinuity in the sac hole pressure, and this is due to the needle movement stopping suddenly. If the needle opened more, it would not reach 2000 bars because the pressure is already decreasing in the rail and the high-pressure line. The form of the pressure at the fully opened state is due to the flow fuse: from the beginning of injection event to the midpoint of injection, the flow fuse mass accelerates and, in the saturated pressure, it has reached a stable velocity.

In the very beginning of the needle seat movement, we can see a steep increase (~0,8ms) which might be a result of the stick-slip phenomena of the friction effect or of

the flow type change. During the time between ~1,2ms and ~1,6ms there seems to be a clear increase in the acceleration of the needle, and it is probably due to the increasing pressure in the sac hole and the increasing flow force. The closing of the needle seat seems to start very fast in the beginning and then accelerate even more.

The needle lift from the top begins earlier than the needle lift from the seat. This difference is due to the needle expanding as the pressure in the control chamber drops. As the needle seat also starts to move, the movement is almost identical. The initial positions are set as zero. Also, it is notable that no bounce occurs in either of the needle lifts.

The needle velocity presented here is the derivative of needle lift (top). In the curve beginning, the first pulse is due to the needle top starting to move, and the second pulse is due to the needle seat starting to move. After that, the velocity oscillation dampens quickly. In the smaller injection events, the closing of the outlet orifice affects a very high negative acceleration, and thus the needle closes almost instantly. In the closing of the needle, there is a small bounce at the beginning of the needle closing, and it's probably due to the pressure oscillations of the sac hole and control chamber. After one pulse, the needle velocity increases exponentially until the needle hits its seat. This acceleration is probably due to the sac pressure decreasing as the flow area decreases along with the needle closure.

Altogether there was a total of 6 different cases which are referred as listed in Table 2. For the optimization runs for verification purposes, we use only case 1 in order to save calculation time.

Table 2. *Six injection cases of the verification data*

Case	**1**	**2**	**3**	**4**	**5**	**6**
Injected quantity [mm^{3}]	1400	20	12	1400	20	12
Pressure level [bar]	2200	2200	2200	1900	1900	1900

5.2 Verification set-up

The inside of the submodel *ModelVerification* can be seen in Figure 20. The picture shows that all the outputs of the simulation model are drawn into their own submodels, which are built identically, excluding the *Injected_quantity* submodel.

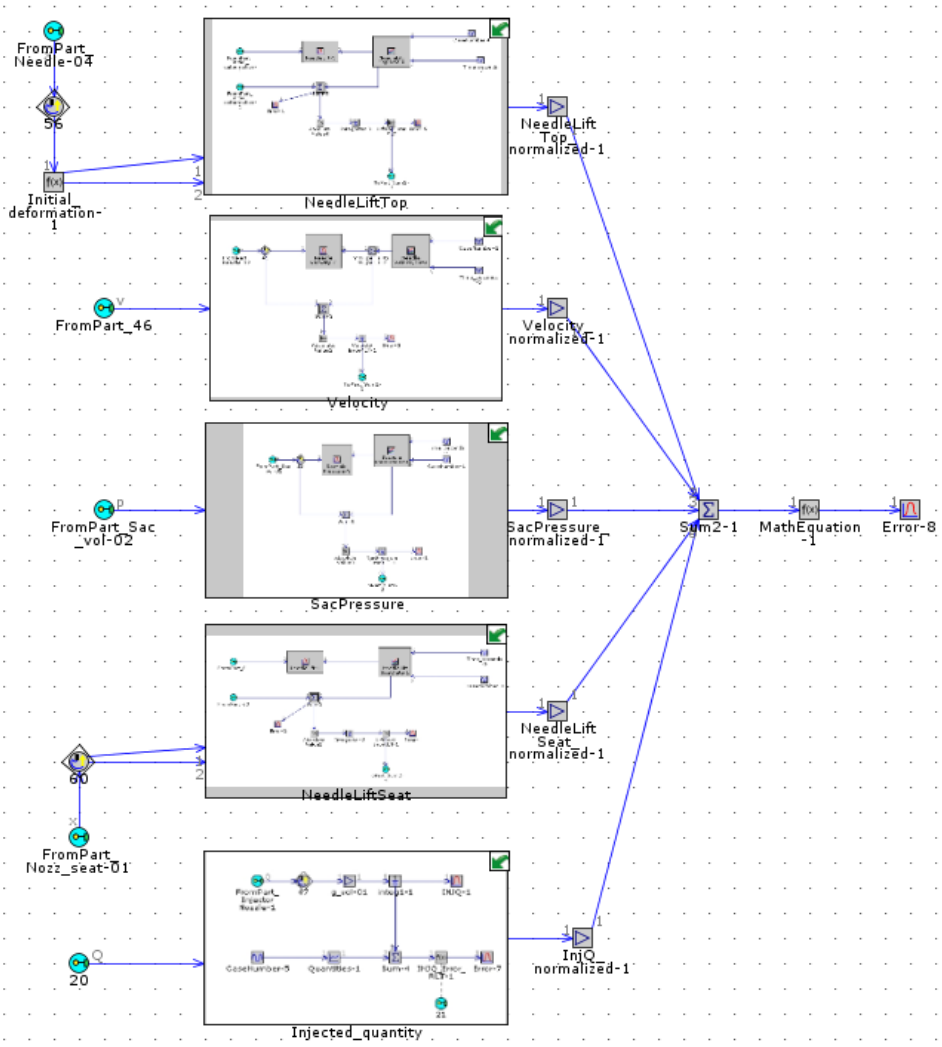

Figure 20. *ModelVerification submodel*

The initial measurement point of the needle lift top is adjusted with the part *Initial_deformation-1*. The outputs of the submodels are the calculated errors for each observed quantity (sac pressure, needle lifts, velocity and injected quantity) which are then normalized by dividing them by the maximum value of the concerning data set in order to balance their effect on the sum of errors. This normalized total error is then set to be minimized in the optimization toolbox in order to find the best fitting parameters. The content of the SacPressure subassembly can be seen in Figure 21.

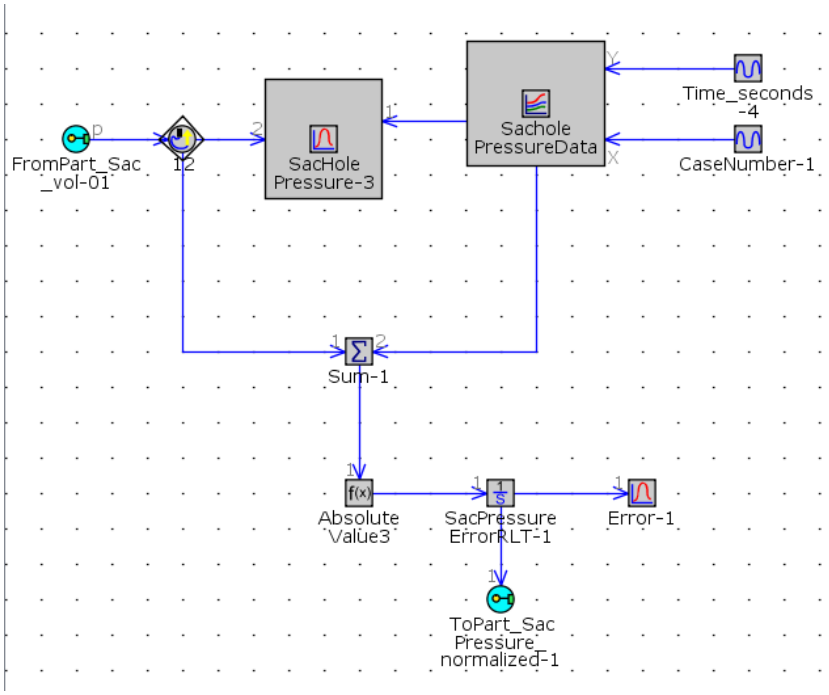

Figure 21. *SacPressure submodel*

The simulated sac hole pressure comes from the *FromPart_Sac_vol-1,* and it is compared with the verification data. This is done first visually in the *MonitorSignal* template, and then an actual error value is calculated within each time step in the *Sum* template. An absolute value is calculated and then integrated, from which the cumulative error is sent to the *ModelVerification* submodel to be normalized.

The verification data is entered into a look-up table consisting of 6 other look-up tables from which outputs are taken at each Case in relation to the simulation time. Within the *SacholePressureData* look-up table, an *XYTableOfTables* named *SacPressures* is determined, as can be seen in Figure 22.

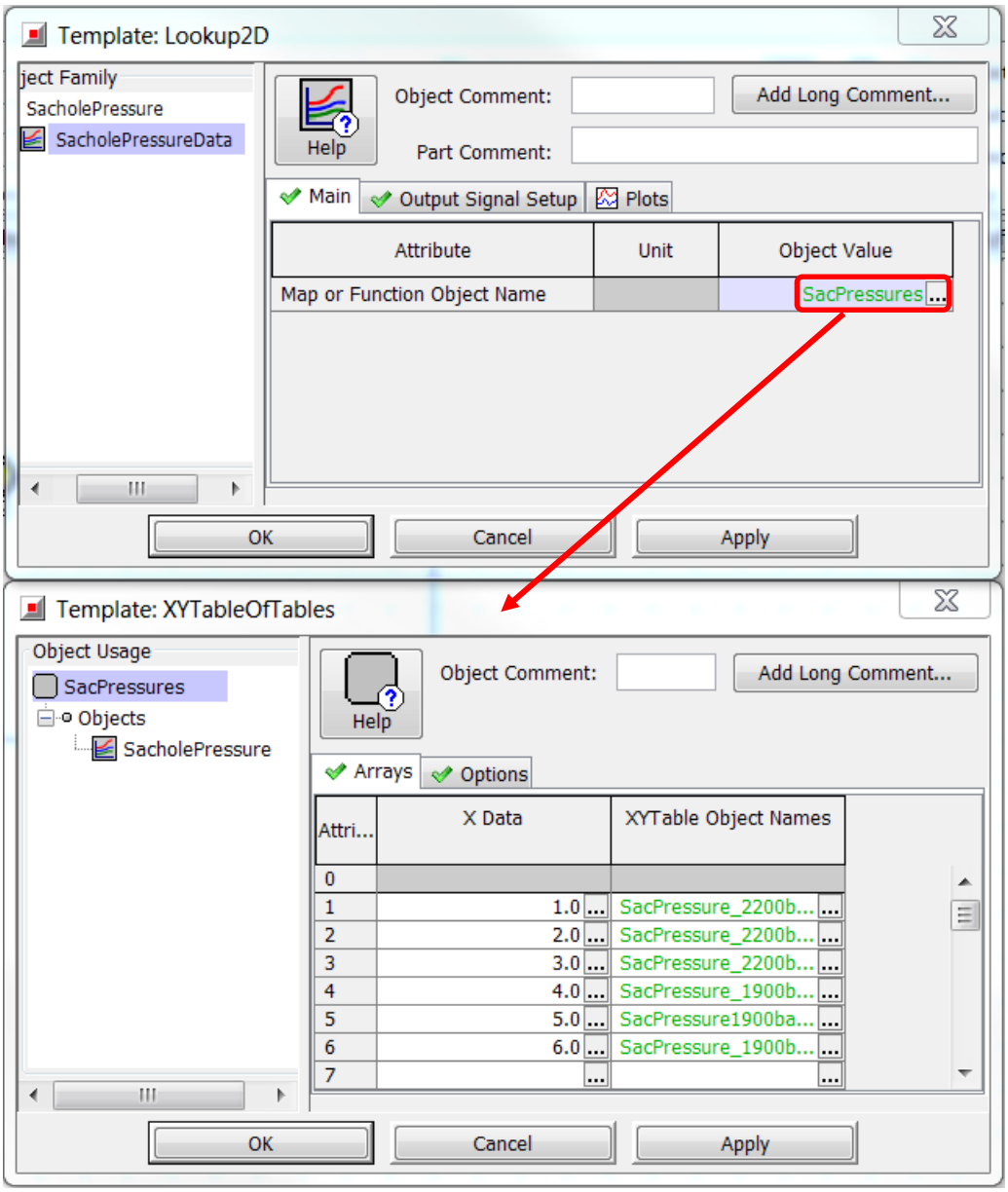

Figure 22. *Sachole pressure look-up tables*

In the *SacPressures XYTableOfTables,* there are 6 different look-up tables which are chosen depending on the input X data numbered from 1 to 6 and defined in the case setup. The look-up tables defined here are the 6 individual cases of the verification data, and the first *XYTable* can be seen in Figure 23.

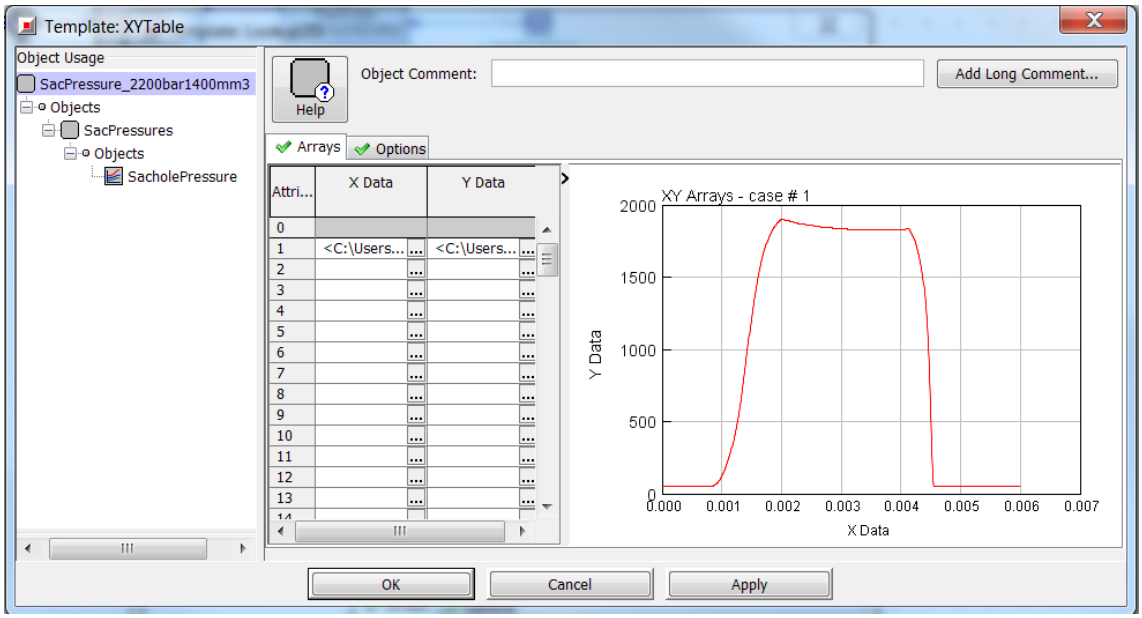

Figure 23. *Measurement data look-up table*

In the X-axis data, we have the measurement time, and in the Y-axis data, we have the observed value which, in this case, is the measured sac pressure. The simulation time is compared with the verification data time, and the table feeds forward the corresponding measured value. When the simulation time is somewhere between two measurement time units, the *XYTable* is set to estimate the measured value using linear interpolation. The other *XYtables* are identical in structure.

5.3 Optimization runs

The simulation model was optimized several times in order to find the critical parameters, and the right parameters to optimize. Notable is that, of course, there are some parameters that should not be varied for verification purposes. These are for example the needle mass, orifice diameters and other exactly known parameters. On the other hand, there wasn't enough information about the system used to create the measured data and therefore there was quite a lot of parameters to guess and optimize. There was no information, for example, on the fuel supply and rail size, so their parameters can be highly off. Additionally, some parameters are just hard to find even when all the dimensions are known, such as the friction parameters and discharge coefficients.

Additionally, the solenoid actuation time and solenoid delay were manually iterated. The delay was adjusted so that the start of needle movement was at the same time as in the verification data. The solenoid actuation time was set for the long injections (cases 1 and 4) so that the simulated beginning of needle closure occurred at the same time as in the verification data and, for the short ballistic injection cases (2, 3, 5 and 6), so that the simulated needle movement reached its top at the same time as in the measurements. This

was done first before any optimizations and then again after a few optimization rounds since the needle dynamics were altered drastically after the first few optimizations.

Having such a scarce amount of information about the system and its parameters, the task for the optimization tool was massive. The number of optimized parameters for one optimization run was as high as nine, and the time to run the optimization was several hours even when using multiple cores at a distributed cluster. A genetic algorithm was used as the search method since it was the most efficient algorithm for optimization with multiple variables.

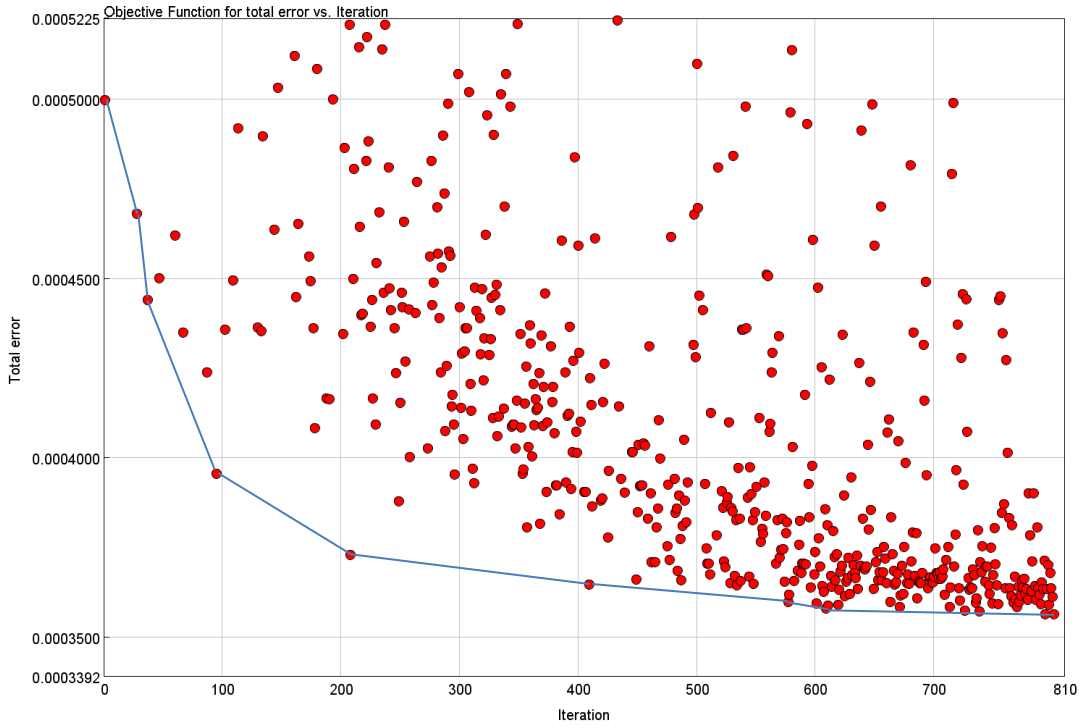

Figure 24. *Minimization of total error*

In Figure 24, a single optimization run can be seen. The total error on the Y-axis is the error introduced in the previous chapter, and the X-axis gives the number of iterations. Each red dot represents one single simulation run, and altogether there is a total of 800 simulation runs. For this run, a total of 9 parameters were optimized. The blue curve has been added to visualize the development of the best fitting parameter set. From the picture, we can clearly see that the development is most rapid during the first 100 simulations, after that the development decreases and after 200 iterations only minor improvement can be seen. In Figure 25, we can see how the total error behaves in relation to outlet orifice discharge coefficient.

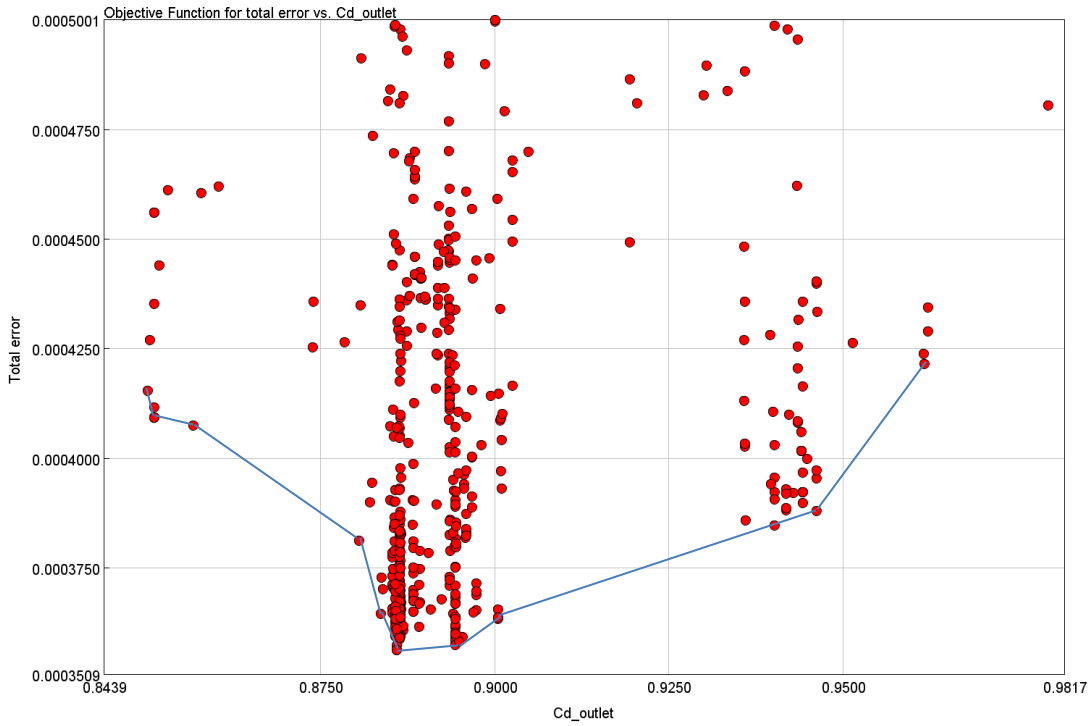

Figure 25. *Total error versus outlet orifice discharge coefficient*

On the Y-axis, we have the same total error as in the previous figure, and in the X-axis we have the discharge coefficient of the outlet orifice. The red dots represent the single simulation runs, and the blue curve has been added to visualize the behaviour of the total error in relation to the outlet orifice discharge coefficient. From the figure, we can see that the best values for *Cd_outlet* are between 0.8750 and 0.91. The optimizer reports the values of the best single set of parameters, i.e. the red dot located at the lowest point in the picture. There are figures also for the other parameters, but it is not purposeful to go through all of them.

5.4 Model fit

The validity of the model is defined by visually comparing the simulated outputs to the verification data, and also by observing the total cumulative error. The best fit was found using the simplified solenoid model and a constant discharge coefficient excluding the cavitation effects for the nozzle holes. In Figures 26-29, we can see the fit of the needle lifts, needle velocity, sac pressure and the injected quantity.

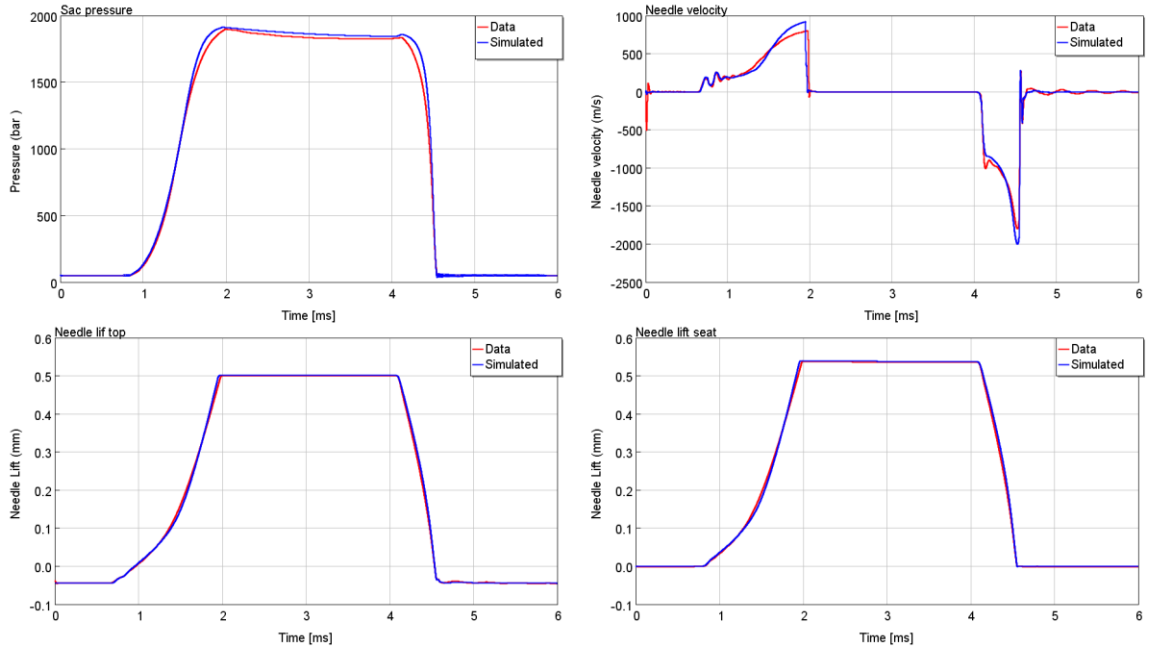

Figure 26. *Model fit for case 1: full injection with 2200 bars*

Evaluating the figures visually, we can see that the model fits the data well. Small differences can be seen in sac pressures and needle velocities, but the forms of the curves are the same, so the basic physical phenomena concerned seems to be right. However, using this optimization method to minimize the error, we should have almost no error at all, if the model is correct and we vary the right parameters. In Figure 27, we can see the needle lift from the seat with 1900 bar supply pressure.

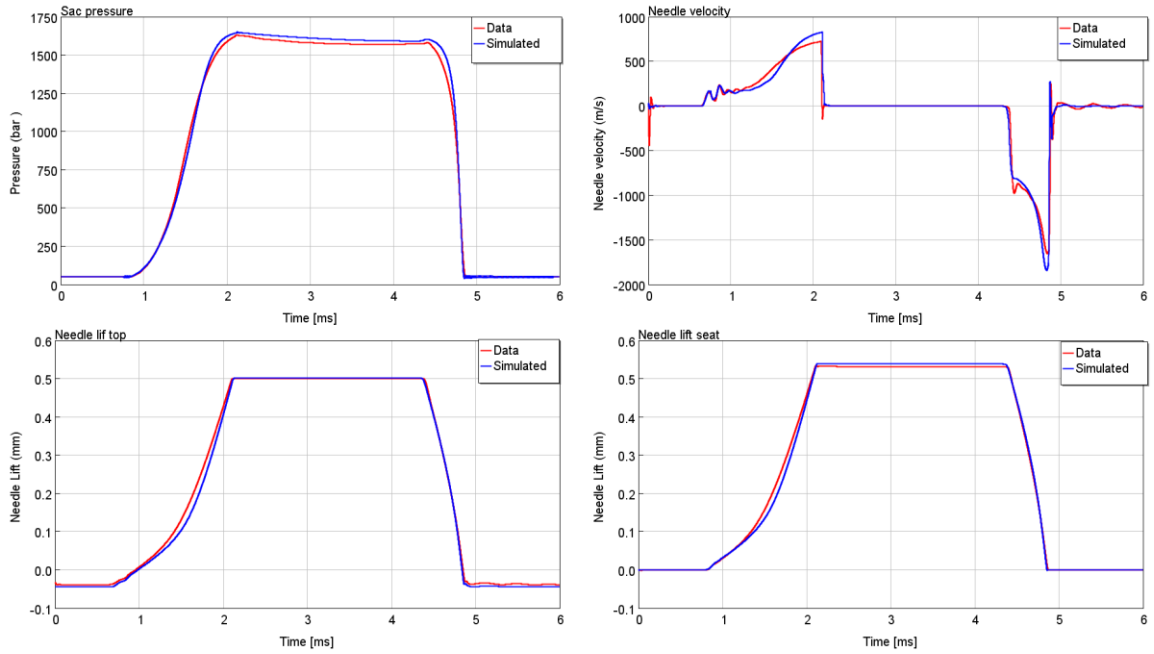

Figure 27. *Model fit for case 4: full injection with 1900 bars*

For the injected quantity of 1400 mm^3 at 1900 bars, the model gives quite accurate results as well. However, there is more error than with the injected quantity of 1400 mm^3 at 2200 bars. This is due to performing the optimization only for the injected quantity of 1400 mm^3 at 2200 bars. We could optimize the model to generate average fitting parameters for all the 6 cases, but this would require 6 times more calculation time. For the remaining four pilot injection cases, only the needle lift (seat) and sac pressure are presented in Figure 28 and Figure 29.

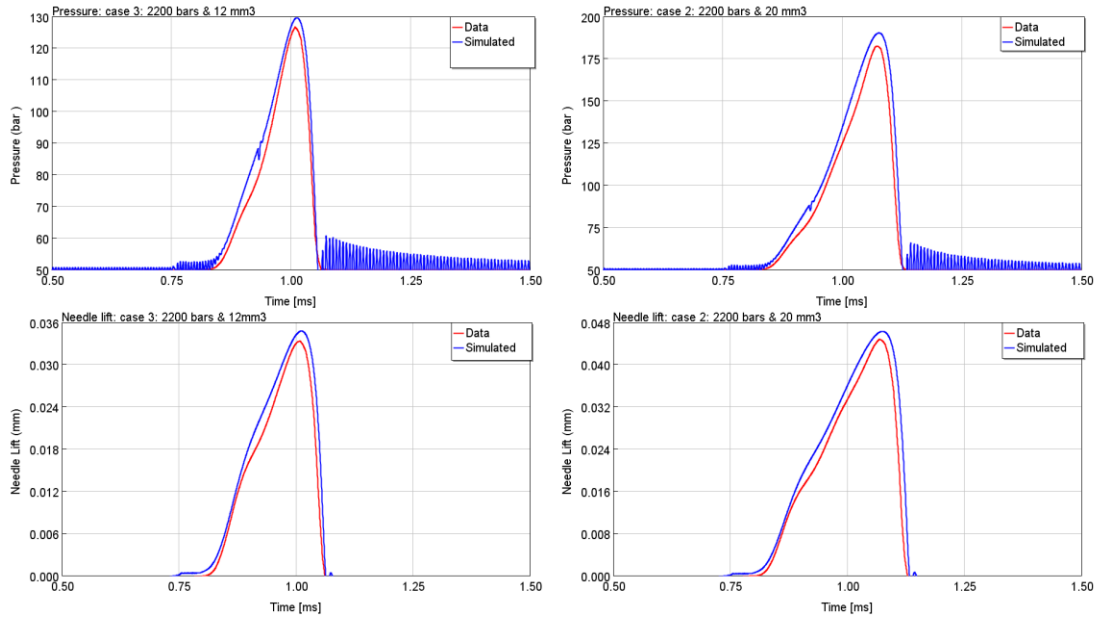

Figure 28. *Model fit for pilot injection cases 2 and 3*

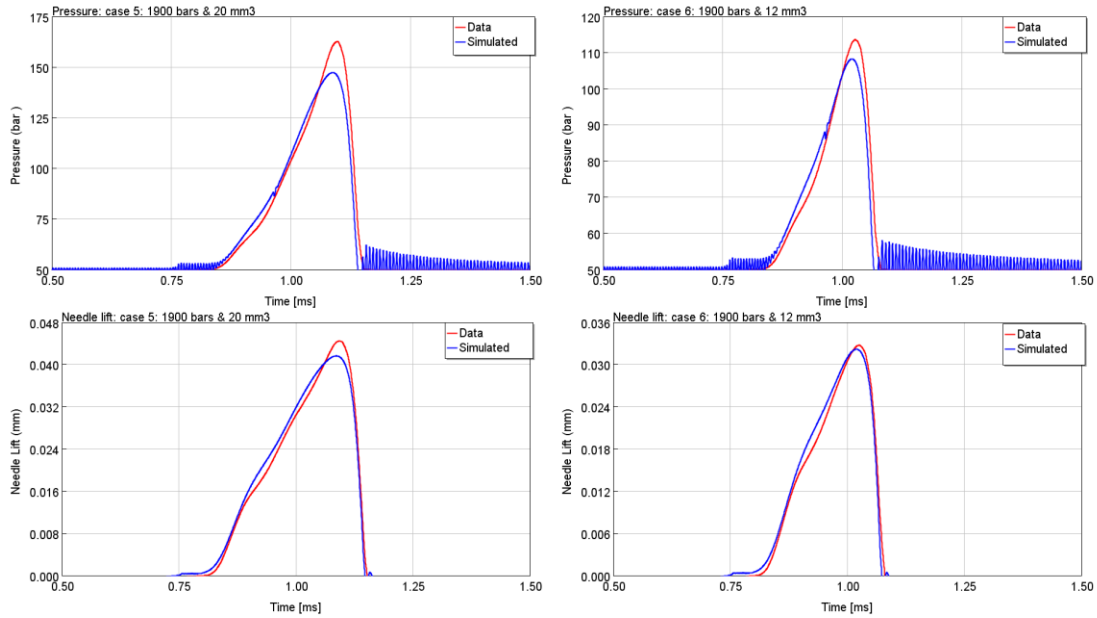

Figure 29. *Model fit for pilot injection cases 5 and 6*

The model fit is good also for the pilot injections. In case 5, there is the biggest error observable visually, and it is probably due to too early switch off of the injection event. The reason for the simulated pressure noise was not found.

In the following table, the measured and simulated injected quantities are presented and compared. Absolute and relative errors are calculated.

Table 3. *Measured and simulated injected quantities for the more simple model*

Case [-]	1	2	3	4	5	6
Measured quantity [mm^3]	1400	20	12	1400	20	12
Simulated quantity [mm^3]	1309	19.9	12.0	1294	17.6	10.6
Error [mm^3]	91	0.1	0.0	106	2.4	1.4
Error [%]	6.5	0.5	0.0	7.6	12.0	11.7

The simulated measured quantities are close to the measured ones, but there is significantly more error in the cases with a lower pressure level. This is probably due to the optimization being performed with the higher pressure level. In case three, there is some error, but the rounding makes it zero with one-decimal accuracy. In cases 5 and 6, the actuation time was observed to be slightly too short, and therefore this would seem to be, at least partly, the reason for their too low injection quantities.

Even though the best fit for the measurement data was found at a simpler simulation model, a more complex one is used with the sensitivity analysis and optimiztion. In this more complex version, the solenoid model is the detailed version, introduced in chapter 4.1 and the cavitation effects are taken into consideration in the nozzle hole flow as the model for calculating the discharge coefficient is the *CdFromGeometry* template. The parameters from which the cavitation and resulting flow are calculated are the orifice diameter and the thickness and rounding of the orifice holes. The fit of the more complex model can be seen in Figure 30 and Figure 31.

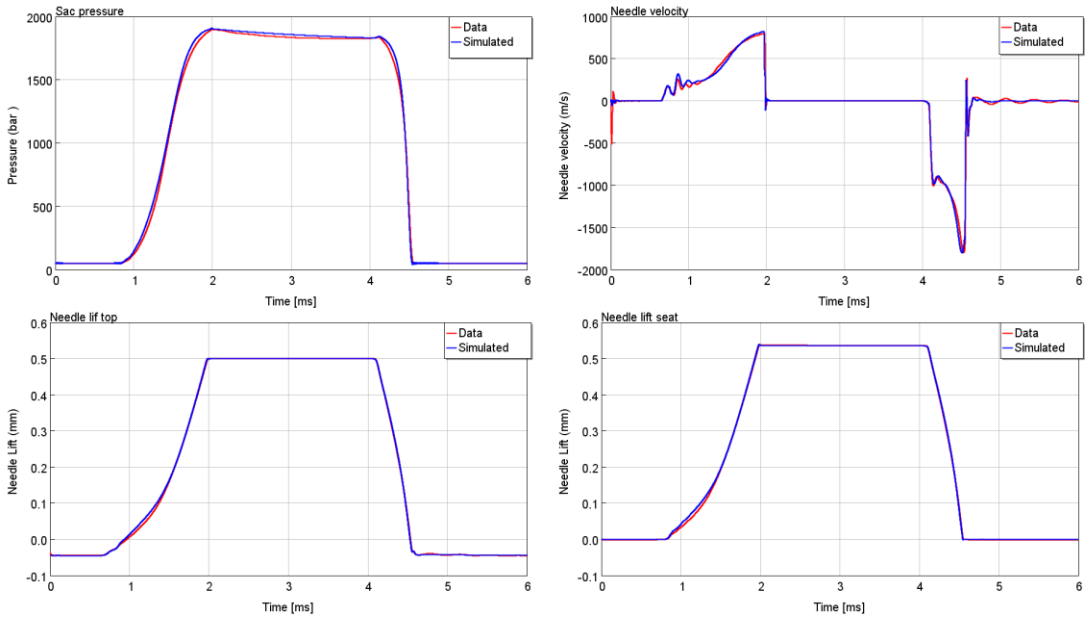

Figure 30. *The more complex model fit for case 1: full injection with 2200 bars*

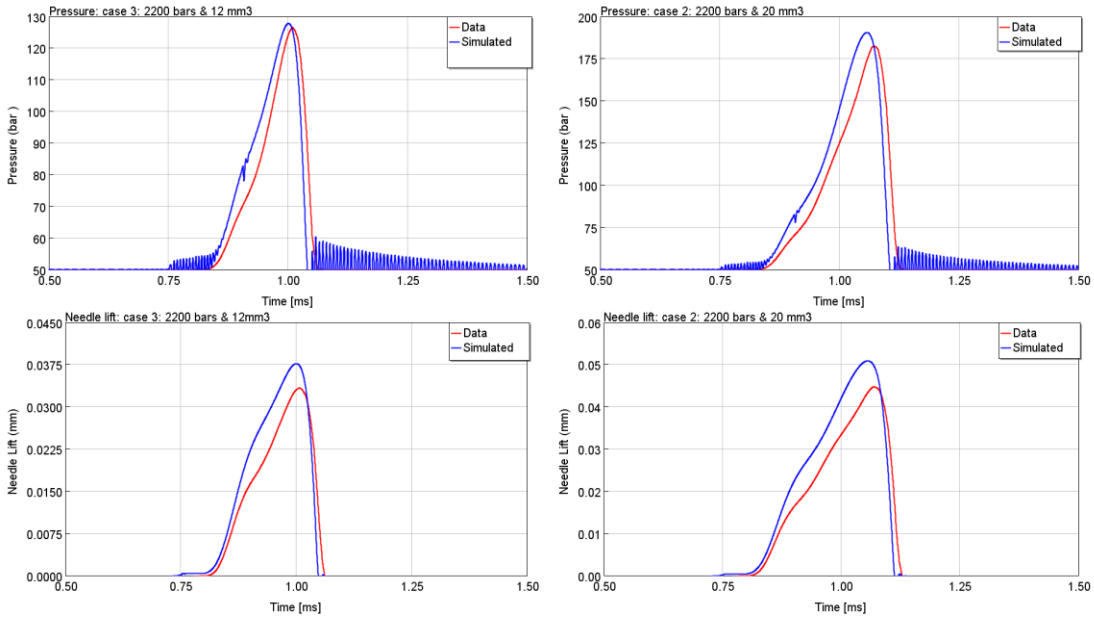

Figure 31. *The more complex model fit for pilot injection cases 2 and 3*

From the figures, we can see that, in the pilot injection, the more complex model does not correspond with the verification data as well as the simpler model previously presented. In the full injection event of the more complex model, there is also a small error in the beginning part of the needle lift. This error is probably related to the modelling of the flow type and the discharge coefficient it yields. Regarding the injected quantities presented in Table 4, the more complex model corresponds with the data almost perfectly, but that is partly due to iterating the actuation times in a way that the simulated injected quantity is made to match with the data.

Table 4. *Measured and simulated injected quantities for the more complex simulation model*

Case [-]	1	2	3	4	5	6
Measured quantity [mm^3]	1400	20	12	1400	20	12
Simulated quantity [mm^3]	1402	20.0	12.0	1401	20.0	12.0
Error [mm^3]	2	0.0	0.0	1	0.0	0.0
Error [%]	0.14	0.0	0.0	0.07	0.0	0.0

6. SENSITIVITY ANALYSIS

In this chapter, sensitivity analyses of the injector are presented. Two different injection events are studied: a full injection event with an actuation time of 3.4 ms and a pilot injection with a variable actuation time always resulting in an injected quantity of 20 mm^3. The analysis is divided into four parts: solenoid, control chamber, needle and nozzle sac; and the study is restricted to observe only one varying parameter at a time. Though in some cases more than one parameter is affected, in those cases either the relation of the varying parameters or the result of the subtraction between the parameters is constant. The purpose of the sensitivity study is to better understand how each individual parameter affects the needle behaviour.

The values that affect the atomization process most are the injection rate, injection velocity (of the spray), and the Sauter mean diameter. The needle lift and the sac pressure do not directly influence the atomization but rather are the causes for the injection rate and velocity curve shape. However, for the reason of understanding the whole injection process, the needle lift and the sac pressure are chosen to be observed in addition to the injection rate and velocity. The Sauter mean diameter is scrutinized only with the sensitivity of the nozzle hole diameter and the number of holes because it is almost the same in the other cases.

In the result figures, the x-axis unit is always milliseconds. The range for the full injection is from 0 to 6 ms and from 0.7 to 1.6-1.7 ms in the pilot injection. The y-axis depends on the unit of the observed parameter and is always set to “auto” so that the simulation software always scales the y-axis values according to the given results.

6.1 Solenoid

In this chapter, the solenoid related parameters are covered, and these are the number of windings, the solenoid airgap, the discharge coefficient of the control valve, and the mass of the control valve. These parameters are chosen to test the effects of both the solenoid electromagnetics and the control valve hydro-mechanics, and they are individually discussed in their corresponding chapters.

6.1.1 Number of windings

The injector sensitivity for the number of windings was tested from 25 rounds of windings to 200 rounds of windings. In this sensitivity study, it is critical to understand the flaws of the solenoid simulation model: the current rise and decrease are always the same though they should be affected by the varying inductance of the solenoid. For this reason,

it is impossible to test the sensitivity of different voltage levels. However, with the number of windings we are already able to influence the shape and intensity of the force generated by the solenoid through which the voltage level affects as well, and therefore we choose to study the windings for this study. The full injection sensitivity to the number of windings can be seen in Figure 32.

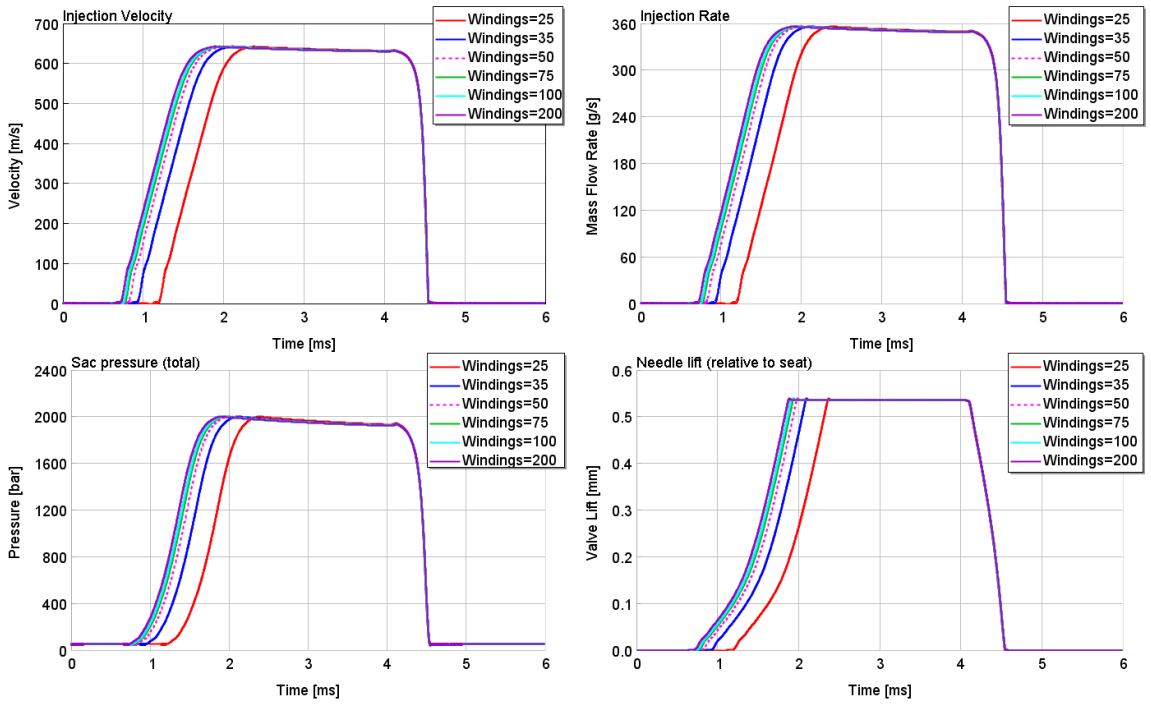

Figure 32. *Full injection sensitivity to the number of windings*

From the figure, we can see that the number of windings affects only the opening delay of the needle lift. However, in reality it should also affect the closing delay of the needle because the discharge of the magnetic field is dependent on the induction of the coil which, in turn, depends on the number of windings. In the simulation model, there is a small difference in how fast the generated force of the solenoid drops, but it is too small to have a noticeable effect on the needle movement.

In Figure 33, pilot injection sensitivity for the number of windings is illustrated.

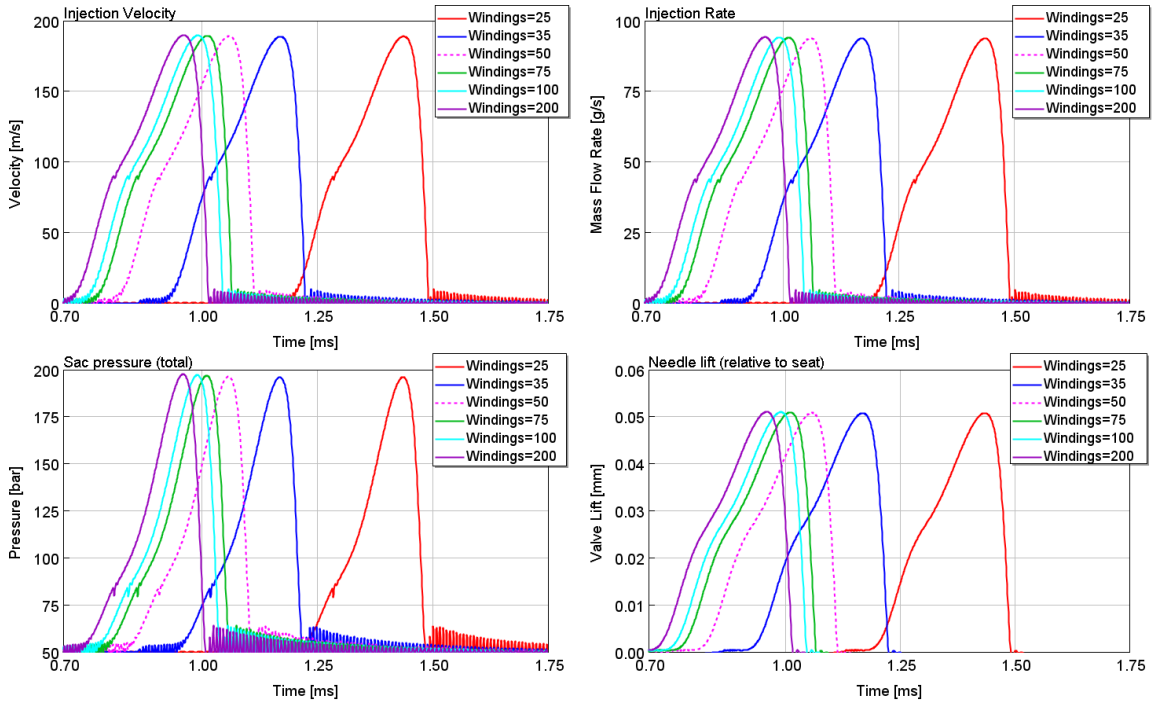

Figure 33. *Pilot injection sensitivity to the number of windings*

There is a considerable delay in the pilot injection, but otherwise, the shapes of the curves are identical. It would seem that it doesn't matter how fast or soon the control valve opens because the needle lift curve shape is not affected by the control valve speed. However, the effect of the solenoid windings to the closing speed of the control valve remains unclear because the change of the solenoid inductance hasn't been taken into consideration. Therefore, we cannot undisputedly say how much the windings affect the shape of the needle lift, but we can surely conclude that it affects the opening delay of the needle.

6.1.2 Control valve mass

In Figure 34, the full injection sensitivity to the control valve mass has been studied. The mass has been chosen to vary from 0.5 g to 50 g's, while the original weight is 3.34 g's.

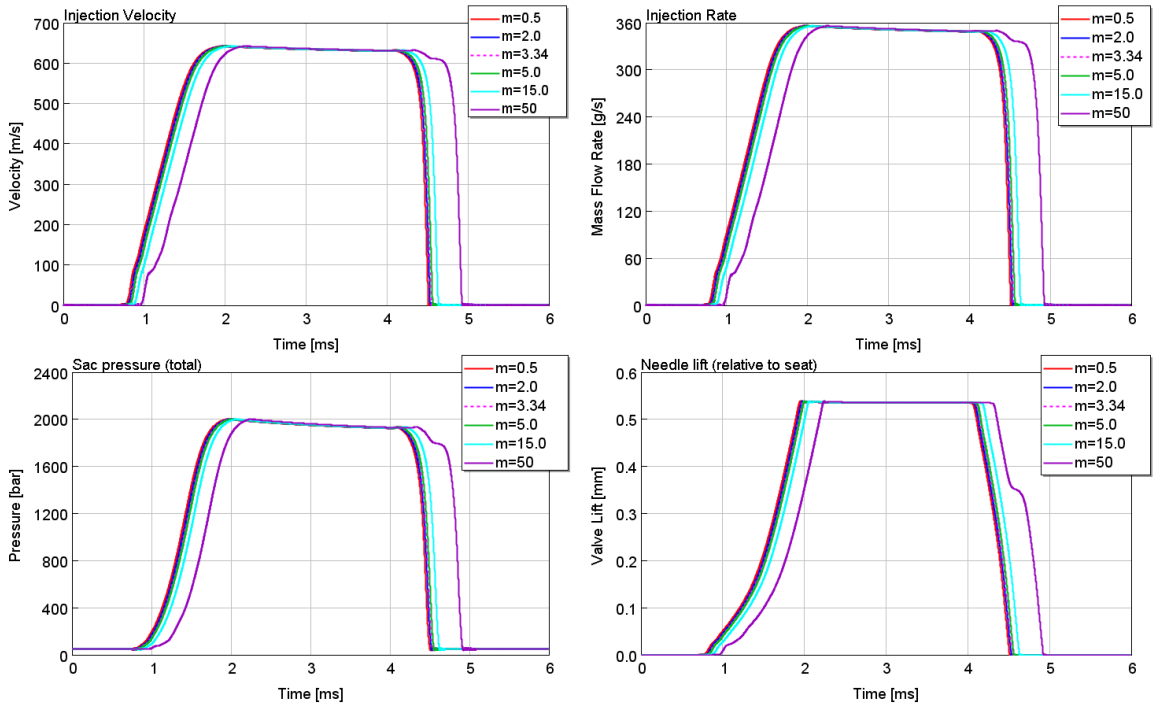

Figure 34. *Full injection sensitivity to control valve mass*

From the figure, we can see that the injector is not very sensitive to the control valve mass. Nevertheless, there is a small increase in opening and closing delay as the mass of the control valve increases. The purple curve that doesn't fit among the others is different due to the unrealisticly high mass of the control valve, causing it to bounce and producing unrealistic results.

In Figure 35, we can see the pilot injection sensitivity to the mass of the control valve.

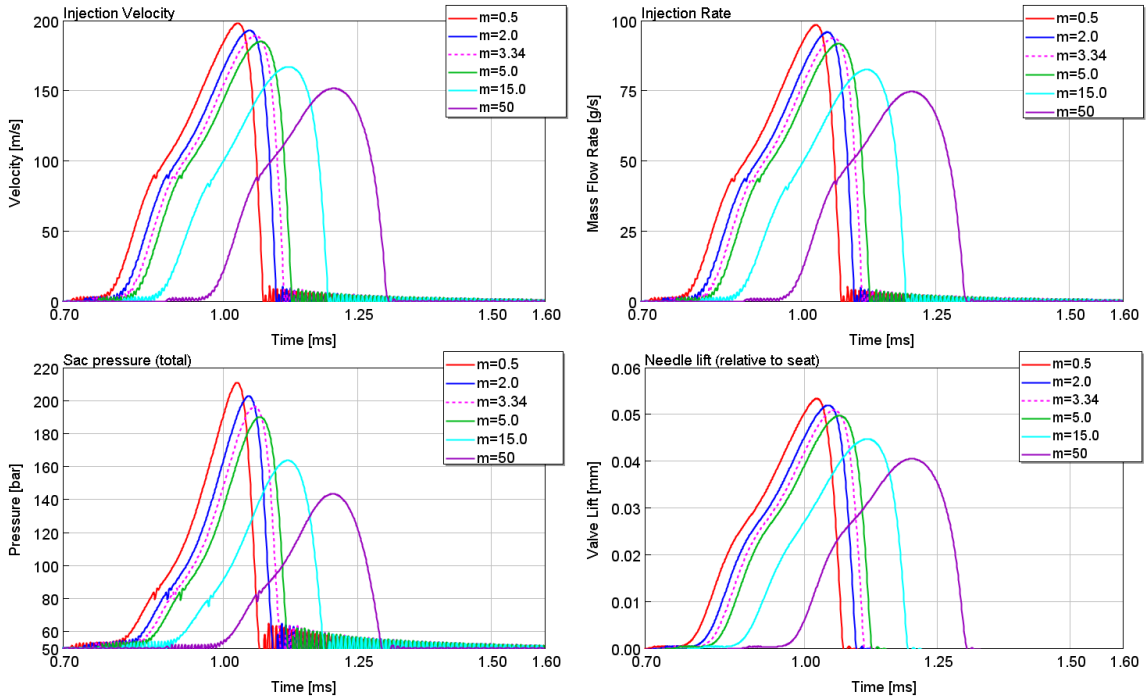

Figure 35. *Pilot injection sensitivity to control valve mass*

We can clearly see that the control valve mass seems to have a medium effect on the pilot injection even though, in the full injection event, we could barely see any difference. This is due to differences in the control valve closing speed: the lighter control valve closes faster, thus the flow direction in the outlet orifice changes more rapidly. In order to understand why the control valve mass affects the pilot injection lift curve shape, whereas the solenoid windings (of the simplified solenoid model) do not, one must understand that the control valve mass affects both the closing and the opening speeds of the control valve, whereas the solenoid windings affect mainly the opening speed and delay of the control valve. The opening time of the control valve does not affect the shape of the needle lift because of the pressure step: the pressure in the control chamber affects the needle lift only after it has decreased low enough to cause needle movement. The closing speed of the control valve, on the other hand, affects immediately the needle movement because, while it is closing it throttles the flow through itself, thus causing the change of flow direction in the outlet orifice to be slow. The different changes of flow rates can be observed in the sharpness of the peaks of the needle lifts: the lightest control valve has the sharpest peak whereas the heaviest control valve has the dullest peak.

6.1.3 Control valve discharge coefficient

In Figure 36, we can see the full injection sensitivity to the discharge coefficient of the control valve. The discharge coefficient was chosen for the study because it represents how much throttling occurs in the control valve, and it is not easy to predict from the geometry how big the throttling in the control valve is in reality.

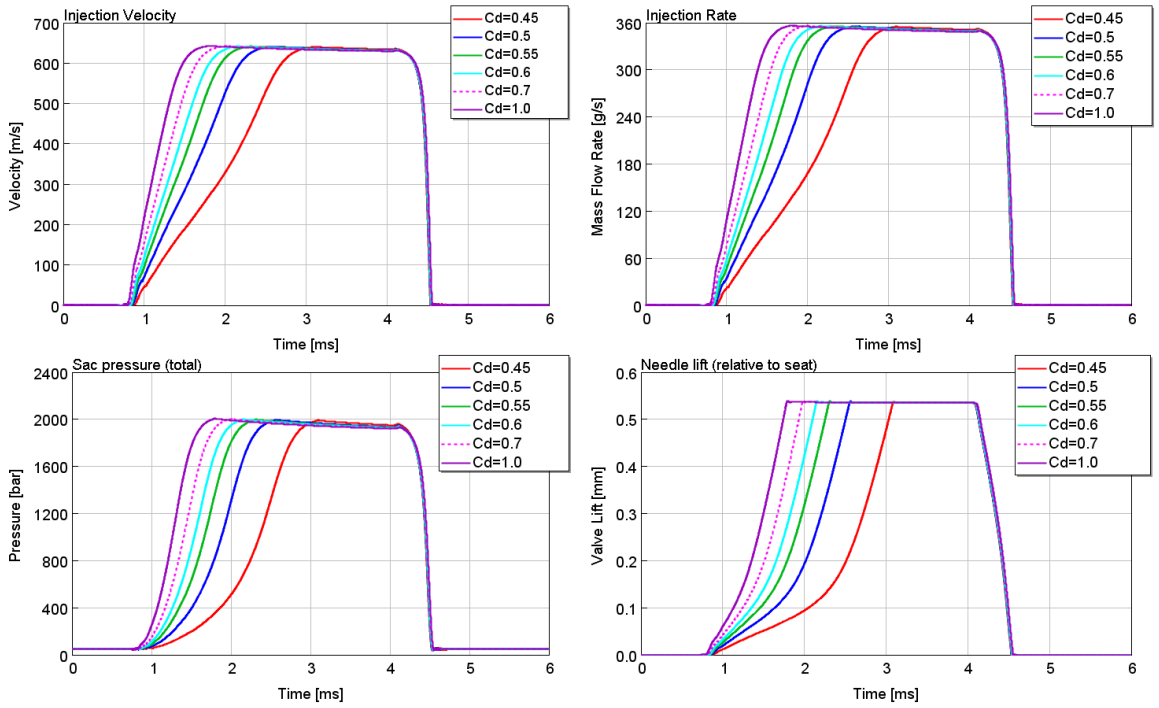

Figure 36. *Full injection sensitivity to the discharge coefficient of the control valve*

From the figure, we can see that the control valve throttling affects significantly the opening of the needle but has no effect on the closing of the needle. This behaviour is due to the injector configuration, meaning that, in the closing phase, the flow doesn't flow through the control valve. Having more throttling in the control valve makes the opening slower. In Figure 37, we can see the pilot injection sensitivity to the discharge coefficient of the control valve.

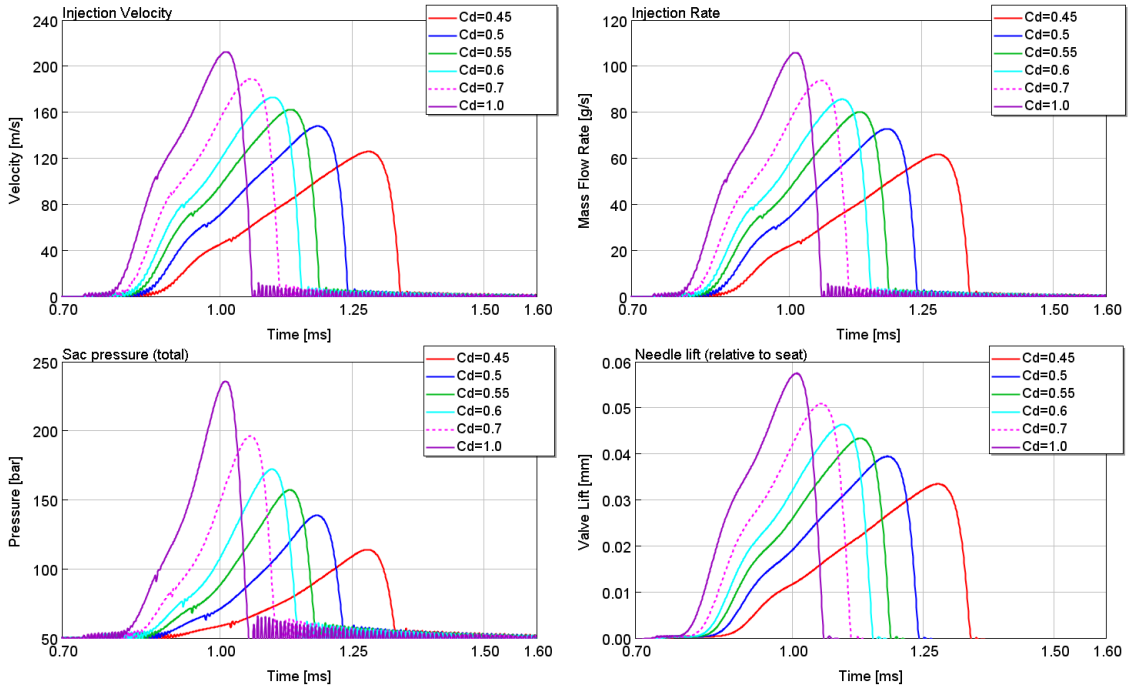

Figure 37. *Pilot injection sensitivity to the discharge coefficient of the control valve*

Having a bigger discharge coefficient results in a faster pilot injection event, and correspondingly, a smaller discharge coefficient results in a slower pilot injection event. The result is in accordance with the full opening sensitivity. The main discovery of this discharge coefficient sensitivity study is that the throttling in the control valve has a significant impact on the whole injection event and therefore should always be taken into consideration in fuel injector design.

6.1.4 Air gap length

In Figure 38, we can see the full injection sensitivity to the solenoid airgap length

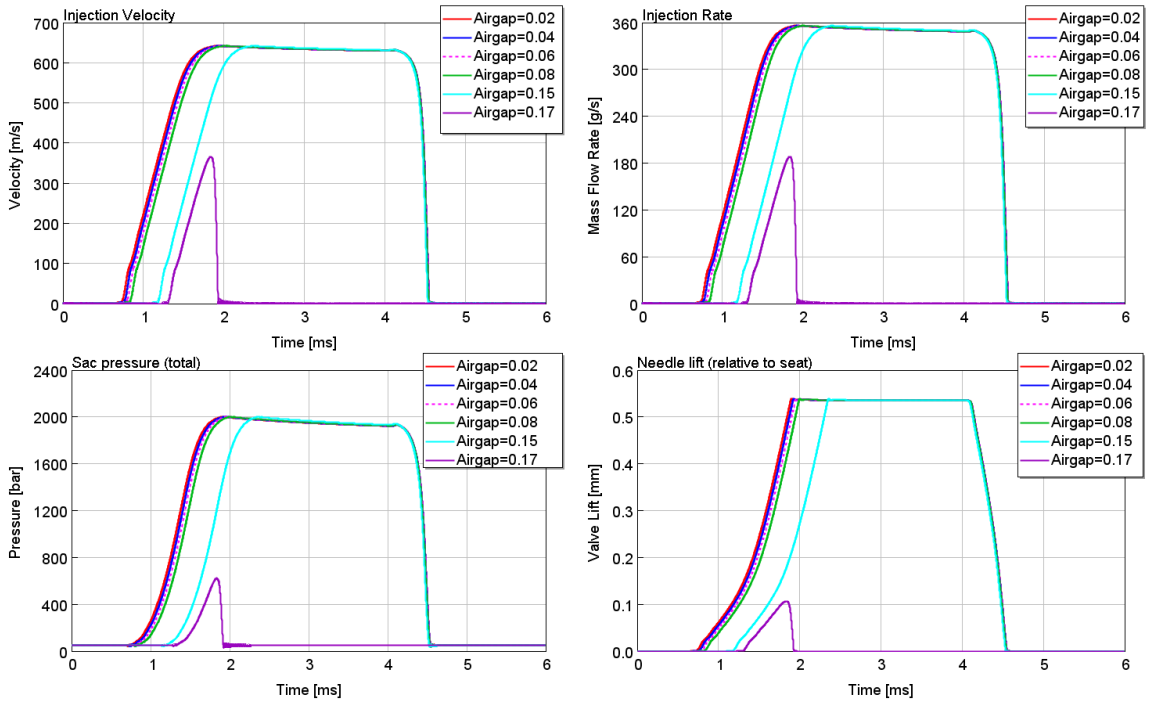

Figure 38. *Full injection sensitivity to the airgap length*

The airgap length seems to affect only the opening delay of the needle. The first two smallest airgap lengths are unrealistic because in those the solenoid pin would sink into the solenoid armature and that is not physically possible. In the case with the biggest airgap length, there is only a pilot-sized needle opening, which is due to the hold current not producing enough force in the solenoid to keep the control valve open. Therefore the needle opens only for a brief amount of time during the boost current, and it looks a bit like the pilot injection event.

In Figure 39, we can see a pilot injection sensitivity to the airgap length.

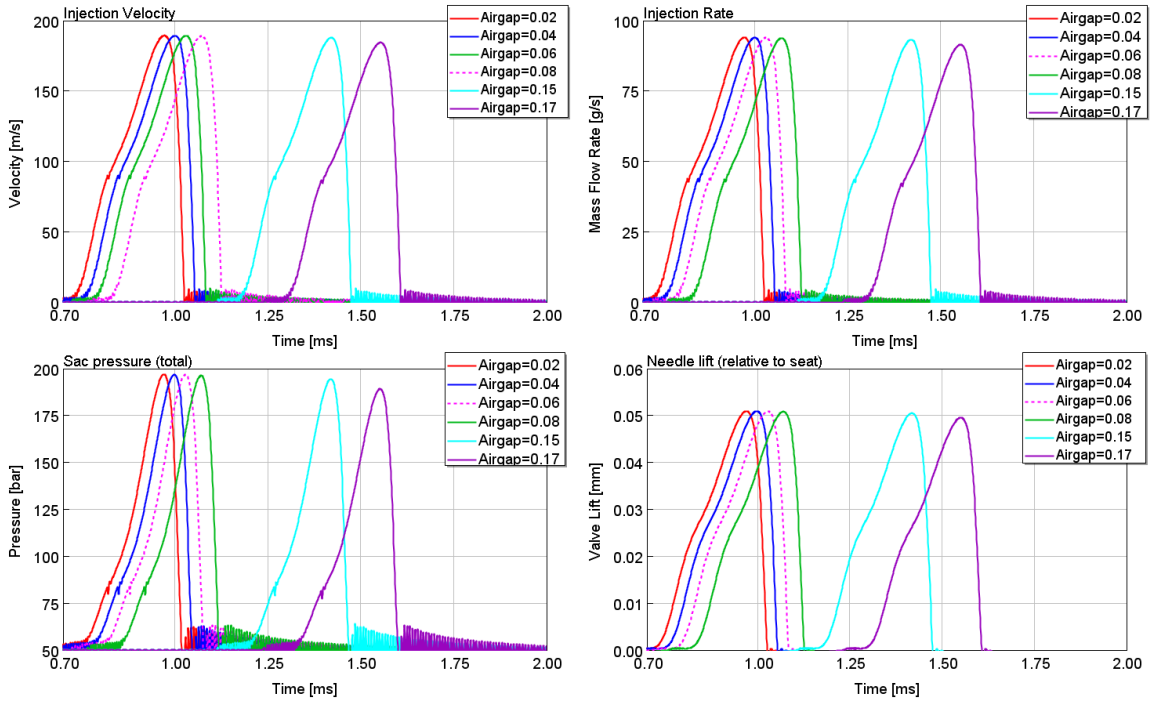

Figure 39. *Pilot injection sensitivity to the airgap length*

The effect of the airgap seems to be in the opening delay of the pilot injection, but otherwise the injection events seem to be identical. Also with the biggest airgap length, the pilot injection event seems to be almost identical with the that of the other airgap lengths. However, also in this case, the oversimplification of the solenoid electro-magnetic model should be noted, as with the number of windings.

In the light of the above-presented solenoid sensitivity analysis results, it's quite safe to say that the control valve opening speed has a minor effect on the studied injector. This lack of effect is partly due to the pressure step: even though the control chamber pressure would begin to sink with different rates, the effect of the control chamber pressure on the needle movement occurs only after the control chamber pressure has decreased low enough. With other injectors with different sizes of pressure steps and orifices, the effect might be different. The control valve closing, on the other hand, seems to play a minor role in the shape of the needle lift. Therefore it can be concluded that, the closing of the control valve should be as fast as possible but the opening of the control valve is not so important. Also in addition to the control valve closing, the flow throttling in the control valve is important.

6.2 Control chamber

The varied parameters for the control chamber were the diameters of the inlet orifice, outlet orifice, filling orifice and the volume size of the control chamber. First, each of them were individually varied, and the inlet and outlet were additionally varied while

keeping their relation–the area ratio–constant. Finally, the three orifices were varied at the same time while keeping their area ratios constant.

6.2.1 Inlet orifice

The inlet orifice variation range was chosen to vary from 0.0 mm to 0.22 mm because with the bigger inlet orifices the needle didn't open anymore. The smallest diameter means that, in practice, there is no inlet orifice, and all the flow goes through the outlet and filling orifices. The resulting needle lifts for a full opening can be seen in Figure 40.

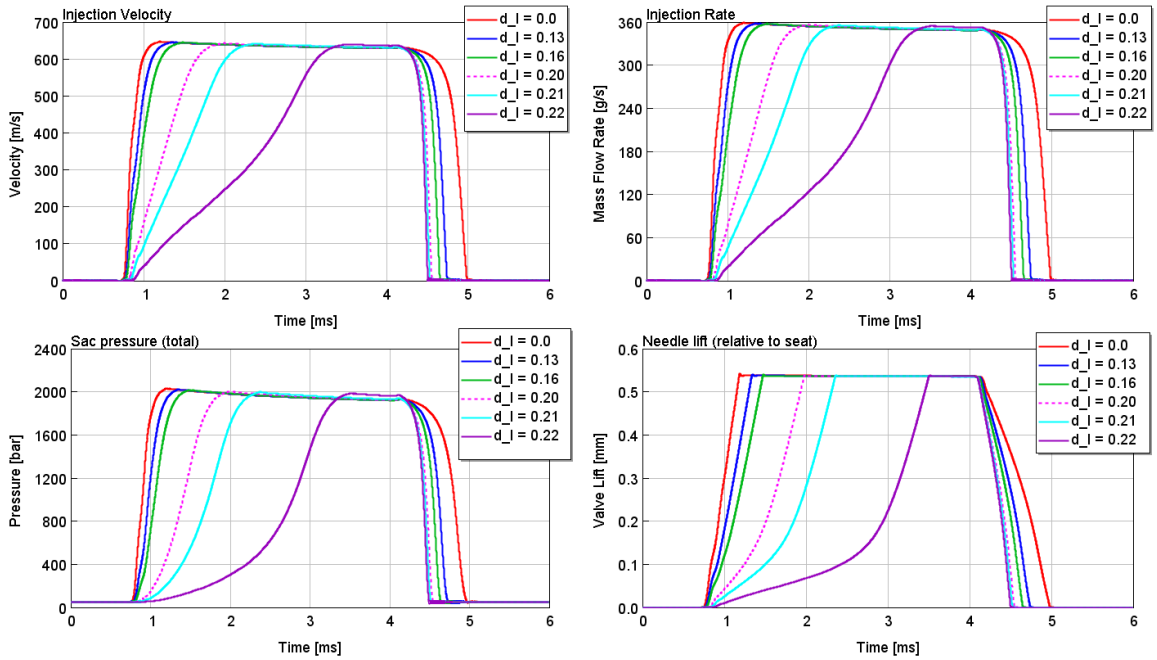

Figure 40. *Injector sensitivity to inlet orifice*

From the figure, we can see that decreasing of the inlet orifice makes the opening faster and closing slower, but the effect on the opening is much bigger than on the closing. The result is as expected, as the smaller inlet orifice results in a higher inlet/outlet orifice ratio which is said to control the needle movement speed [1]. Also, it's notable that, on the closing, the volume flow into the control chamber is the sum of the inlet and outlet orifice flows whereas in the opening it is the difference between the inlet and outlet orifice, and therefore the opening is much more sensitive to small changes in the flow areas than the closing. The corresponding needle lifts for the pilot injection can be seen in Figure 41.

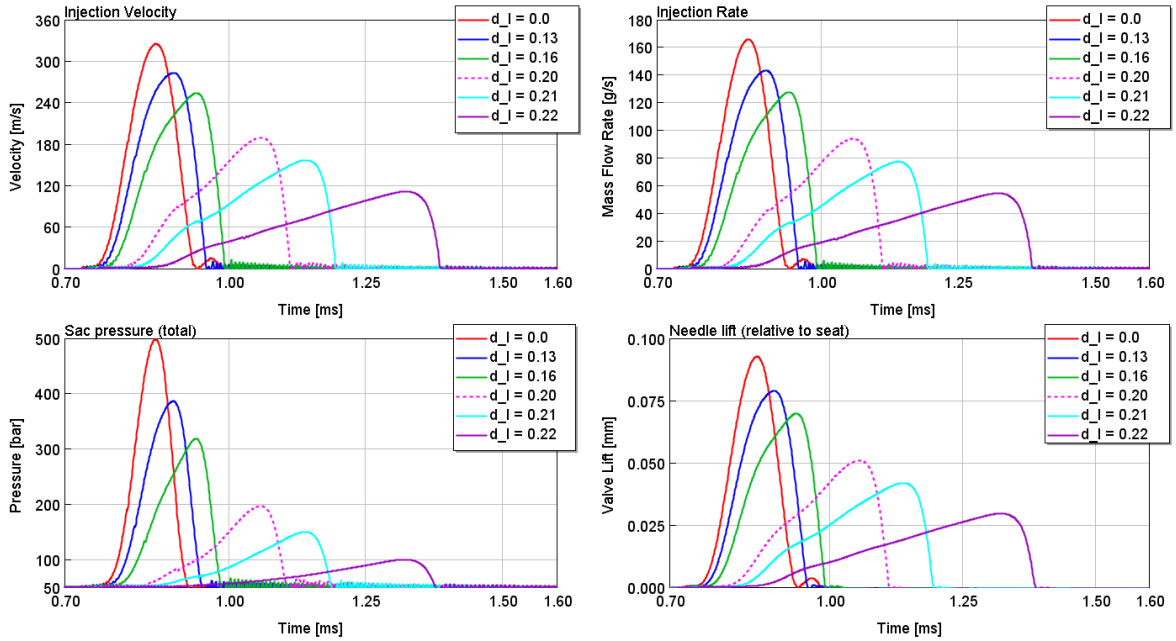

Figure 41. *Pilot injection sensitivity for inlet orifice*

In the pilot injection, there is a considerable variation in the injection events. The faster cases with the smaller inlet orifice values make the injection event very quick and the time of the whole injection very small. The closing speed doesn't seem to differ much.

6.2.2 Outlet orifice

The outlet orifice variation range was chosen to vary from 0.20 mm to 0.30 mm, and the needle lifts can be seen in Figure 42.

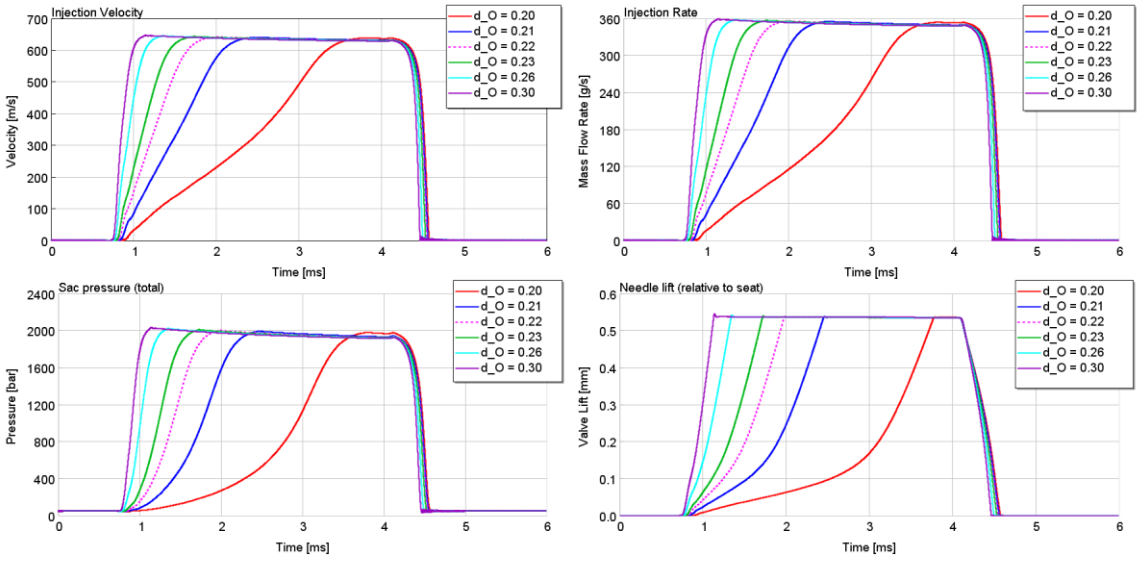

Figure 42. *Full injection sensitivity for outlet orifice*

From the figure, we can see that varying the outlet orifice affects the needle lift in a very similar way as does varying the inlet orifice. Also this behaviour is as expected since the outlet orifice size partly determines the inlet/outlet ratio. The impact to the closing of the needle is almost non-existent because the throttling in the filling orifice is dominant. Also, in this case a faster opening is paired with a minimally faster closing, opposite to what was observed with the inlet orifice sensitivity.

In Figure 43, we can see the pilot injection sensitivity to the outlet orifice.

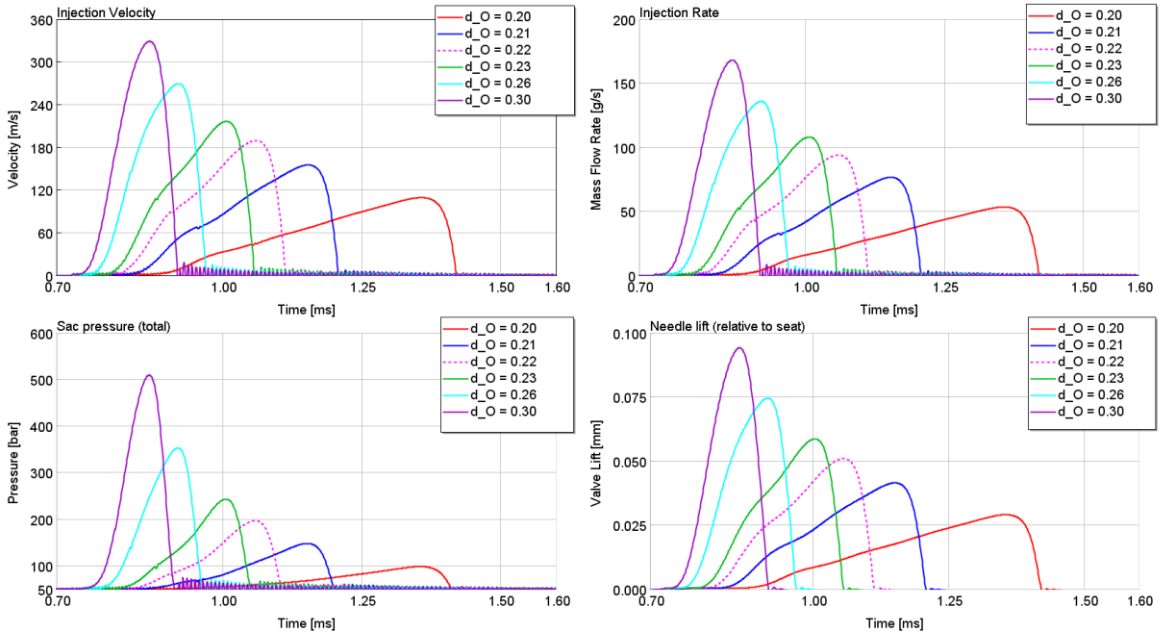

Figure 43. *Pilot injection sensitivity to outlet orifice*

The effect of the outlet orifice to the pilot injection is very similar to the effect of the inlet orifice. A bigger outlet orifice makes the pilot injection very quick and allows the needle to rise higher. In the closing speeds, we can see no considerable differences.

6.2.3 Inlet and outlet orifice

Next, we study the effects of the inlet and outlet orifice together, but we keep their area ratio constant. The ratio between the inlet and outlet are usually chosen to be flow ratios, but as we change the geometrical sizes of orifices, the area ratios are chosen to be observed. The area ratio values of 1.21 and 1.891 are estimated to correspond with the flow ratios of 1.3 and 2.0. Now the outlet orifice range was chosen to vary from 0.11 mm to 0.44 mm and the inlet orifice to range from 0.10 mm to 0.40 mm. The resulting needle lifts can be seen in Figure 44.

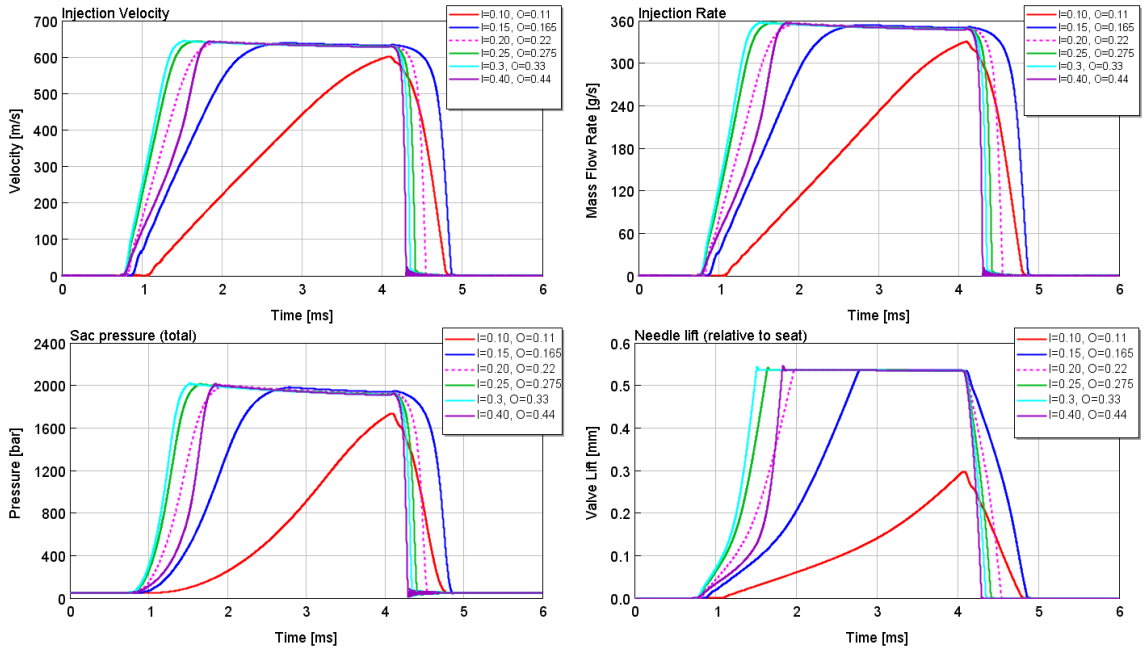

Figure 44. *Full injection sensitivity to inlet and outlet orifice with a constant area ratio of 1.21*

From the figure, we can see that, even though the area ratios of the inlet and outlet orifice remain constant, there are considerable differences between the injection cases. With the smaller orifices, both the opening and closing are slow. Increasing the orifice sizes makes the movement faster until a certain limit is reached, after which the opening rate decreases. This change of opening behaviour we can see in the picture as the purple line that has the biggest values for the orifices. Increasing the orifice size slows down the opening even further until the needle doesn't open at all. The needle movement slowing with bigger orifices is due to the pressure increasing after the outlet orifice, which we can see in Figure 45.

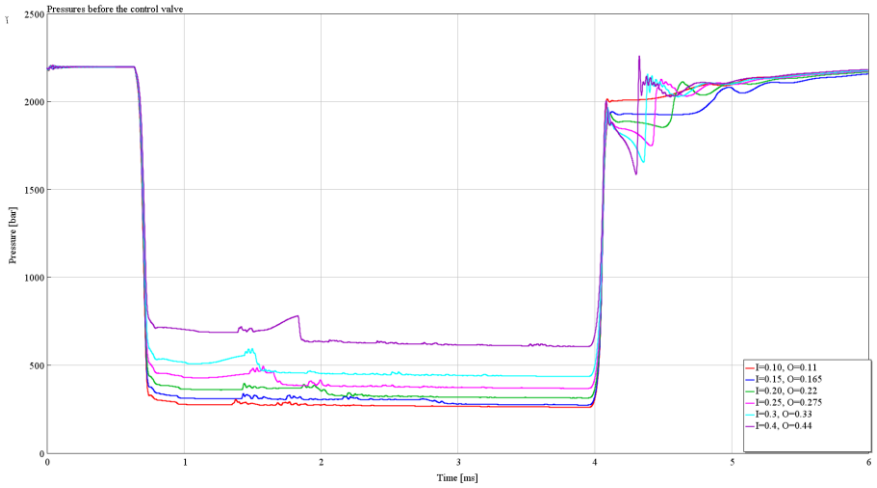

Figure 45. *Pressures after the outlet orifice at full injection and constant area ratio 1.21*

The pressure before the control valve with the biggest orifices has increased to over 600 bars, whereas with the smaller orifices it remains below 500 bars. Also the needle opening causes the pressure to increase as the needle moves. This pressure build-up before the control valve means that the pressure difference over the outlet orifice is smaller, and therefore the fluid flow is less than expected. As the size of the inlet orifice has been increased as well, the fluid flowing in the control chamber increases normally. Now, this causes the actual fluid flow difference in and out of the control chamber to decrease, and therefore the needle movement is slowed down.

In Figure 46, we can see the pilot injection sensitivity at the constant area ratio of 1.21.

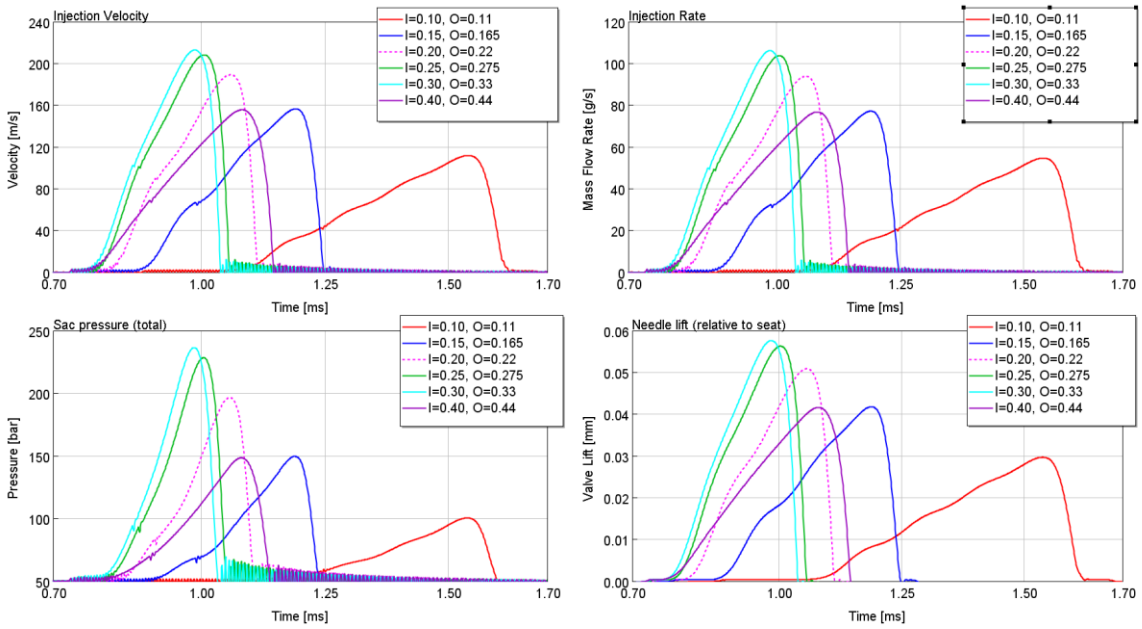

Figure 46. *Pilot injection sensitivity to inlet and outlet orifice size at constant area ratio 1.21*

The pilot injection is affected in the same way as the full injection: bigger orifices result in a faster opening and closing but, with the biggest, one the opening is slow and the closing remains fast.

Figure 47 depicts the full injection sensitivity at a constant area ratio of 1.891 where the values of the inlet orifice vary from 0.05 mm to 0.52 mm and the values of the outlet orifice vary from 0.069 mm to 0.715 mm. The combination of 0.2 mm for inlet orifice and 0.275 mm for outlet orifice is set to have the pink dashed line, though the original values were 0.2 mm inlet and 0.22 mm outlet.

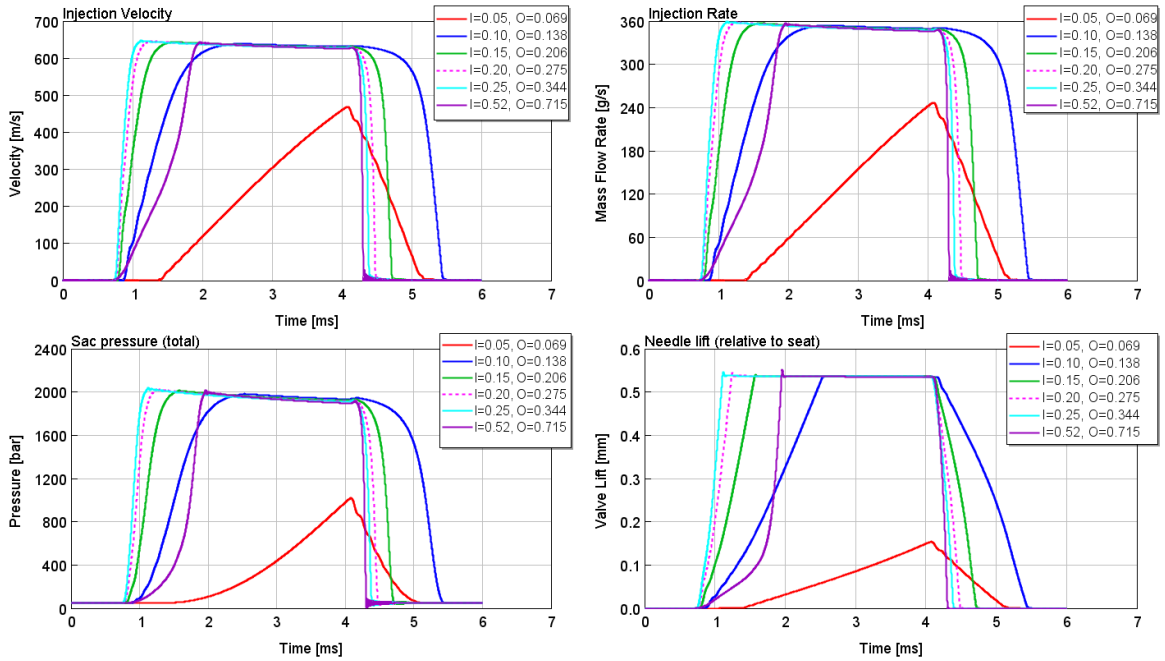

Figure 47. *Full injection sensitivity at a constant area ratio of 1.891*

The injection results are quite similar with a constant area ratio of 1.891 and a constant area ratio of 1.21. First, increasing the orifice sizes makes the injection event faster, but when increased high enough, the opening time decreases due to pressure increasing before the control valve. The difference between the area ratios is that the bigger area ratio is generally faster.

In Figure 48, we can see the pilot injection sensitivity for a constant area ratio of 1.891.

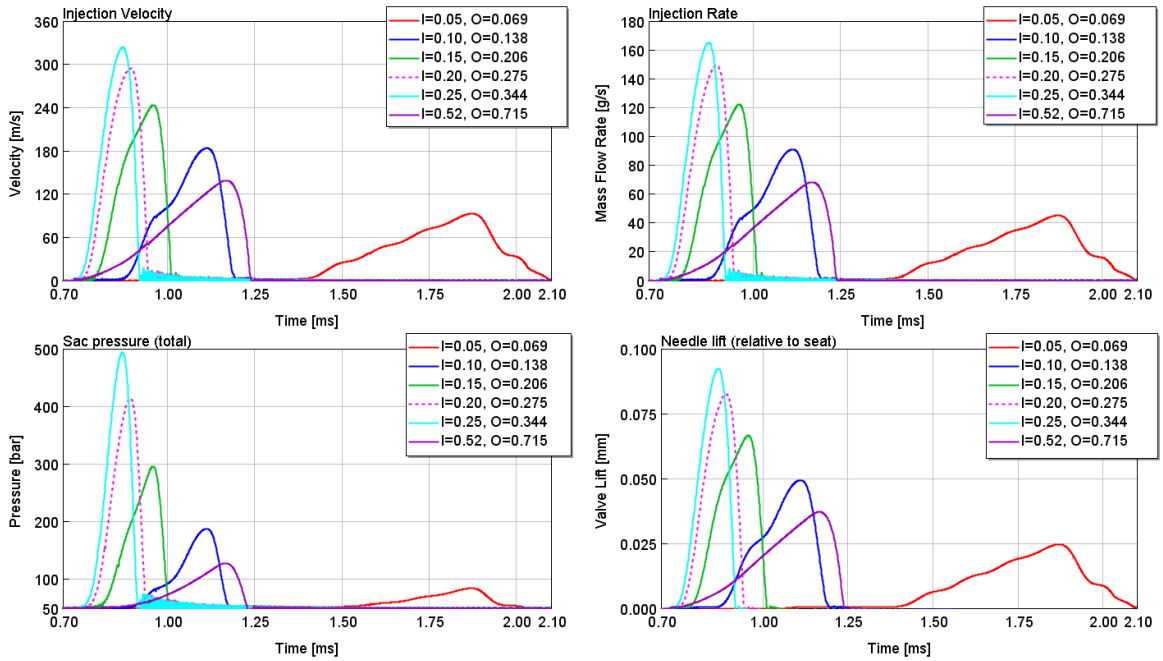

Figure 48. *Pilot injection sensitivity at a constant area ratio of 1.891*

From the figure, we can see that the second highest parameter pair has the fastest injection event, and after it the injection event slows down. Until the biggest parameter pair, the injection events grows faster as the orifice sizes are increased. The speed of the injection event is much higher with an area ratio of 1.891 than with the area ratio of 1.21. Another difference, compared to the constant area ratio of 1.21, is that, with the area ratio of 1.891, the sizes of the orifices can be increased much higher before the slowing of the injection events begins.

6.2.4 Filling orifice

The full injection sensitivity to the filling orifice can be seen in Figure 49. The values for the filling orifice have been chosen to range from 0.0 mm to 0.24 mm.

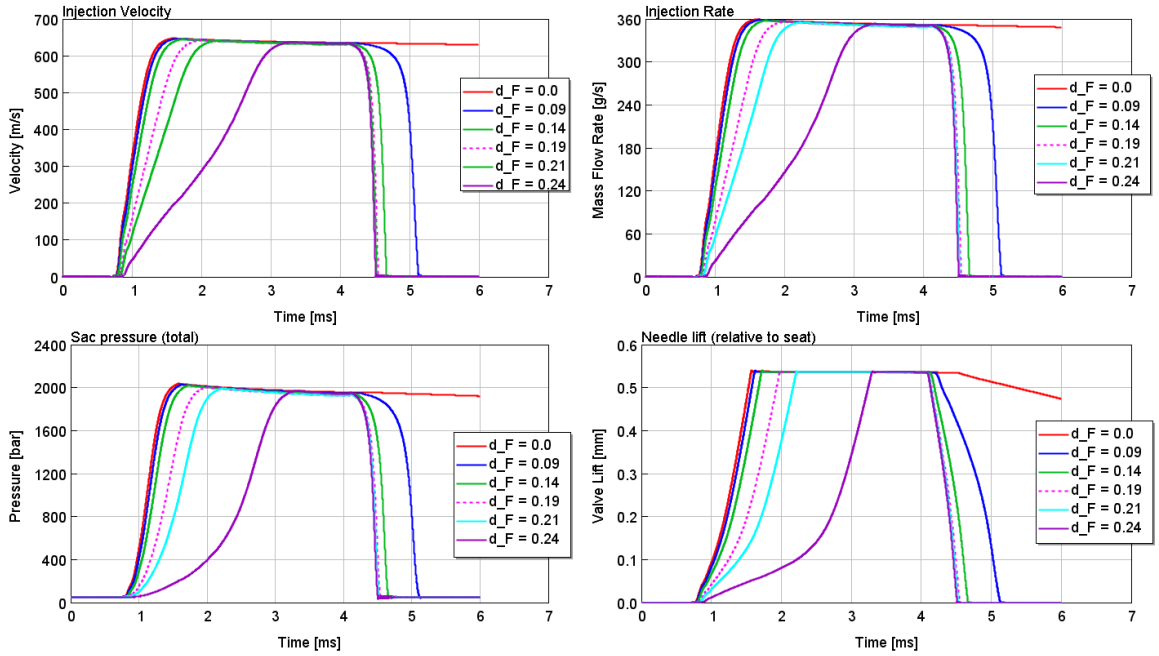

Figure 49. *Full injection sensitivity to filling orifice*

The filling orifice seems to affect both the opening and closing of the injector significantly. Having a bigger filling orifice results in a slower opening and a faster closing. With the value of zero, there is practically no filling orifice and the injector closes very slowly. With the value of 0.24 mm, the injector barely opens but closes very fast.

In Figure 50, we can see the pilot injection sensitivity to the filling orifice.

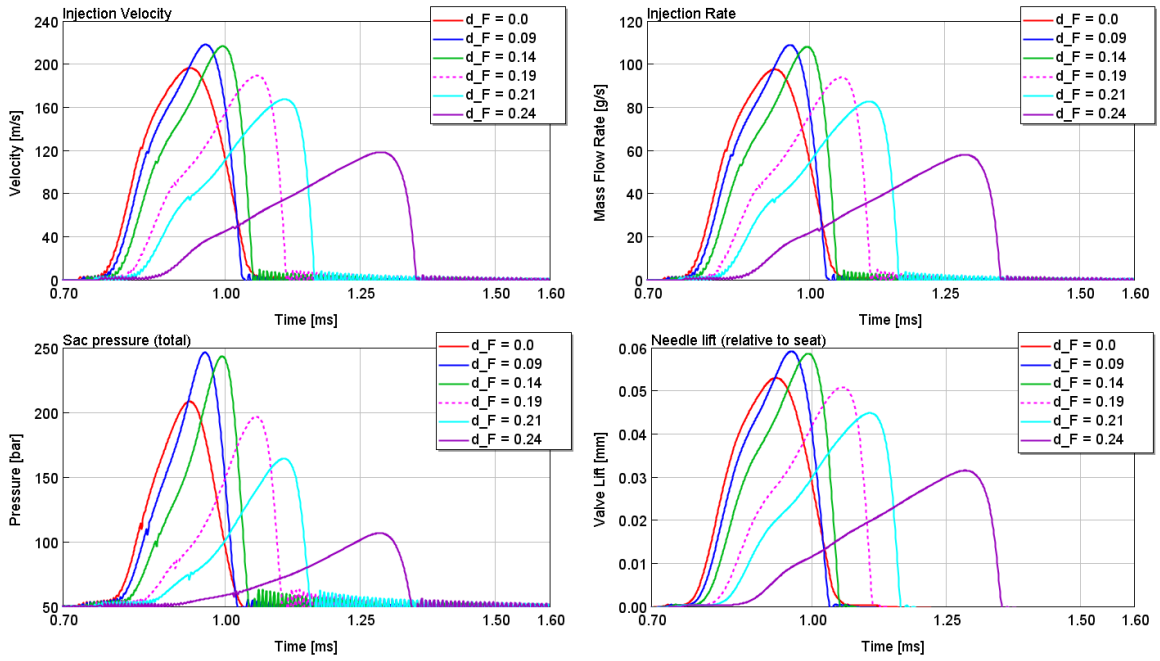

Figure 50. *Pilot injection sensitivity to filling orifice*

From the figure, we can see that, just like in the full injection event, the size of the filling orifice affects both the closing and the opening. The fastest events occur with the values of 0.09 mm and 0.14 mm, and away from these regions, the injection speed decreases. With this in mind, we can infer that, for the fast pilot injection event, both the opening and closing need to be fast.

6.2.5 Inlet, outlet and filling orifice

Finally, all the orifices were varied simultaneously, while keeping their area ratios constant. So, the inlet-outlet area ratio is the same 1.21 as previously, and the area ratio of the filling and outlet is 1.34. The inlet orifice was chosen to vary from 0.13 mm to 0.25 mm, the outlet from 0.14 mm to 0.28 mm and the filling from 0.12 mm to 0.24 mm. The results for the full injection sensitivity to the parameters in question are presented in Figure 51.

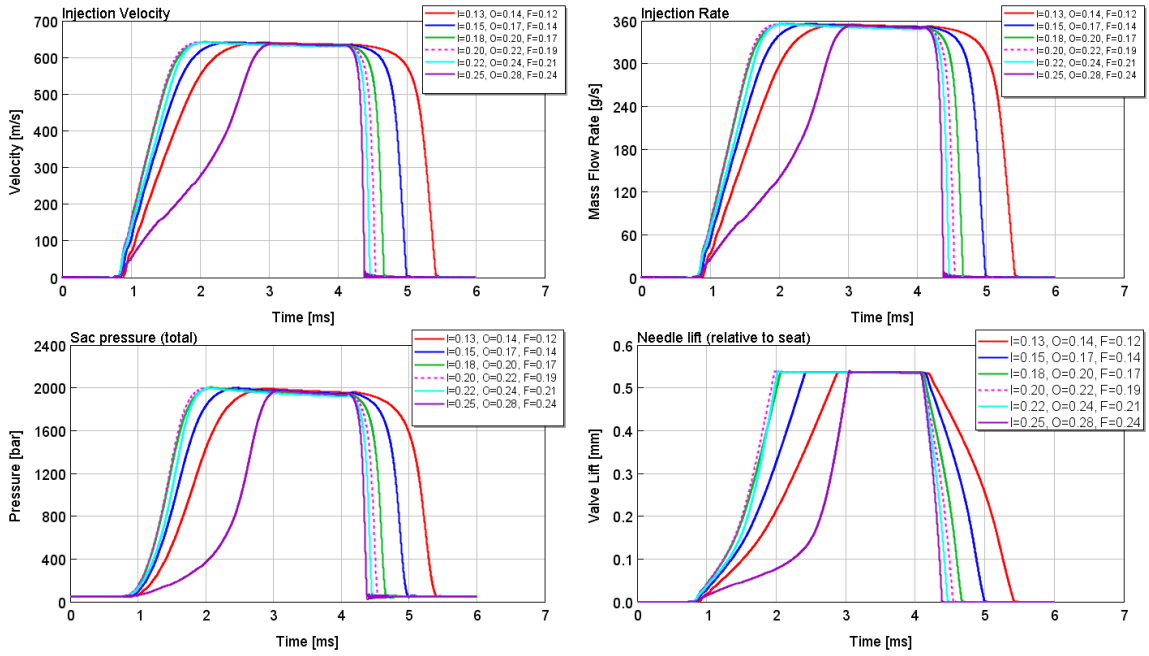

Figure 51. *Full injection sensitivity to inlet, outlet and filling orifices while keeping their area ratios constant*

The results are quite similar to the results with the constant area ratio for only the inlet and outlet orifices. With the increasing orifice sizes, the closing gets faster and so does the opening until high enough values are met and the opening slows down. This slowing is the same effect as seen previously, causing the pressure before the control valve to increase.

In Figure 52, pilot injection sensitivity for the inlet, outlet and filling orifices with a constant area ratio can be seen.

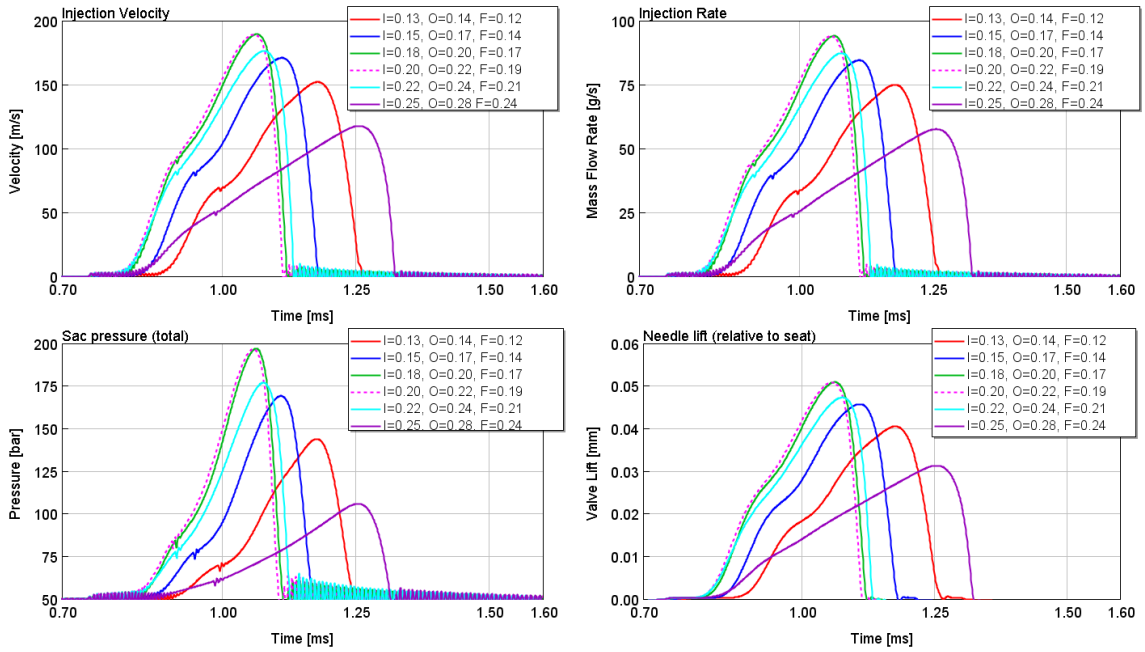

Figure 52. *Pilot injection sensitivity to inlet, outlet and filling orifices while keeping their area ratios constant*

The original values of the orifices seem to be resulting in the fastest injection event. Moving away from these values leads to the injector movement slowing down. Therefore, it would seem that, for the area ratios used, the original sizes of the orifices would seem to be the most optimal ones.

From the results, we interpret that the inlet and outlet orifice sizes are effective for controlling the needle opening but quite ineffective for controlling the needle closing. The filling orifice seems to be the best instrument to control the closing of the needle, though it also affects the opening of the needle. All in all, it should be kept in mind that the inlet-outlet orifice ratio is very important and that the inlet orifice should be smaller than the outlet orifice. The filling orifice can be even slightly bigger than the outlet orifice but not much.

The sensitivity study of the control chamber volume size can be seen in the appendix.

6.3 Needle

The varied parameters regarding the needle were: the spring rate and pretension; the pressure step, meaning the control chamber area; the needle gallery area and the area of the tip of the needle; the needle weight, and the angles of the poppet and seat at the tip of the needle.

6.3.1 Spring

The values of the spring rate have been chosen to range from 0 to 2000 N/m's, and the spring pretension is kept constant at 90 Newton. The value of 2000 N/m was chosen to magnify the impact of the spring. We can see the injector sensitivity to the spring rate in Figure 53.

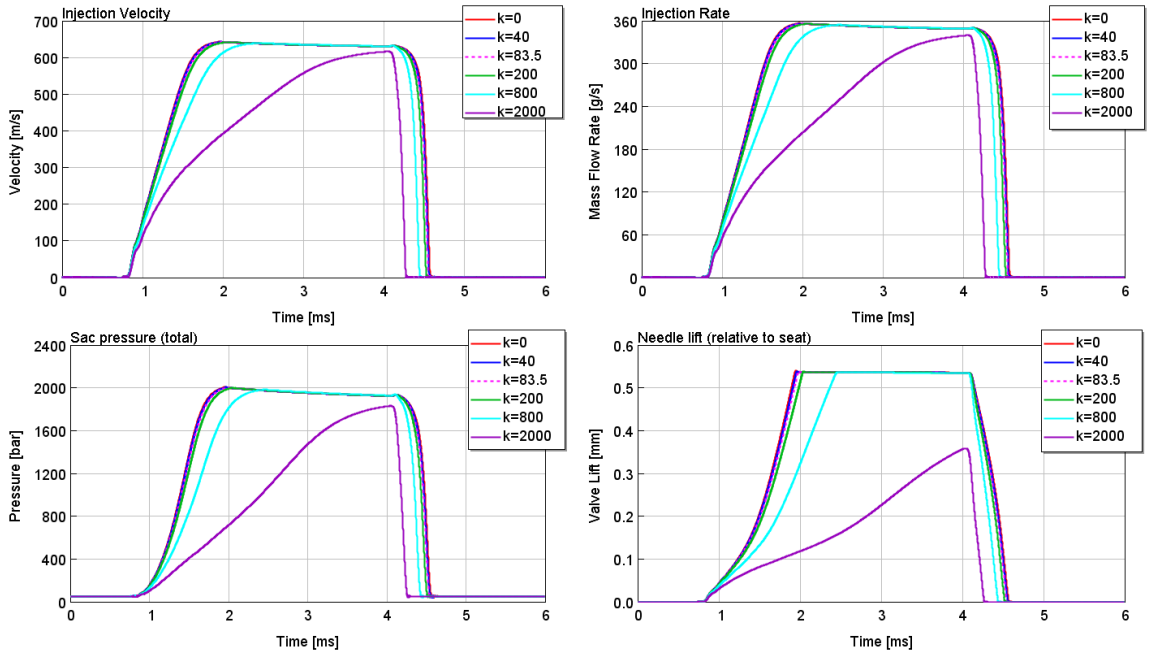

Figure 53. *Full injection sensitivity to spring rate*

From the figure, we can see that, with a higher spring rate, the injector opening speed decreases and the closing speed increases. The start time of the needle lift is not altered even with the highest spring rate. With the spring rate values below 200 N/m's, the effect of the spring rate is very small.

The pilot injection sensitivity to the spring rate can be seen in Figure 54.

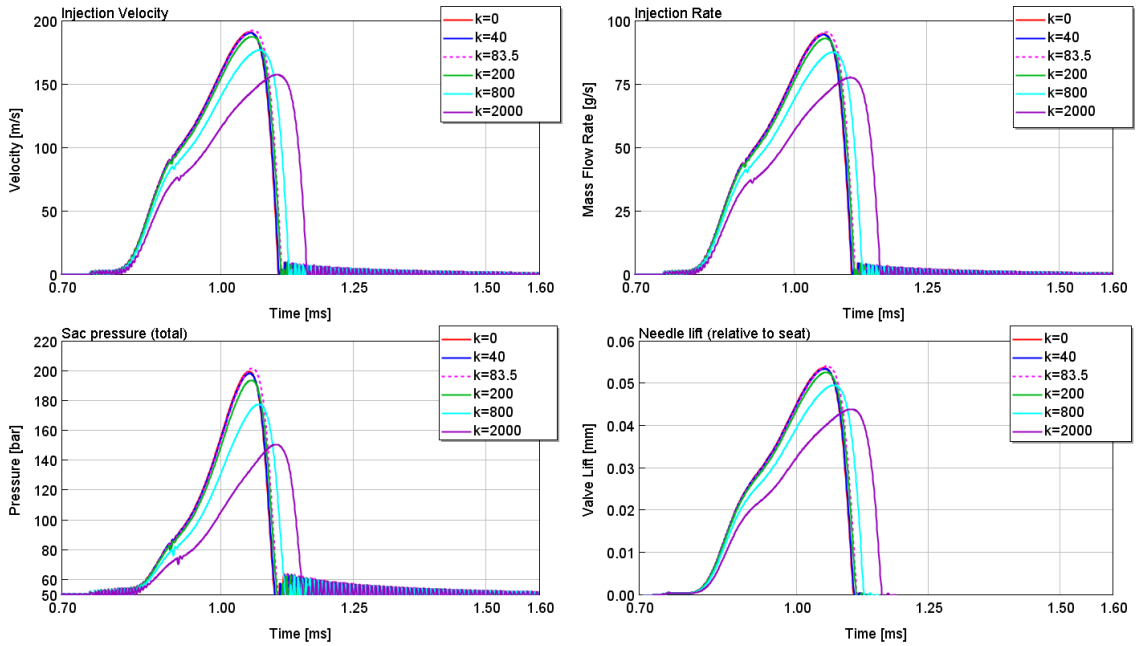

Figure 54. *Pilot injection sensitivity to spring rate*

The pilot injection doesn't seem to be very sensitive to small variations in the spring rate. With the highest spring rates, the movement of the needle seems to become slightly slower, but with smaller rates, there doesn't seem to be hardly any difference.

Injector sensitivity to spring pretension can be seen in Figure 55. The spring pretension values were chosen to range from 0 N's to 300 N's, and the spring rate was kept constant during the spring pretension sensitivity study.

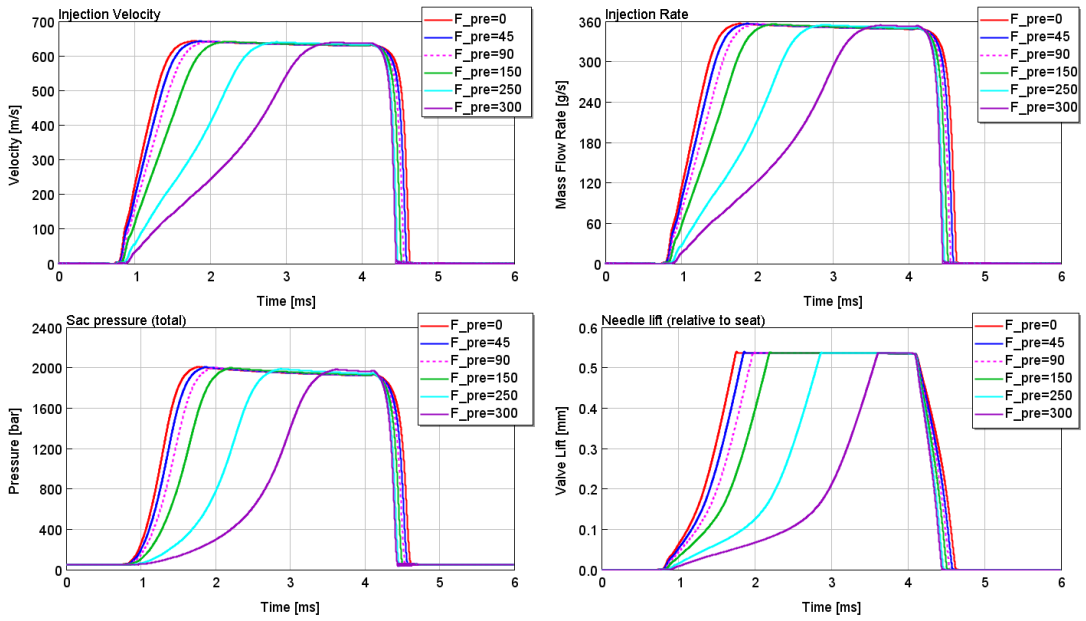

Figure 55. *Full injection sensitivity to spring pretension*

From the figure, we can see that increasing the pretension makes the opening significantly slower and the closing slightly faster. This behaviour is due to the control chamber pressure needing to decrease lower in order to cause movement, and therefore the pressure difference over the inlet orifice grows whereas the pressure difference over the outlet orifice drops. Also, the start of the needle lift is delayed with higher spring pretension values due to the same reason.

In Figure 56, we can see the pilot injection sensitivity to the spring pretension.

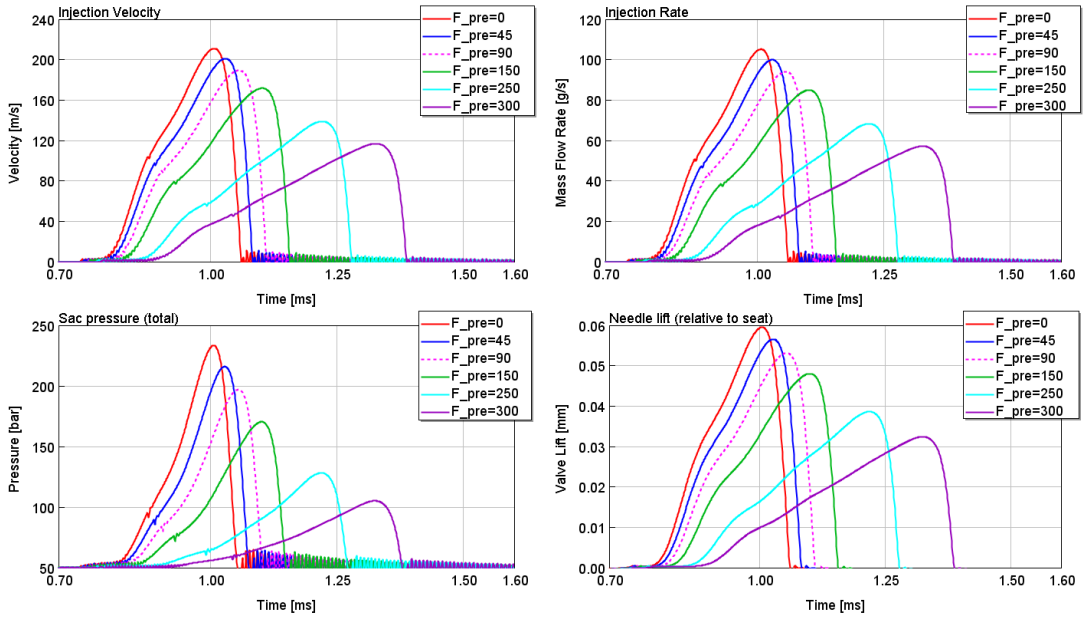

Figure 56. *Pilot injection sensitivity to spring pretension*

The spring pretension seems to considerably affect the pilot injection event as well. With higher spring pretension values, the start of the injection is delayed and the resulting injection event is slower. With lower spring pretension values, the injection event begins earlier and occurs faster. With this certain injector studied, there seems to be more room to make the pilot injection event slower than faster.

6.3.2 Pressure step

The force equations regarding the pressure step are described in chapter 3.2 and Pressure Step Ratio (PSR) is derived there as well (needle lower gallery area divided by the control chamber area). When studying the effects of the pressure step, we need to remember that changing one area affects the size of another area as well. The relationships of these areas are described by the following equation 41, which is the result of the needle being covered by fluid on all sides.

$$A_{sac} + A_g = A_{cc} \tag{34}$$

in which

A_{sac} Area on the needle tip [m^2]

A_g Needle lower gallery area [m^2]

A_{cc} Control chamber area [m^2]

Now, first in this sensitivity study, we vary the values of the needle gallery area and the control chamber area, while the sac hole area is kept constant. The varied parameters and their ratio can be seen in Table 5. The sac area A_{sac} was kept constant during the following analysis.

Table 5. *Variable pressure step values with a constant needle sac area*

Gallery area	6	6.48	7	8.04	14	21
Control chamber area	10.524	11	11.524	12.564	18.524	25.524
PSR	0.578	0.59	0.61	0.64	0.76	0.82

In Figure 57, we can see the full injection sensitivity to a variable pressure step.

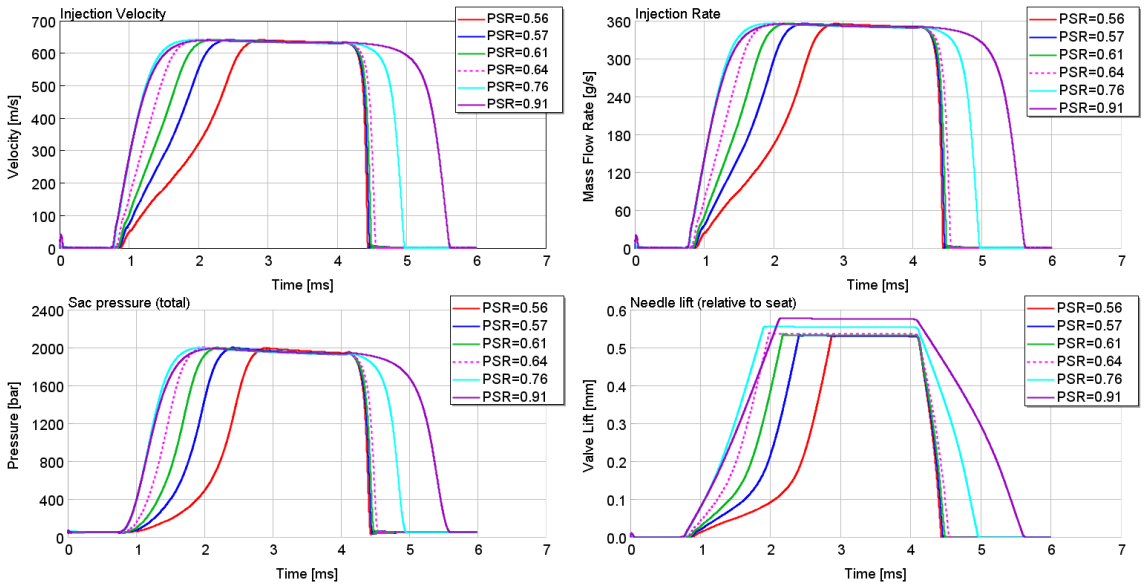

Figure 57. *Full injection sensitivity to variable pressure step*

From the figure, we can see that a big PSR results in a fast opening and a slow closing and, correspondingly a small PSR results in a slow opening and fast closing. Another effect can be seen in the shape of the needle lifts: with a small PSR the kink (curve slope change, i.e. the abrupt bend of the curve) of the curve is big, but with higher PSR's the kink of the curve is non-existent. This kink is the result of the pressure building up in the sac and pushing the needle upwards, and with high pressure step ratios, the part of the generated opening force resulting from the sac area is relatively smaller.

In Figure 58, we can see the pilot injection sensitivity to the variable pressure step.

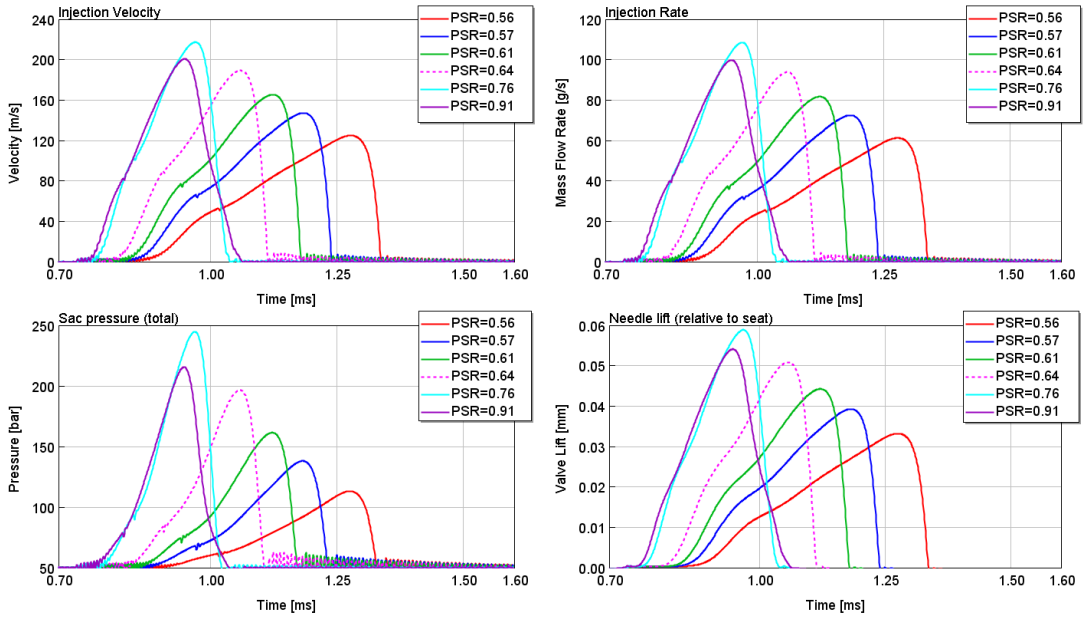

Figure 58. *Pilot injection sensitivity to variable pressure step*

The variable pressure step seems to have similar effects on the pilot injection event as in the full injection event. The fastest pilot injection event seems to be with the pressure step ratio of 0.76 which is slightly bigger than the original pressure step value. With the highest pressure step ratio, the injection event is slower due to its slow closing time, whereas with the smaller pressure step ratios, the injection event is slow due to slow opening. In Figure 59, we can see the full injection sensitivity to a constant pressure step ratio with all of the related areas increased, and its values can be seen in Table 6.

Table 6. *Constant pressure step values, PSR = 0.64*

Gallery area [mm^2]	4.67	5.46	8.04	10.58	15.69
CC area [mm^2]	7.3	8.52	12.57	16.52	24.52
Sac area [mm^2]	2.63	3.07	4.524	5.95	8.83

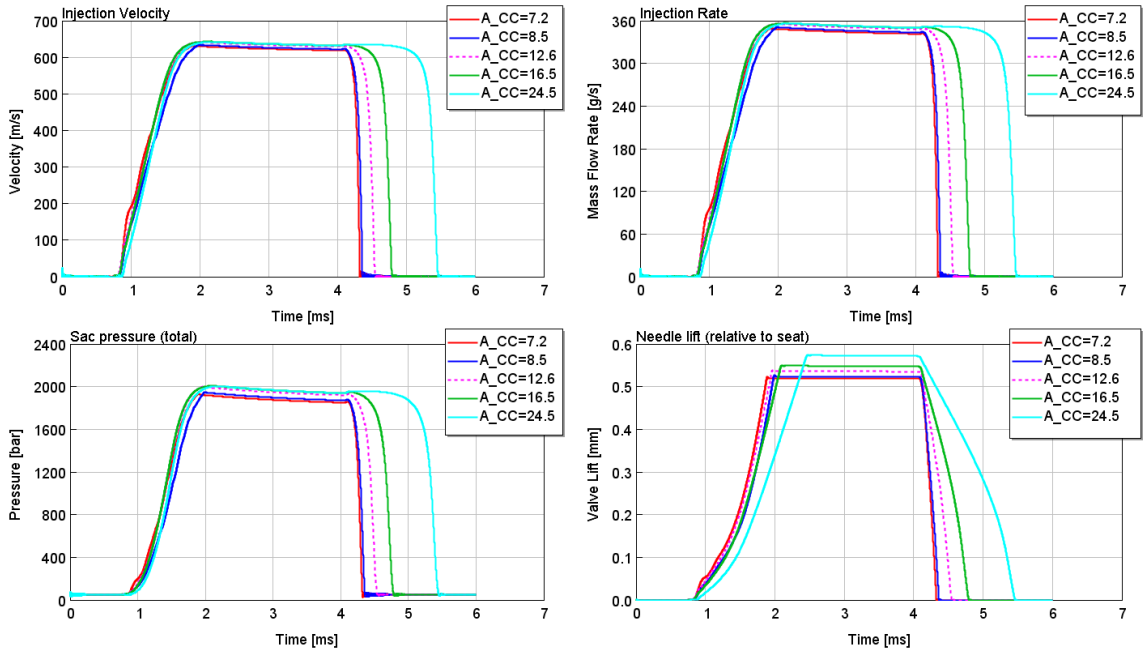

Figure 59. *Full injection sensitivity to a constant pressure step*

The magnitude of the needle areas does not seem to have a lot of effect on the opening of the needle, except that, with the biggest area, the opening is slightly slower. This behaviour is due to the pressure in the control chamber volume changing more rapidly due to higher control chamber area displacing more volume. With the other PSR values, the effect is not so clearly visible. On the closing part, big areas seem to result in a slow closing and small areas with a fast closing. This behaviour is correspondingly due to the pressure in the control chamber increasing slower with the higher control chamber area displacing more volume.

In Figure 60, we can see the pilot injection sensitivity to the constant pressure step ratio.

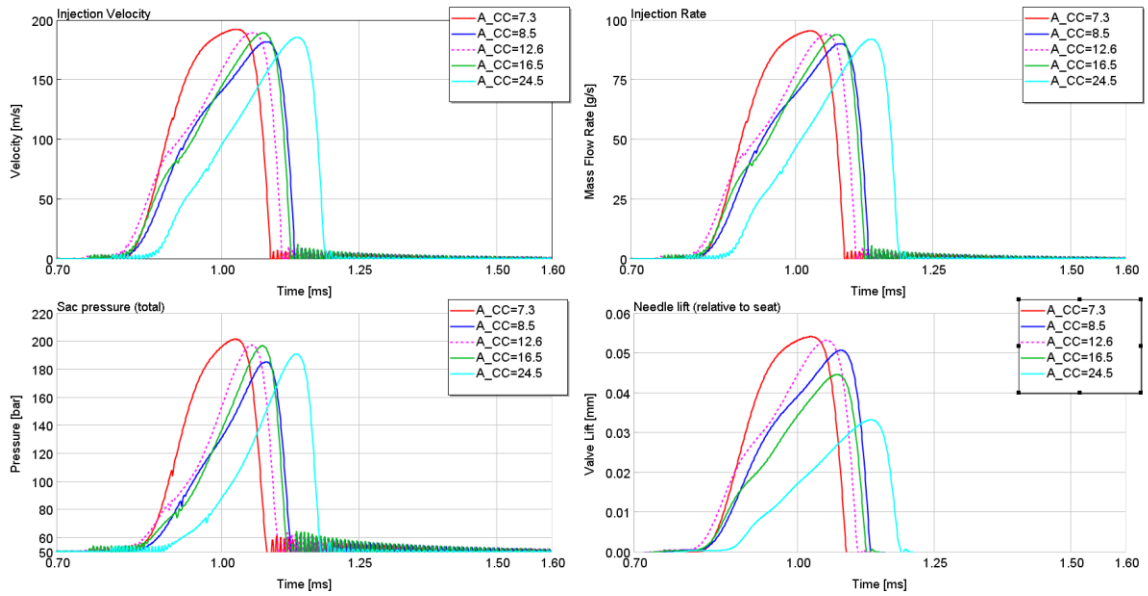

Figure 60. *Pilot injection sensitivity to a constant pressure step*

The injection velocities, flow rates and sac pressures do not considerably differ with different sizes of needle areas, but oddly, the needle lift is quite much smaller with the highest areas. In order to understand this effect, we need to know that when the area of the needle tip increases, so does the effective flow area of the needle tip. Hence, a small needle lift can result in a big opening which, in turn, results in a big sac pressure. The geometry settings for the needle tip are later introduced in Figure 63 and the calculation of the needle tip flow area in Figure 64.

6.3.3 Weight

We can see the injector sensitivity to the needle weight in Figure 61.

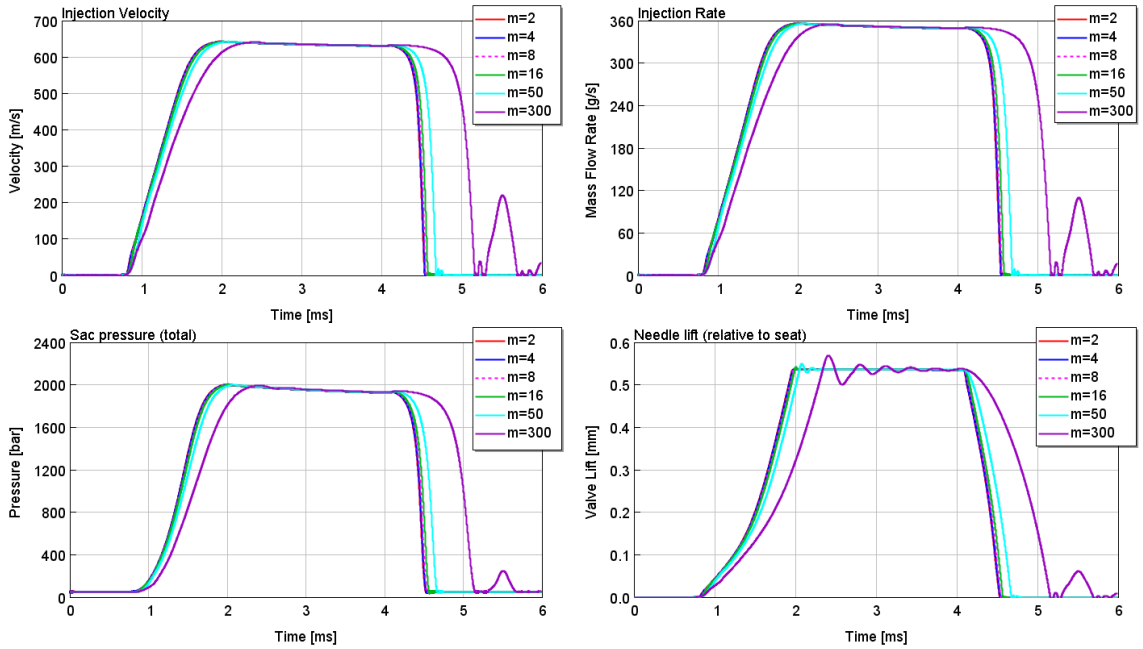

Figure 61. *Full injection sensitivity for the needle weight*

The needle weight was tested from 2 grams to 300 grams, which are actually unrealistic values at the extremums. The main outcome was that the injector is not sensitive to the needle mass even though bouncing started to appear with the 300 gram needle. Figure 62 presents the pilot injection sensitivity to the needle mass.

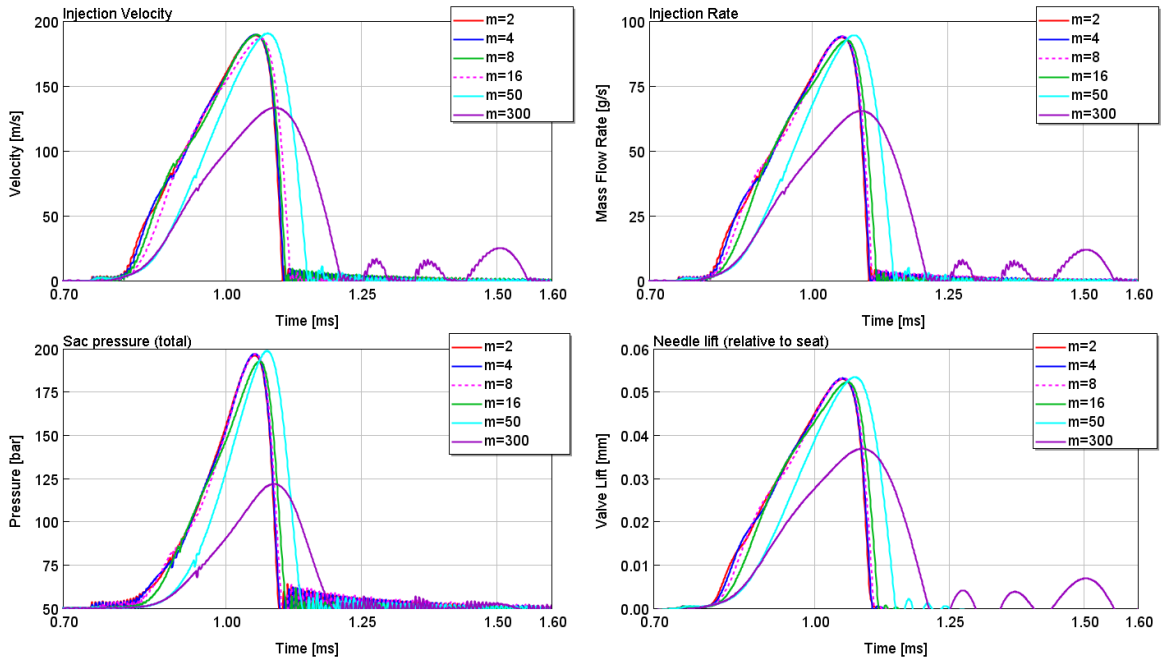

Figure 62. *Pilot injection sensitivity to needle weight*

There was no effect with realistic values even with the pilot injection events. Only the 300 gram needle results in a slower injection event with bouncing.

6.3.4 Tip geometry

In GT-Suite, the properties of the needle tip shape are the input into the *ConicalPoppetConSeat* –template, which is shown in Figure 63. In the figure, we can see an image depicting all the input parameters. Notable is that there is no rod in any of the simulations.

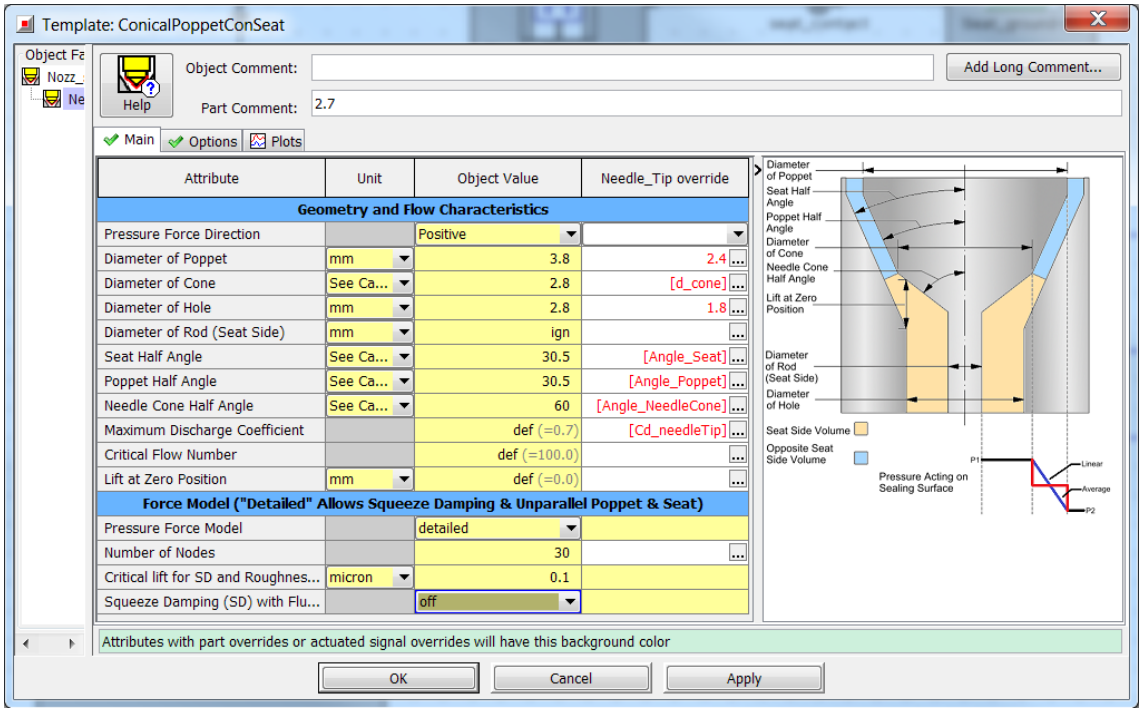

Figure 63. *GT-template ConicalPoppetConSeat*

The varied parameters in the sensitivity analysis for the needle tip shape are the diameter of the poppet and the angles of the seat and poppet (which are varied at the same time). The diameter of the cone is not tested because a CFD analysis would be needed to calculate its effects.

Next, the influence of the poppet and seat angle were scrutinized. In this study, the effective flow area changes also with the different angles, and it leads to differences in the injected quantities. Figure 64 shows the geometry of the needle tip, with which the flow area of the needle opening can be calculated.

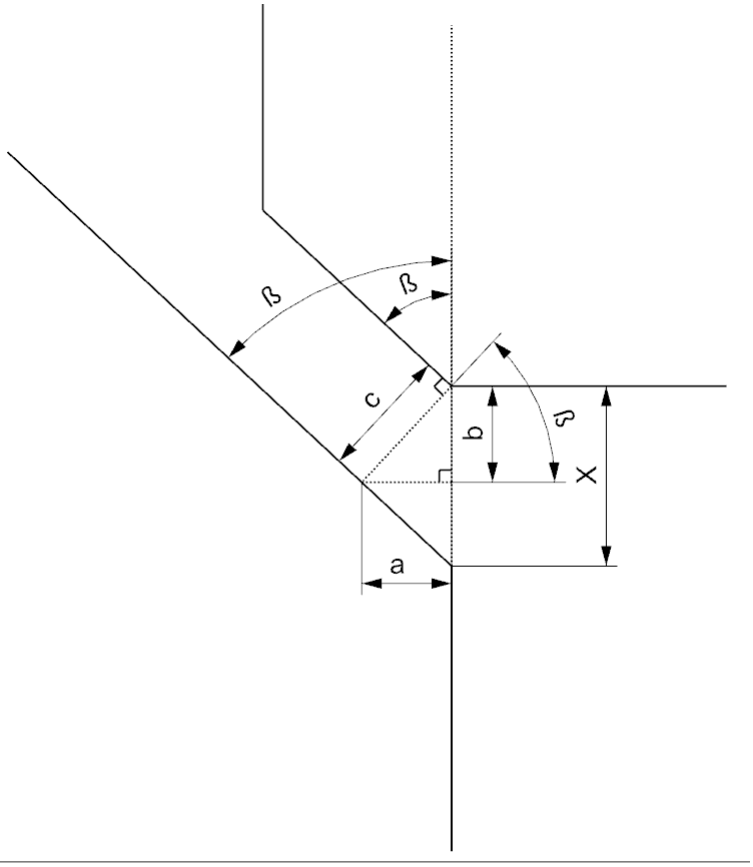

Figure 64. *Needle tip geometry*

When the needle opens, a flow area with the shape of a frustum of a cone emerges. Dimensions a, b and c are calculated by

$$a = \cos\beta \cdot c \tag{35}$$

$$b = \sin\beta \cdot c \tag{36}$$

$$c = \sin\beta \cdot x \tag{37}$$

where

x Needle lift [m]

Now, the in the first two equations, c is substituted

$$a = \cos\beta \cdot \sin\beta \cdot x \tag{38}$$

$$b = \sin\beta \cdot \sin\beta \cdot x \tag{39}$$

The flow area A_{eff} of the needle opening is approximately calculated by

$$A_{eff} = \left(r_{upper} + r_{lower}\right) \cdot \pi \cdot x \tag{40}$$

in which

r_{upper}	Radius of the cone of the needle tip [m]
r_{lower}	Radius of the circle at the needle seat which is at 90 degree angle to the cone diameter [m]
x	Needle lift [m]

The radius of the needle cone tip is known, and the radius of the circle at the needle seat at 90 degree angle to the cone diameter, is the cone radius plus the dimension *a* in the graph. The height of this frustum of a cone is the dimension *b* in the graph.

$$A_{eff} = \left(\frac{d_{cone}}{2} + \frac{d_{cone}}{2} + a\right) \cdot \pi \cdot b \tag{41}$$

Now the values of a and b are inserted into the flow area equation

$$A_{eff} = (d_{cone} + \cos\beta \cdot \sin\beta \cdot x) \cdot \pi \cdot \sin\beta \cdot \sin\beta \cdot x \tag{42}$$

And this equation defines the flow area of the needle as a function of the needle lift and the angle of the seat and poppet.

The needle seat and poppet angles were chosen to vary between 10 and 80 degrees, which means that with 80 degrees the needle tip is almost flat and with 10 degrees it is almost vertical. The angles of the seat is always set to be the same as the angle of the needle poppet, and in the previous figure they were marked as β. In Figure 65, we can see full injection sensitivity for needle seat and poppet angle.

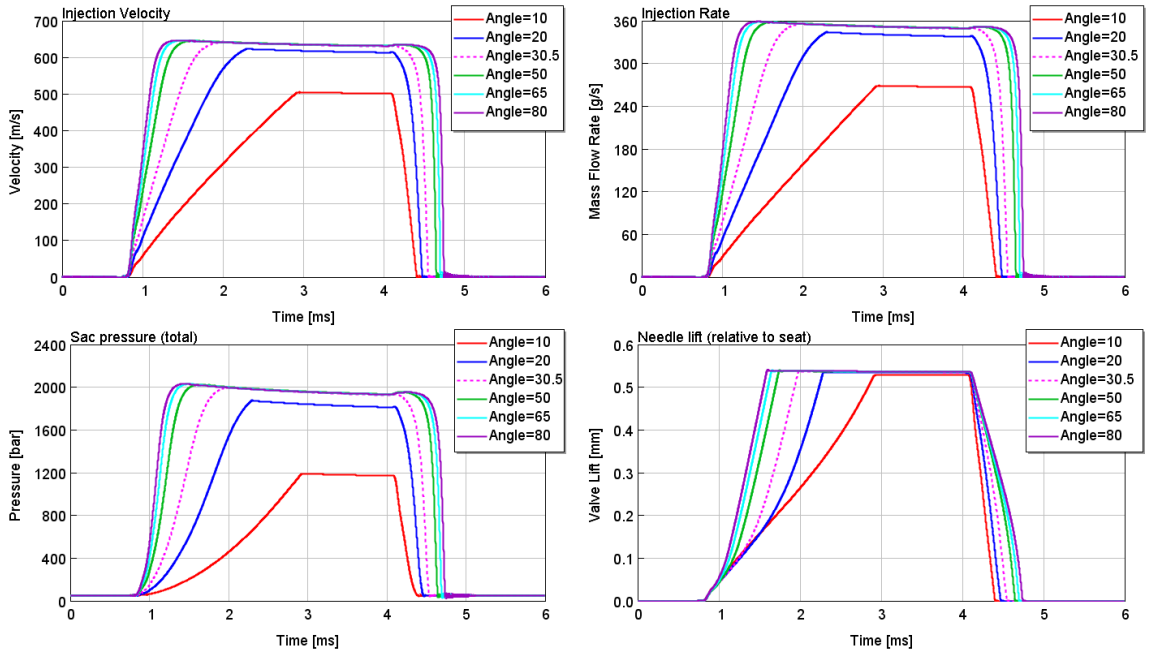

Figure 65. *Full injection sensitivity for needle seat and poppet angle*

From the figure, we can see that a smaller half angle makes the opening slower and the closing faster. This is due to flow area being smaller with the smaller angles, so the rate of flow area during the opening is also smaller, which leads to a slower movement. The results are not entirely true because with different angles the discharge coefficient must be changing also in such a manner that, with bigger flow direction differentiations, the discharge coefficient drops more. This would mean that the smaller angles have a big discharge coefficient and bigger angles have a lower discharge coefficient. Also, the flow forces are somewhat influenced by this, meaning that their impact on the needle lift changes as well. In Figure 66, we can see the effect of the needle seat and poppet angle on the pilot injection sensitivity.

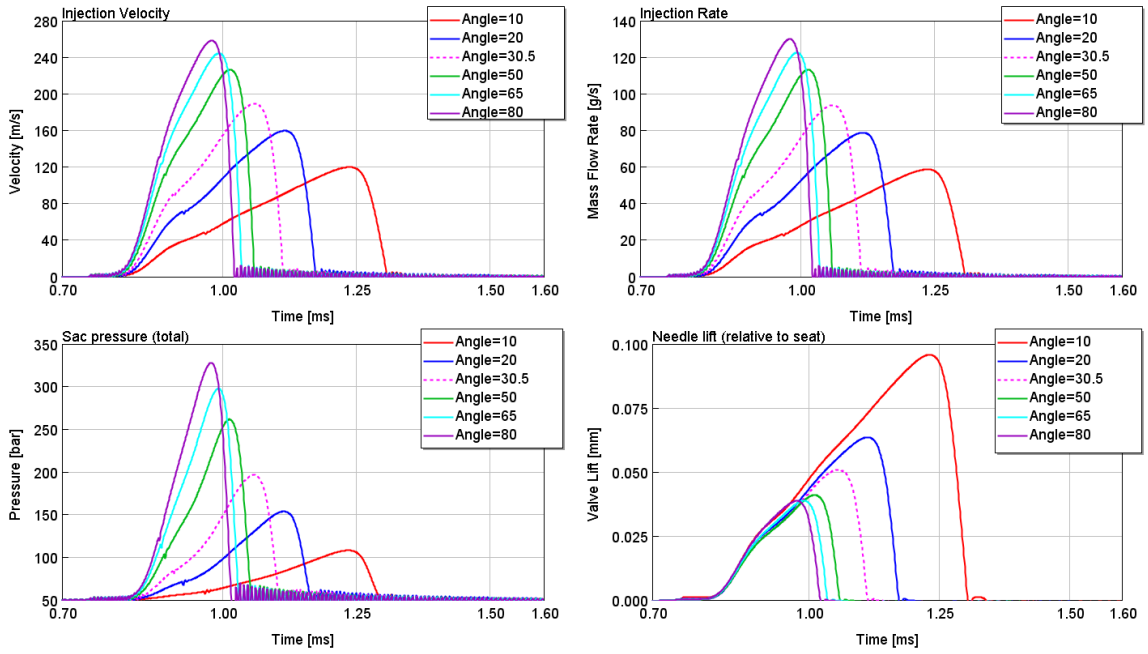

Figure 66. *Pilot injection sensitivity for the needle seat and poppet angle*

We can see that, with the smaller angles, the needle lift needs to rise higher to inject the required amount, whereas with the bigger angles a smaller needle lift is enough. Looking at the injection velocities, we notice that the highest values appear with the highest angles. The result might be somewhat different in reality because the discharge coefficient would be different with different angles. Nevertheless, the results presented here imply that the needle seat and poppet angle has a significant effect on the pilot injection event.

Given these points, the seat and poppet angle seem to be one of the most effective parameters in shaping the pilot injection event though difficult to predict accurately. The pressure step and the spring pretension have a medium effect on the injection event, whereas the needle weight and the spring rate do not have a considerable effect.

6.4 Nozzle sac

The varied parameters regarding the nozzle sac were the sac hole volume, the number of the holes and their diameter, rounding and thickness. Rounding of the holes means how sharp the holes are at the inlet edge, and the thickness of the holes means how deep the orifice is.

6.4.1 Volume

The sac hole volume was chosen to vary from 0.5 mm^3 to 100 mm^3, and the results for the sac hole volume sensitivity can be seen in Figure 67.

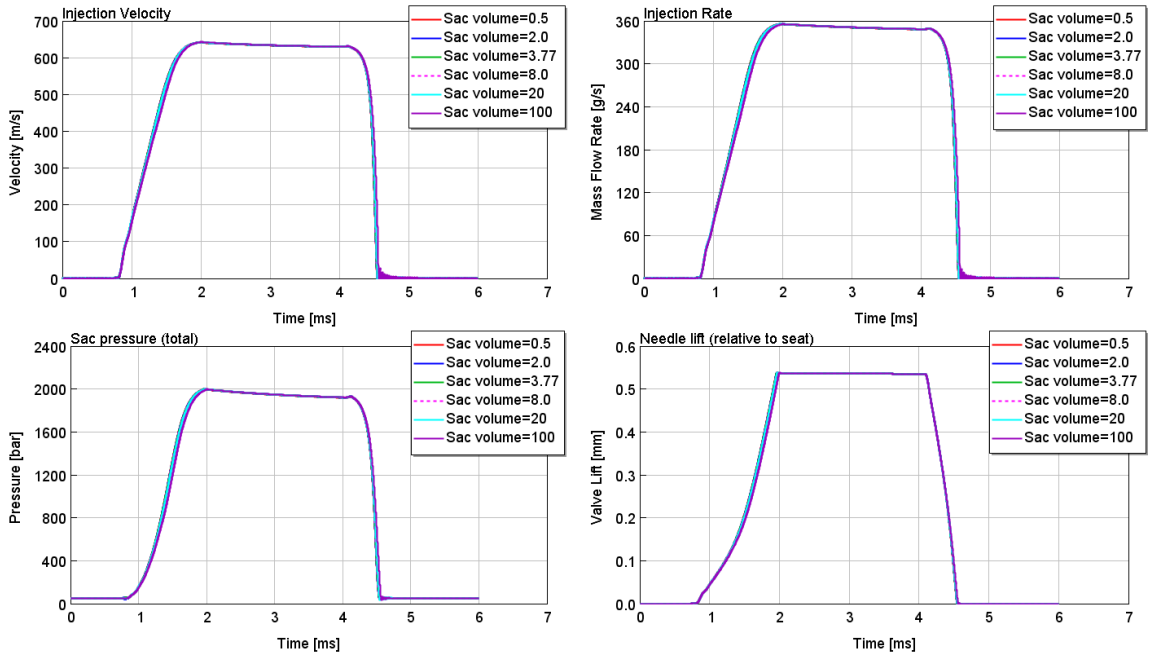

Figure 67. *Full injection sensitivity for sac hole volume*

From the figure, we can see that the sac hole volume size affects the injection process minimally. As the fluid used in the injection is highly incompressible, the result is logical. However, the simulation model used does not have the geometry of the sac hole and therefore cannot properly calculate the effect, because no 3-D fluid flow has been calculated. Nevertheless, looking at the results provided with 1 –D simulations, it would look like the sac hole size is quite insignificant. Figure 68 depicts the same sac hole volume sensitivity for the pilot injection.

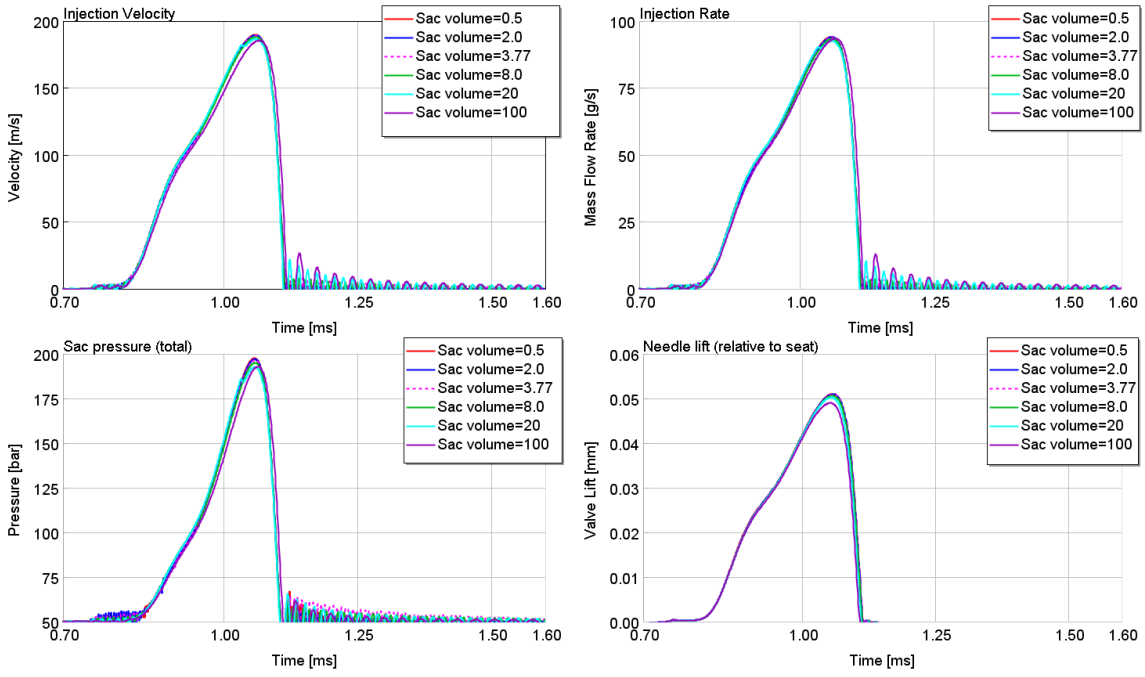

Figure 68. *Pilot injection sensitivity for sac hole volume*

Either in the pilot injection there doesn't seem to be almost any differences with sac volume. The results seem logical in a sense that the fluid used in the simulations is not very compressible, and that the sac volume is a small volume. The results regarding sac hole volume size are further discussed in chapter 8.1, criticism.

6.4.2 Number of holes

In Figure 69, we can see the full injection sensitivity to the number of holes in the sac.

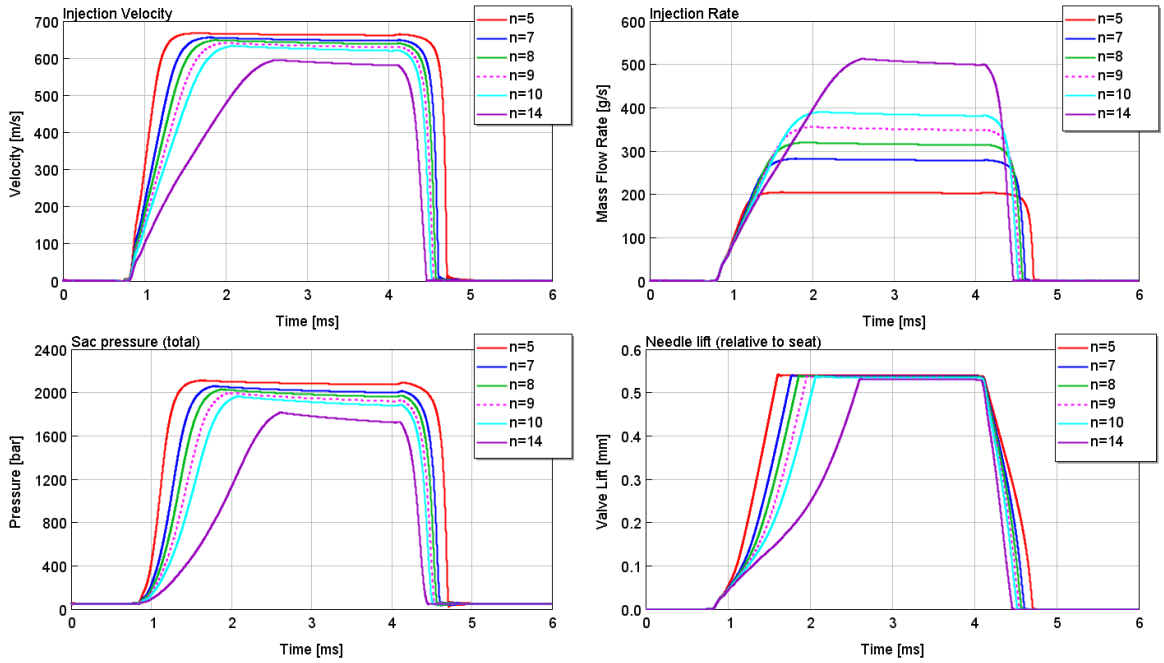

Figure 69. *Full injection sensitivity to number of holes in the sac*

With a higher number of holes the opening is clearly slower than with fewer holes, but then again the closing is faster with more holes. This difference in movement is due to differences in the sac pressure, depending on the flow area of the nozzle holes. Thus, with a small number of orifices, the pressure builds up quickly and shoots the needle up, whereas with a higher number of holes the pressure builds up more slowly and pushes less on the needle. Injection rates are naturally bigger with more holes since there is a bigger flow area. Injection velocities, on the other hand, are higher with the smaller amount of holes, and that is the result of having a bigger pressure difference over the nozzle holes, so there is more flow flowing through a single hole.

Pilot injection sensitivity to the number of holes can be seen in Figure 70.

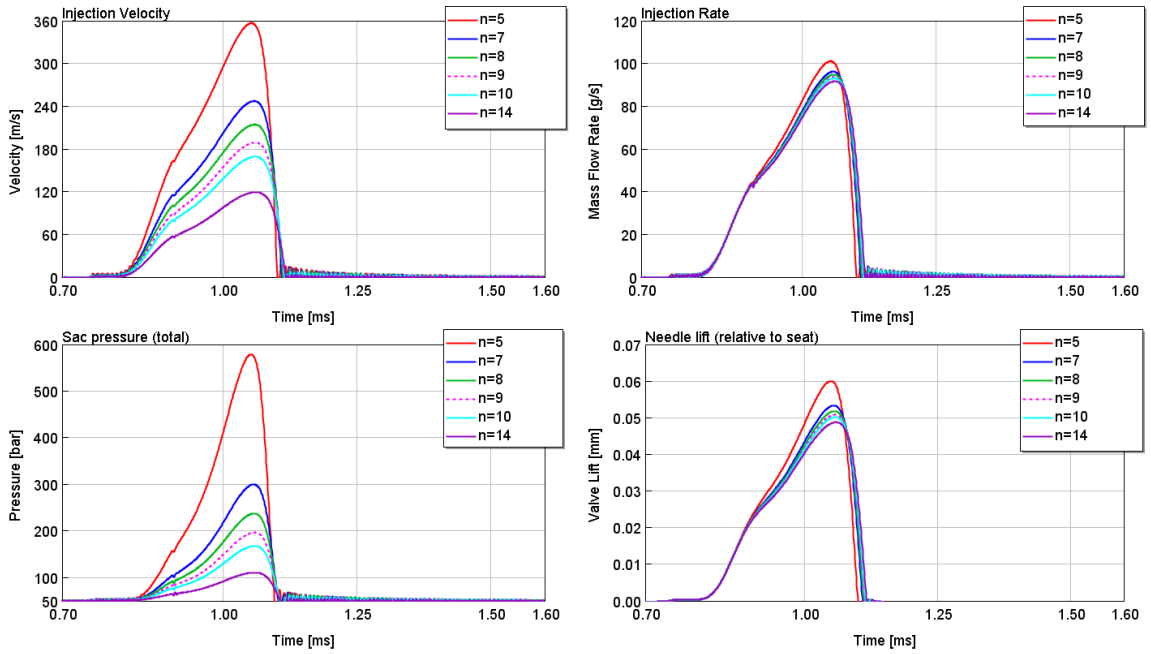

Figure 70. *Pilot injection sensitivity to number of holes*

For the needle lifts, there doesn't seem to be much difference, except that with the smallest number of holes the lift goes slightly higher. The injection rate values follow the needle lift values, but with sac pressure and injection velocity, there are major differences. Similarly to the sensitivity in the full injection event, there is a higher pressure with fewer holes and a lower pressure with more holes, corresponding to differences in the flow areas. Also notable is that the injection rate depends on both the flow area and the pressure difference, whereas the injection velocity depends on the pressure difference but not on the flow area. This relation can be observed in the equations 50 and 51 which have been derived from the equation 17, which was previously introduced in chapter 2.3.2.

$$\dot{m} = C_d A \sqrt{2\Delta p \rho} \tag{43}$$

$$v = C_d \sqrt{\frac{2\Delta p}{\rho}} \tag{44}$$

6.4.3 Hole diameter

The size of the nozzle holes was chosen to vary from 0.23 mm to 0.39 mm, and these results can be seen in Figure 71.

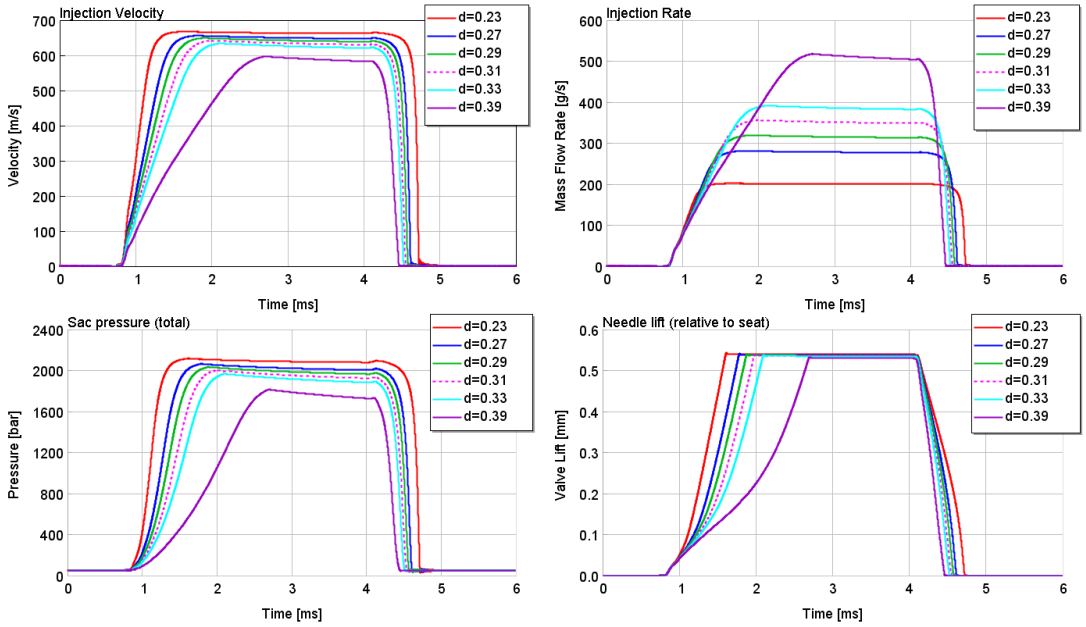

Figure 71. *Full injection sensitivity to nozzle hole diameter*

We can see that the size of the nozzle holes affects exactly the same way as the number of holes, and with the flow area kept the same as with the number of holes, the results in needle opening, injector flow rate and flow velocity are identical. Pilot injection sensitivity to the nozzle hole diameter can be seen in Figure 72.

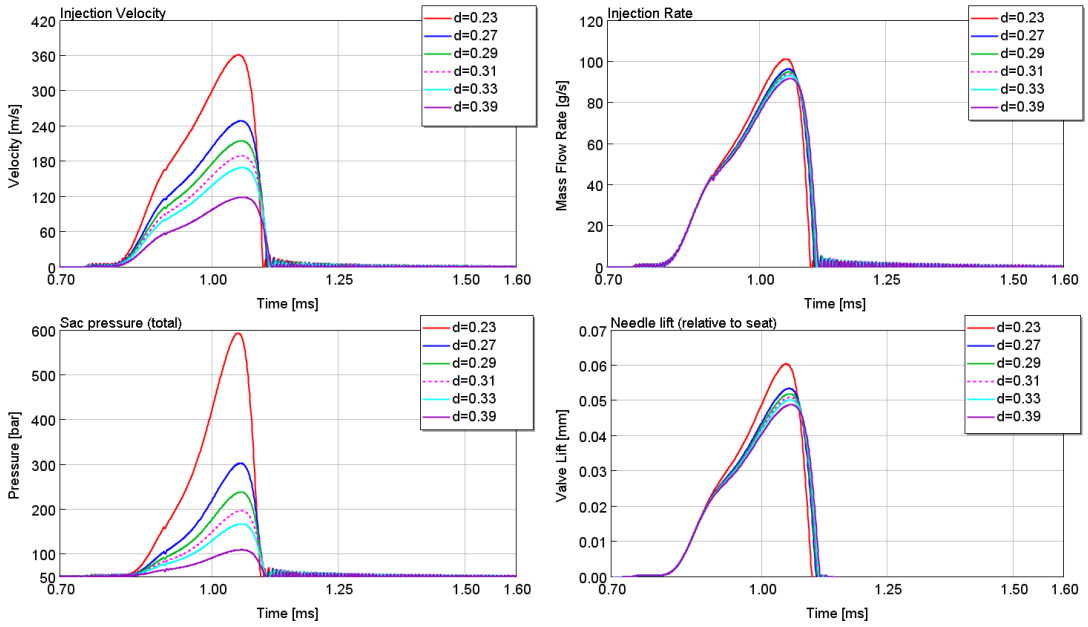

Figure 72. *Pilot injection sensitivity to nozzle hole diameter*

Comparing pilot injection sensitivities of the nozzle hole diameter and the number of holes, we notice that they seem to be identical. Therefore, we can make the deduction that it is the total flow area of the nozzle holes that is critical in the injection event. However, we must once again notice that there have been no CFD calculations for the sac hole flow,

and therefore the cavitation effects are only inaccurately modelled, which has an effect on the injection sensitivity of the nozzle holes.

From the sensitivity analyses of nozzle hole diameter and the number of holes, we can deduct that there is a trade-off between the full injection mass flow rate and the pilot injection flow velocity. As the other increases, the other one decreases, and a good compromise between the pilot injection velocity and the full injection mass flow rate should be sought.

Differences between the nozzle hole diameter and the number of holes can be seen in Figure 73 where Sauter Mean Diameters are depicted for both the number of holes and the orifice diameter.

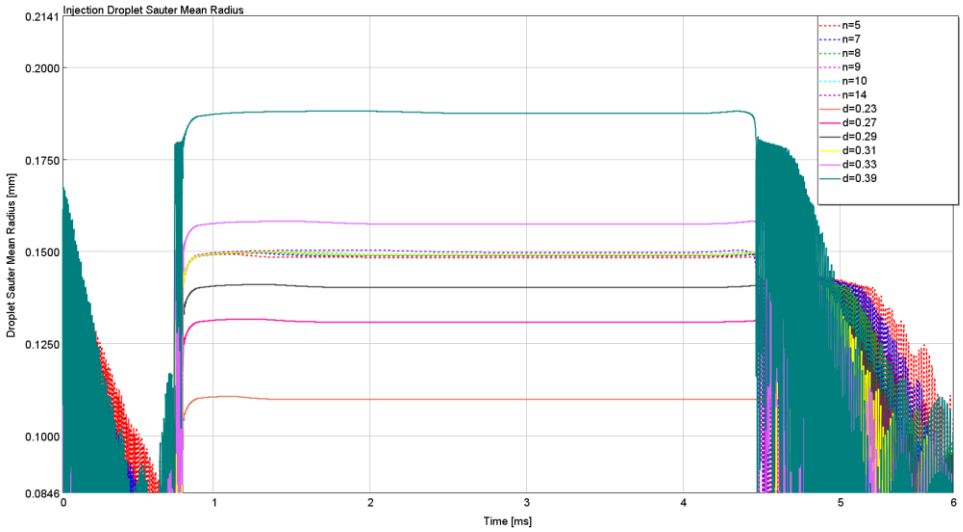

Figure 73. *Sauter Mean Diameter sensitivity during a full injection event*

By varying the number of holes, the Sauter Mean Diameter remained almost at the same level, but with different diameters, the SMD changed significantly. This result is good to keep in mind when we want to alter the SMD and some other outputs at the same time.

6.4.4 Hole rounding

The roundings of the nozzle holes were chosen to vary from 0.0 mm to 10 mm. The outer limits of the ranges are far from reality, but they were chosen to highlight the effects of the roundings. In Figure 75, we can see the full injection sensitivity to the rounding.

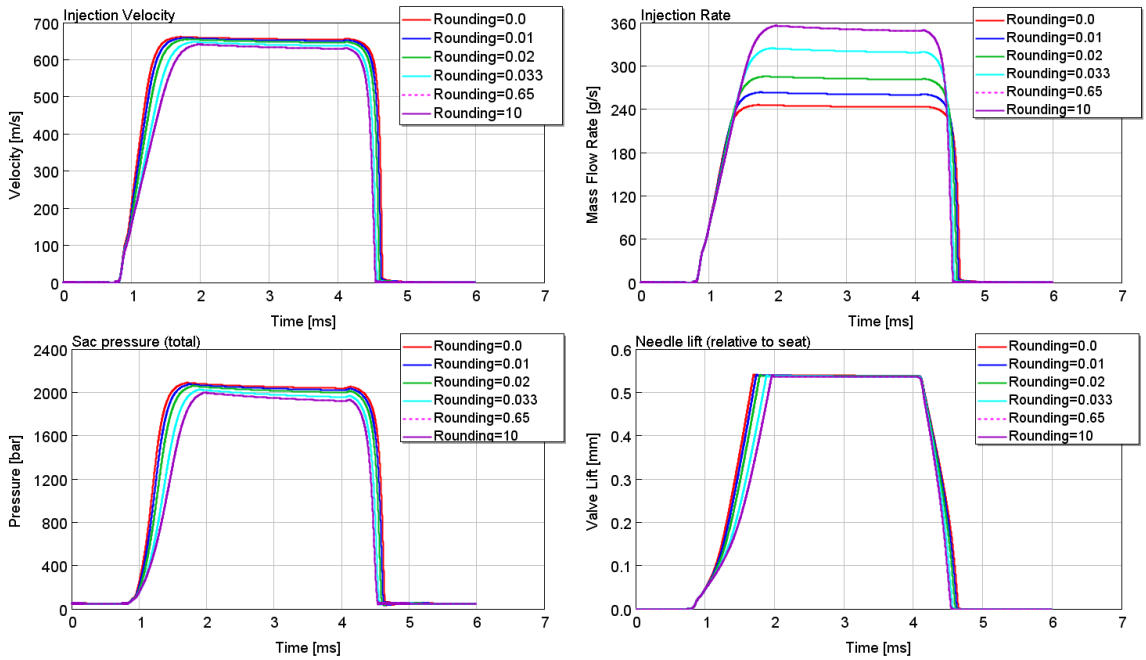

Figure 74. *Full injection sensitivity for rounding of the nozzle holes'*

In the figures, the curve of the original value of 0.65 mm is under the violet curve with the value of 10 mm. The rounding has a minimal effect on the needle lift, sac pressure and the injection velocity, but a high effect on the injection rate. Small values of the rounding make the injector opening faster and the closing slower whereas big values for the rounding make the opening slower and the closing faster. The maximum value of the injection rate increases along the increasing rounding, and it is due to different choking points of the cavitating flow. With the small rounding the flow cavitates earlier, and as the cavitation increases, the effective flow area decreases, leading into the choking of the nozzle hole flow.

In Figure 75, we can see the pilot injection sensitivity to the rounding of the holes.

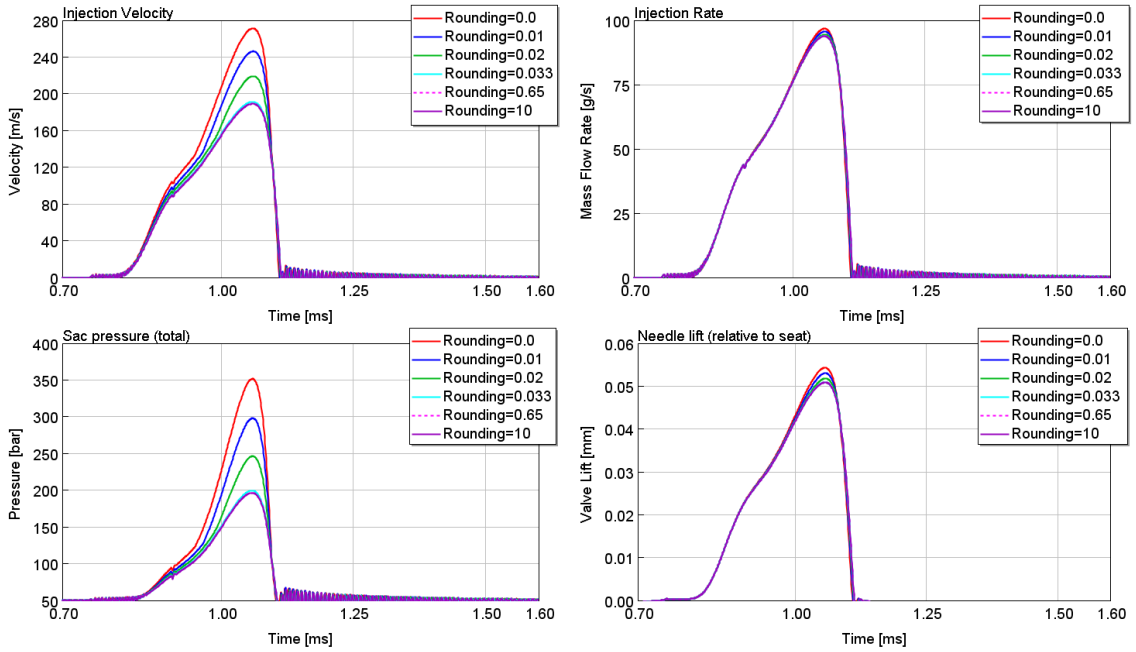

Figure 75. *Pilot injection sensitivity to rounding of the nozzle holes*

The effects of the rounding on pilot injection sensitivity seem to be quite similar to the effects of the different number of holes and hole size. There are no differences if the value of rounding is 0.033 or above, but with the values of 0, 0.01 and 0.02 there are some differences in the injection velocity and sac pressure. The point at which a single sac pressure curve starts to differentiate from the other pressure curves is the point at which the flow enters the super cavitating flow condition. This means that the three simulations with the smallest rounding develop a fully cavitating flow, but the other three simulations do not. This super cavitation phenomenon also means that the effective area of the flow becomes smaller as cavitation increases. Therefore, similarly to the varying geometrical flow areas, the injection velocity varies from case to case, but the injection rate does not.

6.4.5 Hole thickness

In Figure 76, we can see the full injection sensitivity to nozzle hole thickness, i.e. the length of the orifice. The values ranged from 0 mm to 50 mm, 2.5 mm being the original value.

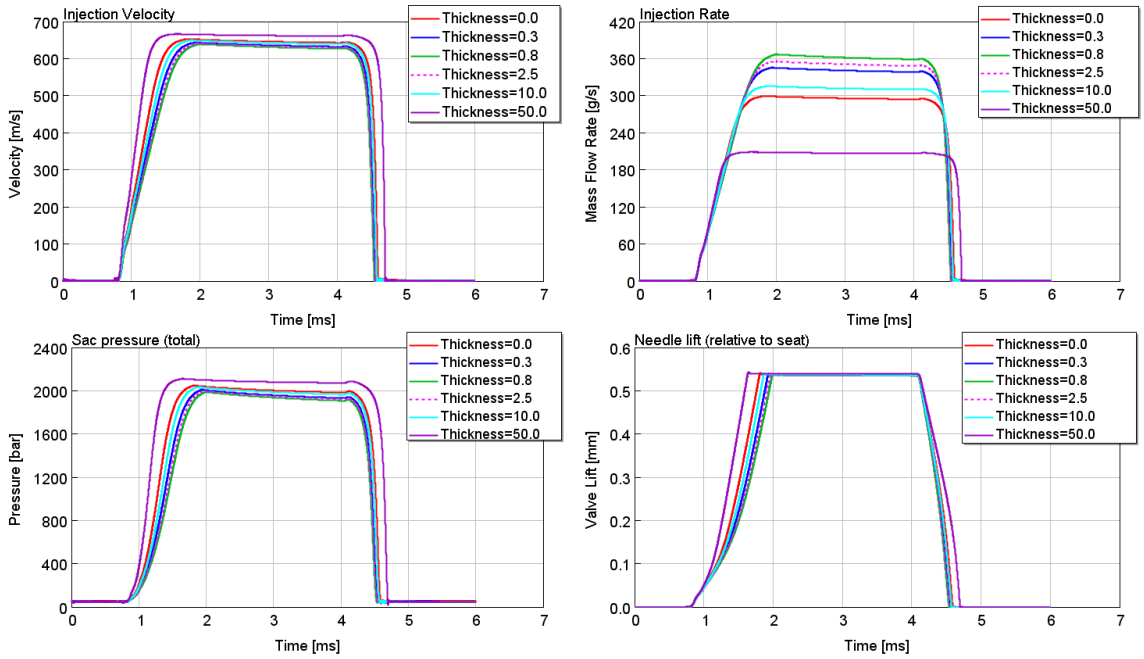

Figure 76. *Full injection sensitivity to nozzle hole thickness*

With the varying thickness, there are some differences in the injection rate and minimal differences in the other three indicators. The simulation with the 50 mm thickness brings the most difference, owing to its unrealistically high value. Growing the thickness from the value of zero first increases the injection rate, and after the thickness grows over 0.8 mm, the injection rate begins to decrease. With the other three monitors, the effect is the same, but smaller and in the opposite direction. By increasing the thickness from the zero value, it gives the flow more length to expand and expand closer to the orifice wall, thus increasing the effective flow area, which leads into a higher flow rate but a smaller sac pressure and flow velocity. Increasing the thickness further, there comes a limit at which the flow never enters the super cavitation zone and the increased length causes more wall friction, which leads to higher pressure loss and therefore decreases the flow rate.

In Figure 77, we can see the pilot injection sensitivity to the thickness of the holes.

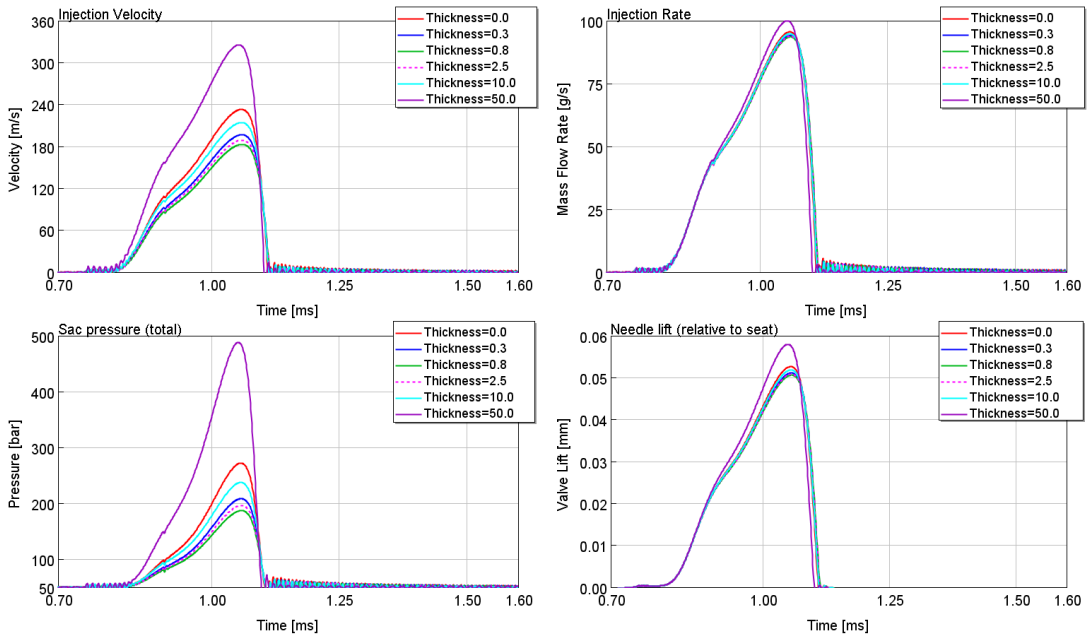

Figure 77. *Pilot injection sensitivity to the hole thickness*

The results are once again quite similar to the flow area and the hole rounding sensitivity. However, like in the full injection sensitivity, the effects of the thickness are nonlinear. First increasing the hole thickness from zero, the sac pressure begins to drop, but after increasing the thickness long enough, the sac pressure begins to increase. Correspondingly with the full injection event, the value of 0.8 mm brings the lowest sac pressure and injection velocity, whereas the value of 50 mm brings the highest sac pressure and injection velocity. This behaviour is again, similarly to the full injection event, due to the wall friction consuming the pressure with the thicker holes, and in the smaller holes the expansion length not being big enough to release the flow velocity energy to pressure energy.

7. OPTIMIZATION

In this chapter, the optimization of the fuel injector is presented. The optimization is done in order to find the most suitable parameter values for the injector studied in this thesis that is, the ones that result in the least amount of emissions. The boundary conditions are explained in chapter 7.1, optimization targets in chapter 7.2, and the results of the optimizations in chapter 7.3. When doing a parameter optimization of a simulation model, gradient-based optimization methods cannot be utilized, and therefore the method used in this thesis is a direct search method: the genetic algorithm, version NSGA-III. Some of the volumes in the injector model are increased in order to save calculation time, but the effects of these modifications are minimal.

7.1 Boundary conditions

A certain set of boundary conditions that limit the injection event always needs to be taken into account. Firstly, in the full injection event, there is the need to have a big enough injected quantity in a certain time zone. In this study, it has been set at the value of 1500 mm^3 within a time period of 4.5 ms. This requirement ensures that the engine is able to produce enough power when needed. In the pilot injection event, the constraint for injected quantity was set to the value of 20 mm^3.

Secondly, we need to limit the amount of stress to the lower part of the needle at closing. When the needle collides with the nozzle body, there is an impact, and the maximum stress resulting from the impact is defined by the material selection. In this study, the yield strength is set to be 700 MPa. In the simulation model, the stress is calculated by dividing the maximum value of the contact part force by the area of the needle tip. This calculation is presented in chapter 4 in Figure 11.

Thirdly, the minimum diameter of the nozzle holes is set to be 0.15 mm because holes smaller than this would be hard to machine precisely. The value is just a rough estimate. The inlet, outlet and filling orifices are not limited by this boundary because the inlet or the filling orifice might even saturate to zero, and in that case, the conclusion would be that the orifice is not needed.

In GT-suite, these parameters are input into the constraints menu tab of the direct optimizer. There, an RLT (Result variable) is selected to be limited, and a lower and an upper limit can be defined. The penalty of the constraint is chosen to be between 0 and 10, while 10 is the ultimately avoided penalty and zero is not avoided at all.

7.2 Targets

From the sensitivity analysis performed in chapter 6, we have learned that we can drastically affect the needle movement and the exit spray properties. With the optimization tool, we can manipulate the most affecting parameters simultaneously instead of simply optimizing one parameter at a time. Now the question remains: What kind of behaviour do we want from the fuel injector?

Looking at the atomization theory (not presented in this thesis), we understand that, in order to maximize atomization, we need to have as much of the spray at the regime four, atomization, as possible. However, the atomization process is complicated and especially difficult to understand in a dynamical process of fuel injection where the spray form and velocity change in relation to the injection time. Therefore, discussions with atomization experts were held, resulting in a target as simple as possible to implement in the simulations, but yet effective for the optimization, and this target is the maximization of flow velocity.

$$f_{opt} = v_{flow} \tag{45}$$

However, having this kind of a target might even be too simple. Hence, there is room for adding more targets while keeping the previously introduced valid. This type of optimization is called multi-objective optimization. In their research, Blessing et al. state the following:

”*Due to gradual throttling of the fuel flow, which also requires much more time than with the PLN system, the atomization of the fuel becomes very poor. This is especially so towards the end of the closing, where the sac hole pressure becomes very low, and will result in dribbling and consequently to increase HC emissions*” [13]

From this quote, it is quite clear that, in order to minimize the time for the bad atomization, the closing time of the needle must be minimized. Now, to add this minimization of the closing time to our optimization function, it must be added as a negative because the previously presented flow velocity is maximized. Therefore, when we maximize a negative value, it moves closer to zero, and thus the closing time is minimized. Moreover, the values of the flow velocity and the closing time must be equally important, and therefore their values are normalized. Now the optimization function looks like

$$f_{opt} = \frac{v_{flow}}{v_{flow\_normalize}} - \frac{t_{closing}}{t_{closing\_normalize}} \tag{46}$$

Furthermore, Sarre et al. states the following:

“*The Sauter Mean Diameter (SMD) is an important spray parameter which indicates the atomization quality and could be directly linked to combustion quality. Two parallel stud-*

ies in SMD measurements of non-vaporizing sprays [21] and engine emissions [27], respectively, have been performed using exactly the same injectors and injection pressures. Results show that the injection systems producing smaller SMD will results in lower particulate emissions." [7]

Thus, we can add the minimization of the Sauter mean diameter as one of our optimization targets. The resulting optimization function looks like the following

$$f_{opt} = \frac{v_{max}}{v_{max\_normalize}} - \frac{t_{closing}}{t_{closing\_normalize}} - \frac{SMD}{SMD\_normalize} \tag{47}$$

which is a maximization problem.

7.3 Results

The optimization of the pilot injection event turned out to be a challenging task for several reasons. First, there are many parameters which in coalescence affect the simulation in an unpredictable way, due which there is a huge number of local optimums in the search space. Second, the injected quantity of 20 mm^3 is so close to the injector not opening at all that, during the optimization process, there are many injection events where the injector doesn't open at all. Third, the target having for the injector to be as fast as possible leads into the injection event being extremely sensitive to any variations in the parameters, which, in conjunction with the small injection quantity, means that the optimums in the search space are extremely steep and narrow. Fourth, there's the problem that in the case of inlet and filling orifice size, it's not their absolute value that matters, but their area ratio to the outlet orifice. Therefore, by making crossover operations, many of the results fail due to having a bad orifice area ratio, mainly meaning that they are bigger than the outlet orifice. Finally, the importance of the actuation time is much higher than that of the other parameters, and the behaviour of the pilot injection event in relation to the actuation time is somewhat difficult to predict. At the beginning of the actuation signal, there's a delay, depending on the other parameters during which the injector doesn't open, and after that the injection rate starts to increase rapidly, gaining a big injected quantity very suddenly. Therefore, the problem is that the optimizer discards the pilot injection events with a fast opening but high injected quantity and tries to reach the optimum via a slower opening and smaller injected quantity. In these pilot injection events, both the actuation time and at least one other parameter need to be manipulated simultaneously to get closer to the optimization target, whereas in the high injection quantity cases, only the actuation time needs to be decreased in order to get closer to the optima. To tackle this problem, a constraint with a small penalty of 1 (maximum penalty = 10) is set to limit the injected quantity to 20 mm^3.

In the following chapters, the results of the optimizations are presented step by step. This means that, in the first result, only pilot injection with 4 variables with the 20 mm^3 constraint and 1 target is considered. In the second results chapter, both the full injection event and the pilot injection event are taken into considerations with 8 variables, all constraints and 2 targets, but the nozzle hole parameters are not varied. In the third result chapter, both the full injection event and the pilot injection event are taken into consideration with all of the constraints and targets, but instead of some of the previously varied parameters, the nozzle hole parameters are varied. These three steps are later referred to as levels 1, 2 and 3. The actuation time is varied independently (meaning different values in the pilot and full injection event) on all levels in order to be able to reach the injected quantity of 20 mm^3 in all parameter sets and also to vary the fully open time in the full injection event with different closing times (to fulfil the boundary condition of sufficient injection quantity within a certain time period).

7.3.1 Pilot injection with 4 variables

In the first optimization, only the actuation time and the inlet, outlet and filling orifices were taken as variables. The only boundary condition was the maximum injected quantity of 20 mm^3, and only the pilot injection was optimized. In Figure 78, we can see the development of the maximum flow velocity with relation to iteration rounds.

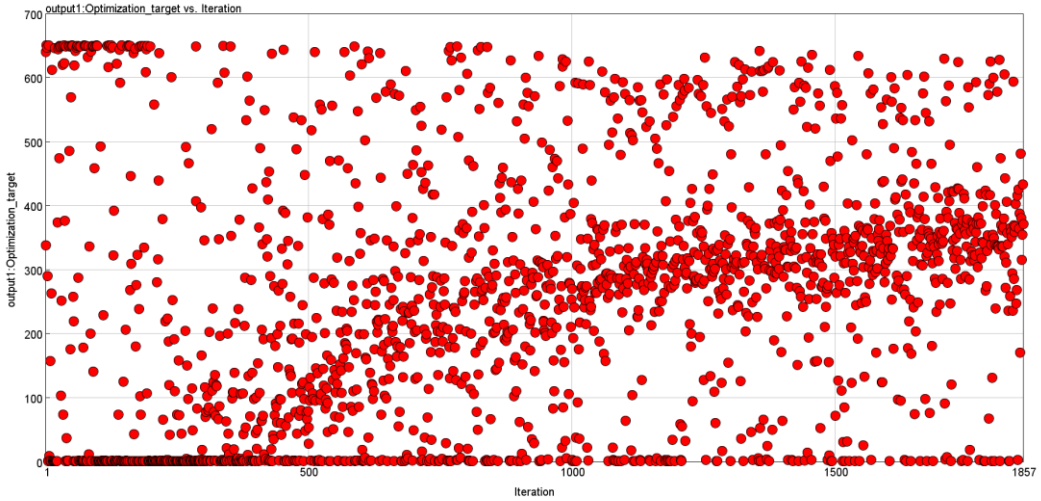

Figure 78. *Level 1 optimization target development*

In this optimization, it took a considerable amount of single simulation rounds to get to the maximum optimization output of 372 m/s. This optimization tardiness is probably due to the small sizes of the local optimums in the search space. The resulting parameters are presented and compared to the original values in Table 7.

Table 7: *Level 1 optimized parameter values*

Parameter:	Original value:	Optimized value:	Difference	Difference [%]
t_actuation [ms]:	0.39	0.15	-0.24	-62
d_outlet [mm]:	0.22	0.38	+0.16	+73
d_inlet [mm]:	0.20	0.14	-0.06	-30
d_filling [mm]:	0.19	0.18	-0.01	-5

The size of the outlet orifice is 73 % higher, while the inlet orifice is about 30 % and the filling orifice only 5 % smaller. The result is as expected because the outlet orifice was the biggest influencing factor in the sensitivity analyses. In Figure 79, we can see the level 1 optimized injector performance compared to the original performance.

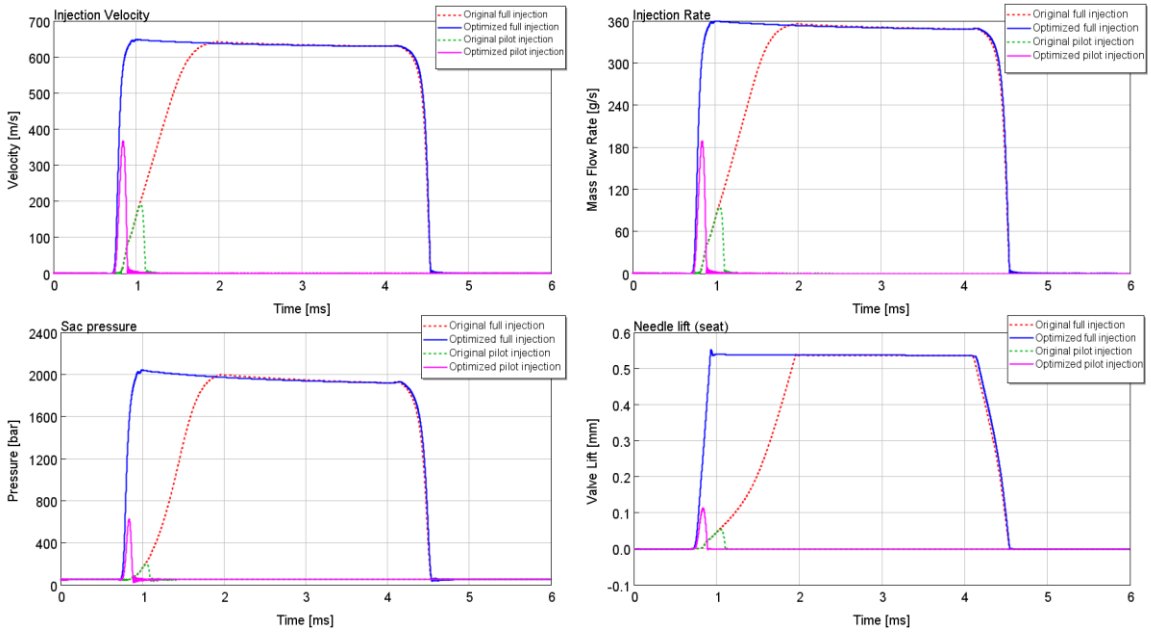

Figure 79. *Level 1 optimized performance vs. original performance*

Now the optimized pilot injection is clearly a lot faster than the original pilot injection. The original maximum of flow velocity was about 190 m/s, and the optimized maximum flow velocity is about 370 m/s or about twice higher than the original. The closing speed of the needle is almost identical with the two full injection cases even though the inlet and filling orifices have been decreased, and this is because the outlet orifice size has increased so that it throttles less also in the closing movement of the needle. The closing times of the pilot injection event are almost the same, both lasting 55 µs, but the optimized pilot injection event moves a longer distance, hence being faster. In Figure 80, we can see both the lift of the needle and the lift of the control valve. The green dashed line is the maximum opening of the control valve.

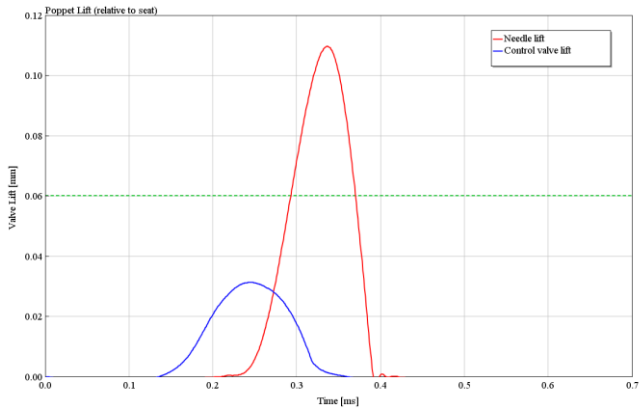

Figure 80. *Needle & control valve lift*

From the figure, we can clearly see that now the needle movement is so fast that the control valve lift doesn't have time to open fully. Therefore, in order to make the opening even faster, we would need to make the control valve lift faster. So even though in the sensitivity analysis it was stated that the solenoid electro-magnetic parameters do not significantly affect to the resulting pilot injection event, it is no more the case with the faster, optimized version of the injector. Though, by tuning the parameters of the solenoid model, the speed of the control valve could be improved, it is not performed in this thesis. The unrealistic behaviour of the solenoid model brings discredit as such, and therefore it is best to leave the improvement of the solenoid performance for the future.

7.3.2 Full and pilot injection with 8 variables

In the second optimization, both the full injection and the pilot injection event were considered with 8 variables consisting of 7 sweep parameters: inlet, outlet and filling orifices, the pressure step (lower gallery area and needle poppet diameter as variables and the control chamber area as their sum), and the spring rate and spring pretension. The actuation time was varied independently so that it altered freely between the two cases. Its values, however, were ranging from 1 ms to 5.5 ms in the full injection event, and in the pilot injection, the range was divided by 10 because the pilot injection event is so sensitive to small changes in the actuation time and, therefore, it is good to limit the search space. All of the constraints were taken into consideration, and the target was to maximize the flow velocity in the pilot injection and to minimize the closing time on both the pilot injection and full injection events. The parameters for the nozzle hole were not varied. In Figure 81, we can see how the model is made to change a boundary and a target in the two cases

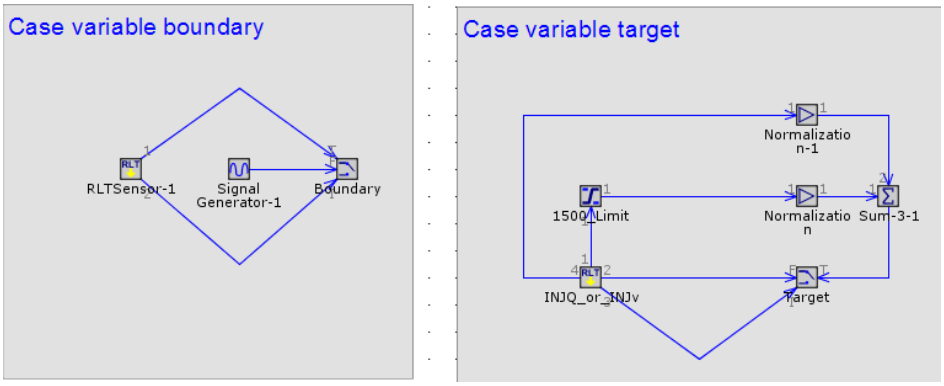

Figure 81. *Varying targets and boundaries case by case*

In the variable boundary case, the RLT sensor senses the injected quantity and the case number and sends them forward to the switch part. From the signal generator, a constant value of 10 is sent to the switch. The case number is the control input of the switch, determining which of the switch inputs the switch output is: the constant value of 10 or the injected quantity. The switch output is then sent to the constraint section of the optimizer setup. With this configuration, the injected quantity is set to be limited to 20 mm^3 in the pilot injection, whereas, in full injection the boundary condition is never violated because the constant value of 10 is always smaller than the boundary value of 20.

The case variable target is a very similar configuration. The sensed values of the RLT sensor are the casenumber, the injected quantity and the closing time of the full injection event. There the case number is again controlling the switch output, and the outputs of the switch are sent to the optimizer. The target of the pilot injection is made in the ScalarPerformance submodel, which can be seen in the appendix A. The full injection event target is a subtraction of the normalized injected quantity which is limited to 1500 and the normalized closing time of the full injection. With this configuration, the model is set to reach the amount of 1500 mm^3 in the full injection while minimizing the closing time of the needle.

In Figure 82, we can see the development of the optimization target in relation to iteration rounds. The target value is calculated as the average of the pilot injection target value and the full injection target value.

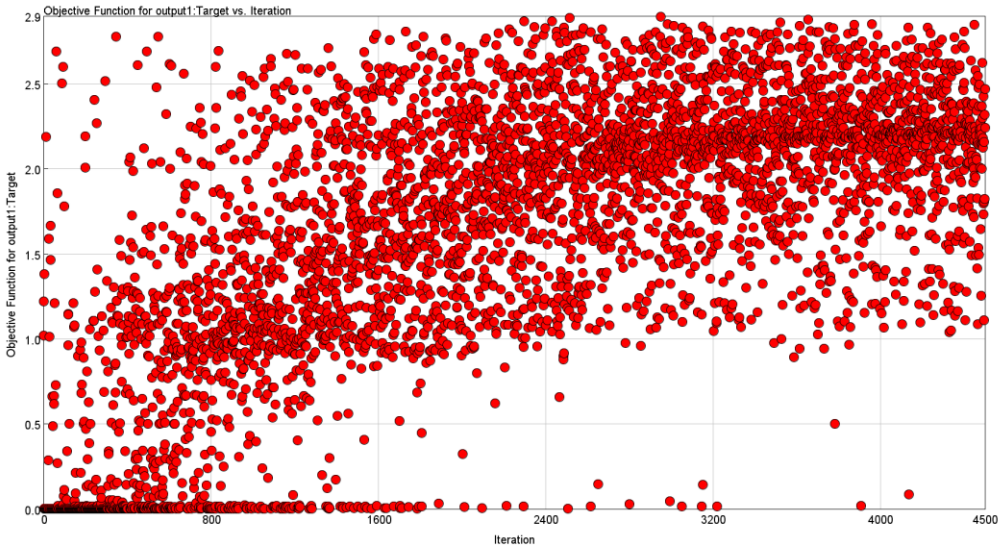

Figure 82. *Level 2 optimization target development*

From the figure, we can see that the optimization is very slow and it takes many iterations to move forward. The total amount of iterations was 4500, after which the optimization target was saturated, which means that a better solution could not have been found by running the optimization even further.

In Table 8, we can see the optimized parameter values versus the original values and their differences.

Table 8. *Level 2 optimized parameter values*

Parameter:	Original value:	Optimized value:	Difference	Difference [%]
Actuation time [ms]:	0.39	0.21	-0.18	-46.2
Outlet orifice [mm]:	0.22	0.47	+0.25	+113.6
Inlet orifice [mm]:	0.20	0.22	+0.02	+10.0
Filling orifice [mm]:	0.19	0.21	+0.02	+10.5
Needle gallery area [mm^2]:	8.04	10.01	+1.97	+24.5
Needle poppet diameter [mm]:	2.4	3.47	+1.07	+44.6
Spring rate [N/mm]:	83.5	114.1	+30.6	+36.6
Spring pretension [N]:	90	300	+210	+233.3

The actuation time is decreased to about half of its original value. The outlet orifice is more than twice as big as before, but there are only about 10 % differences in the inlet and filling orifices. The needle gallery area is 24.5 % bigger than before, but the poppet diameter of the needle is 44.6 % bigger than before, which means a considerable increase in the needle poppet area and the control chamber area. The spring rate is up by 36.6 %, and its importance can be questioned, as the spring rate mainly has an effect with the full injection event, probably making the initial closing speed faster and in this way decreasing the whole closing time. The spring pretension is 233.3 % higher than the original

value, and it is at its limit. The resulting injection events are compared to the original ones, and they can be seen in Figure 83.

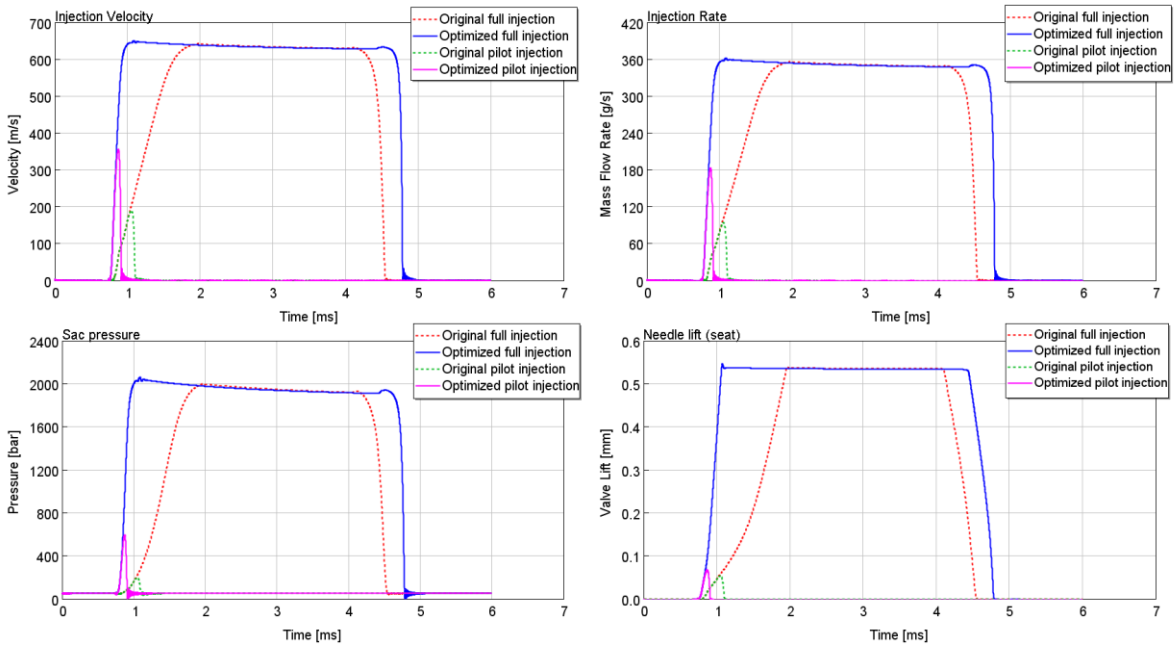

Figure 83. *Level 2 optimized versus original injection outputs*

In the full injection event, both the opening and closing speeds of the needle are faster, but especially the opening speed. The pilot injection opening is also much faster, and the closing speed only slightly faster: the original closing time of the pilot injection is 55 µs, and the optimized closing time of the pilot injection is 41 µs. The sac hole pressure is a lot higher in the optimized pilot injection than in the original pilot injection. This is partly due to the needle tip having a bigger diameter which leads to a bigger flow area in relation to the needle lift. The optimized injection velocity is about 355 m/s, and the original injection value is about 190 m/s. The high injection velocity and mass flow rate are caused by the high sac pressure.

7.3.3 Full and pilot injection with nozzle parameters

In the third optimization, both the full injection and the pilot injection events were considered with 8 variables consisting of 7 sweep parameters: inlet, outlet and filling orifices, the nozzle parameters for the nozzle hole diameter, the number of nozzle holes, hole thickness and the rounding. The actuation time was varied in the same way as in the previous optimization chapter. All of the constraints were taken into consideration, and the target was to maximize the flow velocity and to minimize the SMD in the pilot injection and to minimize the closing time on both the pilot injection and full injection event. In Figure 84, we can see the development of the optimization target in relation to iteration rounds.

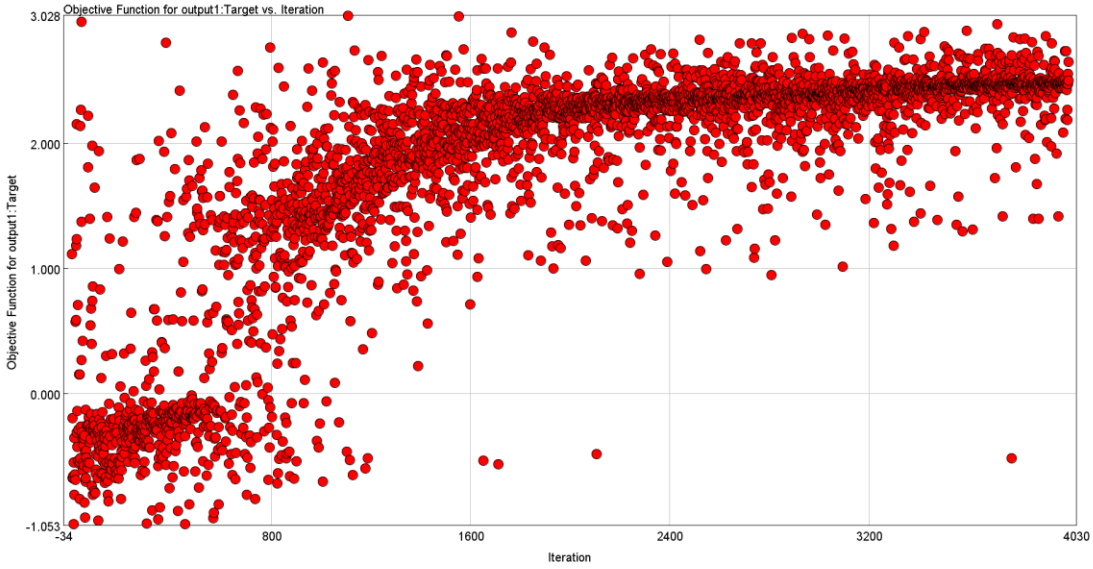

Figure 84. *Level 3 optimization target development*

We can see that the optimization target saturates, and it would not considerably improve with further iteration rounds. It takes about 800 iteration rounds in order to find parameters with which both the pilot injection targets and full injection targets are achieved.

In Table 8, we can see the optimized parameter values versus the original values and their differences.

Table 9. *Level 3 optimized parameter values*

Parameter:	Original value:	Optimized value:	Difference	Difference [%]
Actuation time [ms]:	0.39	0.18	-0.21	-54
Outlet orifice [mm]:	0.22	0.27	+0.05	+23
Inlet orifice [mm]:	0.20	0.14	-0.06	-30
Filling orifice [mm]:	0.19	0.20	+0.01	+5
Number of nozzle holes []:	9	19	+10	+111
Nozzle hole diameter [mm]:	0.31	0.20	-0.11	-35
Hole thickness [mm]:	2.52	6.4	+3.9	+156
Hole rounding [mm]:	0.64	0.74	+0.09	+14

Similarly to the previous optimization levels, the value for the outlet orifice increases and the filling orifice remains roughly the same. The inlet orifice has decreased by 30 %, like in the first optimization result. The number of nozzle holes has been increased to 19 and their diameter has been decreased by 35 %. The amount of the nozzle holes was limited to 19, so it saturated to the maximum allowed value. A boundary condition for the nozzle holes could have been added to limit the minimal distance between the nozzle holes to avoid nozzle sac break-up, but it was thought that the break-up can be avoided with good nozzle design, and having the holes with different horizontal alignment. The value for the

nozzle hole thickness increased by 156 %, but as the original value was uncertain, the difference might be smaller in reality. The hole rounding also increased by 14 %, but looking back at the sensitivity of the hole rounding, it doesn't seem to have any difference with so high values. The injection events resulting from those values can be seen in

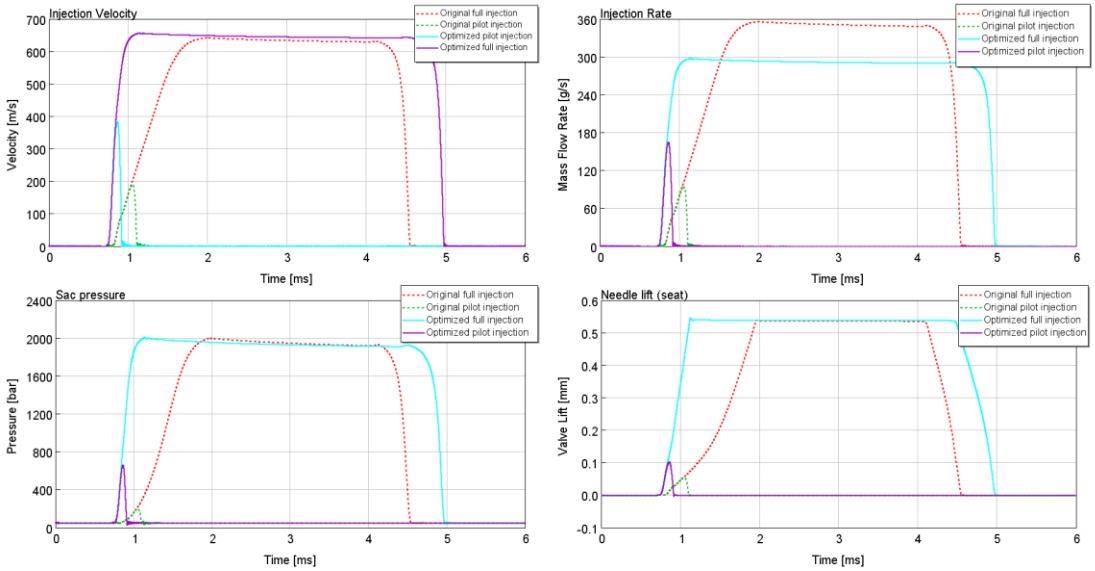

Figure 85. *Level 3 optimized versus original injection outputs*

Again, the pilot injection velocity is about double the higher as in the original injection event. The closing time, on the other hand, has increased from 55 µs to 57 µs, and the SMD has decreased from 0.15 mm to 0.09 mm. This result would implicate that a fast closing of the needle cannot be reached simultaneously with a small SMD. The mass flow rate in the full injection event has decreased significantly, and the injected quantity in the optimized case remained at 1466 mm^3 though 1500 mm^3 was set as the boundary condition. This result further amplifies the interpretation made during the sensitivity analysis of the nozzle hole diameter, that there is a trade-off between a good pilot injection and injecting enough quantity in a time zone.

7.4 Arising problems

Maximizing the injection spray velocity does not bring only bliss but also trouble. With the needle opening being extremely fast, it is also extremely sensitive to any changes in the operating conditions. For example, small variances in the actuation time would lead to the injection quantity strongly increasing or no injection at all. Also, the effects of the surging rail pressure or the fluid temperature would bring even more inaccuracy to the pilot injection than before. Therefore, with the increasing speed of the pilot injection, there is also an increasing need for more accuracy in the control of the injected quantity.

With that said, there would need to be a new kind of optimization, where both the tolerance and the injection velocity would be taken into consideration.

8. DISCUSSION

In this chapter, some criticism is given for the thesis results and how they were created. These things should be taken into account in the future when doing more injector simulations. Also, possibilities for improvements for the future development are discussed.

8.1 Criticism

During the building of the injector simulation model, many of the parameters needed were inaccurately measured and some of them were only guesses. Especially, the fuel rail before the injector was just tuned in a way that the pressure in the sac hole was at the right level. And there are a few components between the rail and the sac hole which have an effect on the pressure level of the sac hole. Therefore, there is a possibility that a good match with the verification data was achieved with quite incorrect parameters. Having a set of 6 injection cases of verification data does bring some relief on the matter, but even more would have been better.

In the verification data, the size of the needle bounce was tiny. And this should be doubted. If there were no pressure at all, surely there would be a bounce. But with the varying pressure load, it's hard to predict how the deformation and the needle bounce work together. Contacts between the colliding parts have been modelled with the *Contact* template within the simulation software with parameters that were default values and guesses. By increasing the speed of the needle and the control valve, the significance of the contact parameters and the demand for the modelling accuracy increases. Especially important in the pilot injection event is the "apply damping if gap less than" parameter input as it influences the closing speed of the control valve. In this study, it was set to 5 micrometres.

Another oddness of the model is that the cavitation in the 0.31 mm injector nozzle holes has been taken into account but not that in the inlet, outlet and filling orifices which are about the size of 0.20 mm. This simplification was done to ease the verification process: the cavitating model is a more complex model, and it brings more parameters for the verification, making it more difficult to find the correct parameters. If the orifices were to cavitate, it would have a significant effect on the movement of the needle. Nevertheless, a good fit with the verification data was found even without the cavitating orifices.

In contrast to the previous simplifications of the model, a dynamic friction model was added to the simulation model, creating more variables and making the model more complicated. This can be justified by arguing that the needle might easily be moving eccentrically or that, in the beginning of the needle movement, it is pressed to the needle seat and, because of the obliqueness, stretches the needle seat slightly open. This stretching

would lead into a dry contact movement in the very beginning of the needle movement. Although this friction behaviour might be true, it was noted that the friction affects the needle movement very little, and a good verification fit can be reached even without the friction model.

Another question that arose was the initial state of the sac hole. In laboratory conditions, there is no ignition of the gas and no combustion process, so there the sac is always filled with the same fuel. But how about in the real engine where the fuel actually burns? Does the fuel inside the sac burn as well, or does it remain fully liquid? The case could also be that the fuel burns partly and, at the start of the injection event, there is a mixture of liquid fuel and gases from the partly burned fuel. In any case, the initial state of the sac has some kind of an effect on the pilot injection case with small injection quantities because gas behaves in a very different way compared to liquid fuel.

When increasing the size of the outlet orifice, the flow through it grows, and it is clear that more pressure strains the control valve. In this thesis, it has not been taken into account how much force and pressure the control valve can take. However, there must be a limit after which the durability of the control valve is lost.

The solenoid model used in this thesis is a very simple one, and it does not consider the inductance of the solenoid though it probably has a significant effect on the injector performance. This simplification might distort the thesis results in a considerable manner.

A field that has completely been left out of the scope of this thesis is the energy consumption. As the injector always uses some of the fuel as the control leakage, increasing the sizes of the outlet and inlet orifices also increase the amount of the energy spent on controlling the needle movement. The injector energy efficiency plays also a role in the whole engine energy efficiency. There could be a possibility to minimize the energy consumption of the injector without significantly worsening the injector performance.

8.2 Future research

During the thesis work, a simple FEM model of the injector needle was built and the needle deformations were roughly estimated. This dynamic strength analysis for the needle would be good to estimate properly since the dynamic deformations of the needle influence the pressure of the control chamber and the opening delay of the injector. Furthermore, the deformations both at the top of the needle and at the guide of the needle top have an effect on the amount of leakage flow from the spring chamber to the control chamber. One of the boundary conditions was the maximum stress on the needle tip, and its limit was only a rough estimate. In reality, it is the stress caused by the needle tip to the nozzle body that limits the needle speed and diameter.

Another object that reacts to the varying pressure is the orifice. With increasing pressure, one would expect the orifice to widen. As the flow through the orifice increases, the pressure inside the hole is more and more dynamic, which means that the force acting on the orifice inner surface is smaller. However the force acting to the orifice wall before the orifice remains the same, and the force acting on the orifice wall after the orifice is smaller due to the throttling of the orifice. With this in mind, the study would consist of a fluid dynamical part in which the pressure distribution would be solved and the strength analysis part with a focus on the deformations of the orifices. The orifice size variations have a significant effect mainly on the nozzle holes but also on the inlet, outlet and filling orifices.

One possible method of achieving the objectives of both a good pilot injection and full injection could be having different kinds of nozzle holes. Big cavitating nozzle holes would provide a good pilot injection, and as the pressure increases, the cavitation would choke the flow for the full opening. Small non-cavitating nozzle holes would provide the fuel needed in the full opening, and only a minor flow in the pilot injection.

The simulations performed during this thesis work were in a laboratory environment, meaning that the combustion chamber was modelled as a pot with a constant pressure of 50 bars and liquid fuel. In reality, of course, the environment is the combustion chamber of an engine, and the pressure is around a few hundred bars, depending on the engine. This kind of simulation in the engine environment would give understanding on how the behaviour of the injector differs within an engine compared to the simulation environment of laboratory conditions. The difficulty would be in obtaining reliable measurement data and in the verification of the model.

8.2.1 Co-simulations

As seen in the results presented in this thesis, the injection rate shape can be formed into several different shapes and the needle closing and opening movements can be individually varied. Therefore it comes to a question: what are the desired outputs? Are the targets presented in chapter 7.2 sufficient?

According to Blessing et al. [13], there are several factors that interactively affect the whole combustion process. The main parts of the combustion process are the hydraulics of the injector (which is studied in this thesis), the fluid dynamics in the injection nozzle, spray formation and atomization, and finally the ignition and the combustion phase. Blessing writes that studying only one part of the injection process at a time does not bring understanding of the whole process. Given these points, there is a need for a comprehensive co-simulation that would include all the four main parts of the combustion process.

The core of the co-simulation should be the hydraulic injector model because it affects the other parts of the co-simulation significantly. The first co-simulation to add could be the fluid dynamics model in the nozzle hole, which would bring accuracy to the modelling of cavitation, information about the pressure and velocity distribution inside the nozzle hole and more understanding on the primary break-up of the exiting flow. The next part to add would naturally be the atomization model for the spray. This model would bring in-depth knowledge about the transformation of the liquid into vapour, droplet size distribution, spray angle and penetration, and spray pattern and distribution of fuel within the combustion chamber. Eventually, a model for the combustion event would be added, and that would bring knowledge on the ignition, diffusion combustion and the formation of emissions. Adding all of these simulations together would create more possibilities to the optimization of the injector: the reduction of emissions could be done by adjusting the parameters of the injector, and the resulting simulated emissions would be immediately observed. However, it is notable that the 3D CFD calculations consume a lot of calculation time whereas the hydraulic 1D simulations do not, and therefore running several optimization runs would consume a huge amount of time. Moreover, interconnecting these models could be problematic.

In addition to the above mentioned co-simulations, also a 3-dimensional model of the solenoid electromagnetics could be included. In the solenoid model used in this thesis work, the effects of inductance were not modelled, and therefore the model remained deficient. Understanding the solenoid effects is particularly important when multiple injection events within a single stroke are studied because the solenoid affects especially the opening delay of the control valve. Furthermore, the solenoid inductance affects the closing speed of the control valve, which in turn influences the pilot injection. After modelling the magnetics of the solenoid, the electric circuit and its automation system would need to be modelled because the solenoid electro-magnetism is a dynamic system where electric parameters affect the magnetic outputs and the magnetic parameters affect to the electric outputs correspondingly.

8.2.2 Optimization double loop

When optimizing the pilot injection event, there was the problem that the injected quantity was usually quite far from the desired pilot injection quantity. That resulted in a huge number of simulation runs in order to reach the simulation runs close to the targeted quantity. For this reason, we understand that there is a need for first evaluating if the chosen parameters can reach the value of the chosen pilot injection quantity and, if they can, then set the control signal to yield the equivalent volume. Figure 86 depicts the characterized optimization loop planned to ease this problem, and in this work it is referred as the “optimization double loop”.

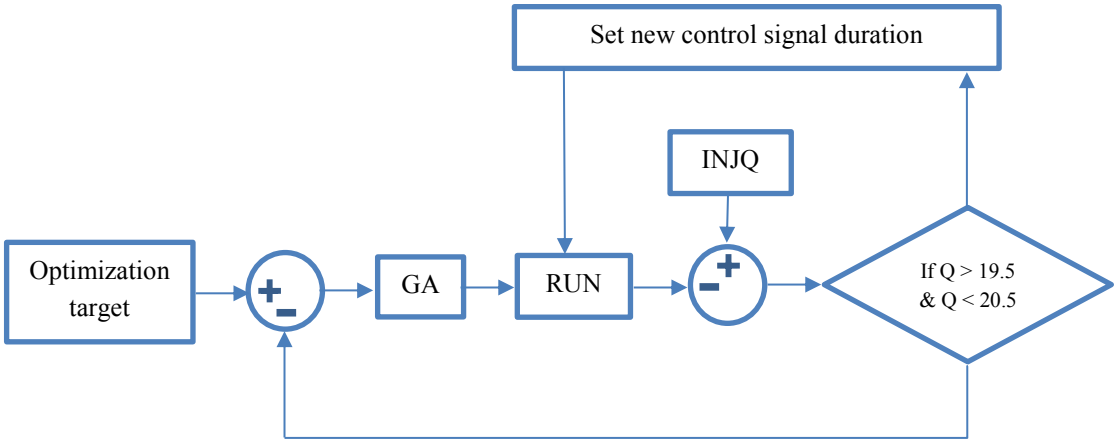

Figure 86. *Vision of double loop optimization for pilot injection*

The optimization target is a target defined by the user, and it could be one of the targets introduced in the optimization chapter. In the first block, the optimizer calculates how far it is from the target and, based on that information, the genetic algorithm (GA) chooses the parameter sets to the mating pool. Always after a simulation run (RUN), the deviation from the desired pilot injection quantity is calculated and, if it is too far off the target (INJQ), the actuation time should be tuned and a new parameter set should be rerun. This would be the other loop of the optimization, i.e. the iteration loop for the actuation time. The control algorithm for the control signal length could be a simple bisection method or a more sophisticated algorithm designed to effectively find the root for this certain application. Hence, most of the parameter sets returned for the genetic algorithm would result in a very close value for the targeted injection quantity and therefore would ease the selection method of the genetic algorithm

8.2.3 Dual control valve

In dual fuel engines, there is the need to utilize two different fuels efficiently. From the fuel injector point of view, this means that the pilot injection event in the gas mode needs to be fast, whereas the full injection event in the diesel mode needs to be energy efficient. And as we see from the results in chapters 6 and 7, to make the pilot injection event faster, the outlet orifice size needs to be increased. This modification leads to more fluid flowing as control flow, which means less efficiency in the full injection event. Therefore, we can doubt if these two objectives can be reached with the current configuration.

By installing two control valves into an injector, the opening speed of the valve can be easily modified. It shouldn't affect the closing speed of the needle for the full injection event but, for a pilot injection event, it might result in small differences if the control valve closings are not fully identical. In the implementation, there would need to be two solenoids and two control valves mounted on parallel flow paths. In a pilot injection, both of these solenoids would be opened, but in full opening, only one of the solenoids would be opened. In this kind of an approach, it is good to notice that the importance on the

throttling in the control valve increases and, therefore, the modelling of the pressure losses on the control valve should be accurate. A hydraulic scheme of the dual control valve injector can be seen in Figure 87.

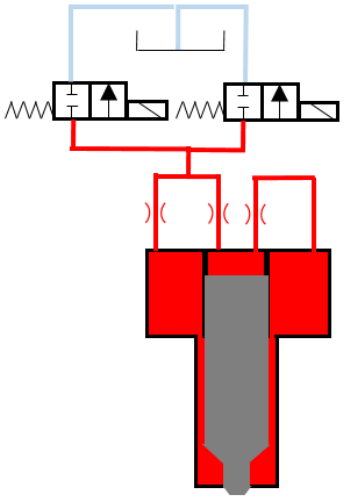

Figure 87. *Dual control valve*

The advantage of the dual control valves is the possibility to control the injection event on the basis of the mode the engine is running in. With this configuration, it is possible to reach a fast opening in the pilot injection and minimal control leakage during the full injection. This kind of a functionality would result in less emissions from the pilot injection event while having a good energy efficiency in the full injection event. Additionally, the control valve system becomes more reliable as the injector can still perform even with one control valve locked in closed position.

A low side of the dual control valve is in increased costs, as more components cost more money. Also, a little more space is needed, and there can be technical difficulties in synchronizing the two control valves to close exactly at the same time in the pilot injection event. If they are not closed exactly at the same time, the pilot injection event slows down, which reduces the presented advantages.

9. CONCLUSION

This master's thesis examines fuel injector operation and simulation. The main focus is on studying the pilot injection and optimizing it to reach the maximal atomization level. The pilot injection is especially important in dual fuel engines where it is used to ignite the combustion event. As the use of dual fuel engines increases, the importance of a good pilot injection grows as well.

By reading this thesis, the reader can get an idea how a fuel injector operates and how individual parameters affect the whole injection event. Even though the main focus is on the pilot injection, also the full injection event is considered, and the effects between these two injection events can be compared. For example, if one wants to compare two quite similar injectors, one can find the differing parameters and see their effects from this thesis. In Table 10, the potential of studied parameters are evaluated with a scale low-medium-high and briefly clarified in the comment section. The potential is defined by the parameters influence to the pilot injection.

Table 10. *Summary table: a parameters influence on pilot injection*

Studied parameter:	Potential:	Page:	Comment:
Inlet, outlet & filling orifice	High	56	These are the basic and the most effective parameters to control the needle movement. Inlet/outlet ratio mainly defines the opening speed, and the sizes of filling and inlet orifices together define the closing speed.
Seat & poppet angle (in the needle tip)	High	75	Seat and poppet angle has a significant effect on the pilot injection, and a small effect on the full injection. However, its effects are hard to estimate precisely.
Number of nozzle holes	High	81	Decreasing the flow area improves the pilot injection significantly. The problem with that is to get sufficient injected quantity in the full injection event.
Nozzle hole diameter	High	82	Same as with the number of nozzle holes above, but affects also the sauter mean diameter, i.e. the 'blob' size of the spray.
Pressure step (control chamber area, needle gallery area & needle tip area)	Medium	69	The pressure step means the shape and size of the needle. It is not the most effective parameter, but it should always be considered in needle design.
Discharge coefficient of the control valve (throttling on the control valve)	Medium	52	In this thesis, the discharge coefficient of the control valve represents the throttling of the control valve. With a big outlet orifice, the pressure before the control valve should be observed.
Spring pretension (spring of the needle)	Medium	67	Spring pretension affects the opening delay and the movement speed of the needle, both during the pilot injection and the full injection.
Nozzle hole rounding	Medium	84	Sharp edges advance start of cavitation and therefore increase the pilot injection spray velocity. Cavitation also limits the full injection flow rate. CFD calculations needed to estimate properly.
Nozzle hole thickness (hole length)	Medium	86	Hole thickness affects the injection events in a similar way as the hole rounding. Results are hard to interpret, and CFD calculations would be needed to estimate properly.
Solenoid electromagnetics (windings, airgap)	Low	48	In the specific injector studied in this thesis, the solenoid performance did not limit the pilot injection speed. However, that might not be the case with every injector. Also the solenoid simulation model in this thesis was oversimplified, and the results are therefore unreliable.
Control valve mass	Low	50	The control valve mass plays a minor role in the movement speed of the control valve.
Spring rate (spring of the needle)	Low	67	The spring rate would need to be highly adjusted in order to have an effect. There's not a lot of room for improvement of the pilot.

Hence, the outlet, inlet and control orifices are clearly the most effective parameters, which is in conjunction with the basic guidelines presented in the Bosch Common Rail book. The pressure step had some effect but not as much as with the orifices. Solenoid electromagnetics had very little effect, but the electromagnetic simulations were not fully reliable. On the other hand, the throttling in the control valve influenced the opening speed of the needle significantly, but there was no effect on the closing speed. The spring rate of the needle had almost no effect on the pilot injection, and in the full injection, it needed to have very high values to have a considerable effect. On the contrary, the spring pretension had a medium effect on both the pilot injection and the full injection. The seat and poppet angle was also found to have a high influence on the movement of the needle, but it must be said that their effects are too hard to predict accurately with 1D simulations. The number of holes and the hole diameter had a very significant effect on the needle movement, and it was noted that the flow velocity increased with the decreasing flow area. The only significant difference between the two was observed in SMD, smaller hole diameters naturally resulting in a smaller SMD. The nozzle hole rounding and thickness also resulted in quite similar effects, having a medium effect on the pilot injection, but a big effect on the flow rate during the full opening of the needle.

One of the important results found in this thesis was that, in the control valve movement, the opening speed of the control valve does not affect the pilot injection event, but the closing speed of the control valve does. The reason for this behaviour was found to be in the pressure step, meaning that the decreasing speed of the control chamber pressure does not matter until the needle begins to move. Then again, on the control valve closing movement, the needle is already moving upwards, and therefore even the slightest difference in the control chamber pressure results in a difference in the needle movement. With that said, we can conclude that there is a need to maximize the control valve closing speed, even though its significance is quite small.

The optimization is presented in three different stages, each stage more complex than the previous and adding something more to the optimization. On the first level, only the pilot injection was optimized with the varying parameters of actuation time, inlet, outlet and filling orifice. On the second level, both the full injection and the pilot injection were simultaneously optimized with 8 variables. On the third level, both injection events were optimized and some of the nozzle hole parameters were changed. With this kind of an approach, the reader can see how the results differ at each stage of the optimization, and it is easier to follow the implementation of the optimization. The optimization process introduced here can be applied to any injector, but it is notable that the optimal values are valid only for the injector studied in this thesis. In addition, the optimization focuses mainly on the pilot injection, and therefore the process is not valuable for non-dual fuel performing injectors. The original and the optimized values for the three stages of the optimization can be seen in Table 11.

Table 11. *Original vs. optimized parameter values*

Parameter:	Original value:	1st optimization:	2nd optimization	3rd optimization
Actuation time [ms]:	0.39	-62% (0.15)	-46% (0.21)	-54% (0.18)
Outlet orifice [mm]:	0.22	+73% (0.38)	+114% (0.47)	+23% (0.27)
Inlet orifice [mm]:	0.20	-30% (0.14)	+10% (0.22)	-30% (0.14)
Filling orifice [mm]:	0.19	-5% (0.18)	+11% (0.21)	+5% (0.20)
Needle gallery area [mm^2]:	8.04	-	+25% (10.01)	-
Needle poppet diameter [mm]:	2.4	-	+45% (3.47)	-
Spring rate [N/mm]:	83.5	-	+37% (114.1)	-
Spring pretension [N]:	90	-	+233% (300)	-
Number of nozzle holes [-]:	9	-	-	+111% (19)
Nozzle hole diameter [mm]:	0.31	-	-	-35% (0.20)
Hole thickness [mm]:	2.52	-	-	+156% (6.4)
Hole rounding [mm]:	0.64	-	-	+14% (0.74)

In all of the optimization results, the outlet orifice size is drastically bigger than in the original, and therefore we can conclude that it is the single most important parameter affecting on the needle movement. The optimization results undisputedly present that if the injection event is needed to improve, then the outlet orifice size needs to increase. Faster injection events, however, bring along more stress, and this should be taken into consideration.

As shown above, fuel injectors have many parameters which greatly affect the injection event. The individual effects of parameters are easy to study, but the effects of changing multiple variables at a time are impossible to predict without simulations. All in all, the injection event is a dynamic process where many parameters in conjunction affect the injection process.

REFERENCES

[1] R. B. GmbH, Diesel Fuel-Injection System Common Rail, Stuttgart: GmbH, Robert Bosch, 2005.

[2] M. S. Wärtsilä, *Wärtsilä 34DF Product Guide,* 2016.

[3] University of Oulu, *Elementtimenetelmät 3,* Oulu, 2016.

[4] C. Canudas de Wit, K. J. Åström, P. Lischinsky and H. Olsson, "A New Model for Control of Systems with Friction," *IEEE Transactions on automatic control,* March 1995.

[5] J.-P. Karjalainen, High-Pressure Properties of Hydraulic Fluid Dynamics and Second Order Polynomial Prediction Method, Tampere, 2011.

[6] H. Kauranne, J. Kajaste and M. Vilenius, Hydraulitekniikka, Helsinki: WSOY, 2008.

[7] C. von Kuensberg Sarre, S.-C. Kong and R. D. Reitz, "Modeling the Effects of Injector Nozzle Geometry on Diesel Sprays," *SAE technical paper series,* 1999.

[8] R. P. Benedict, Fundamentals of pipe flow, New York: Wiley, 1980.

[9] Taulukot.com, "Taulukot.com," 2017. [Online]. Available: http://www.taulukot.com/fysiikka/fysiikka_kaavoja/#s%C3%A4hk%C3%B6-_ja_magnetismioppi. [Accessed 6 9 2017].

[10] A. D. Belegundu and T. R. Chandrupatla, Optimization Concepts and Applications in Engineering, New Jersey: Prentice-Hall, Inc, 1999.

[11] T. Ohrn, D. Senser and A. Lefebvre, "Geometrical Effects on Discharge Coefficients for Plain-Orifice Atomizers," *Atomization and Sprays,* vol. 1, no. 1, pp. 137-153, 1991.

[12] L. C. Ganippa, S. Andersson and J. Chomiak, "Transient Measurements of Discharge Coefficients of Diesel Nozzles," *SAE Technical Paper Series,* 2000.

[13] M. Blessing, G. König, C. Krüge, U. Michels and V. Schwarz, “Analysis of Flow and Cavitation Phenomena in Diesel Injection Nozzles and its Effects on Spray and Mixture Formation,” *SAE Technical paper series,* 2003.

[14] M. Linjama, *Lecture slides on a basic course of digital hydraulics,* Tampere, 2015.

APPENDIX A: SIMULATION SUBMODELS

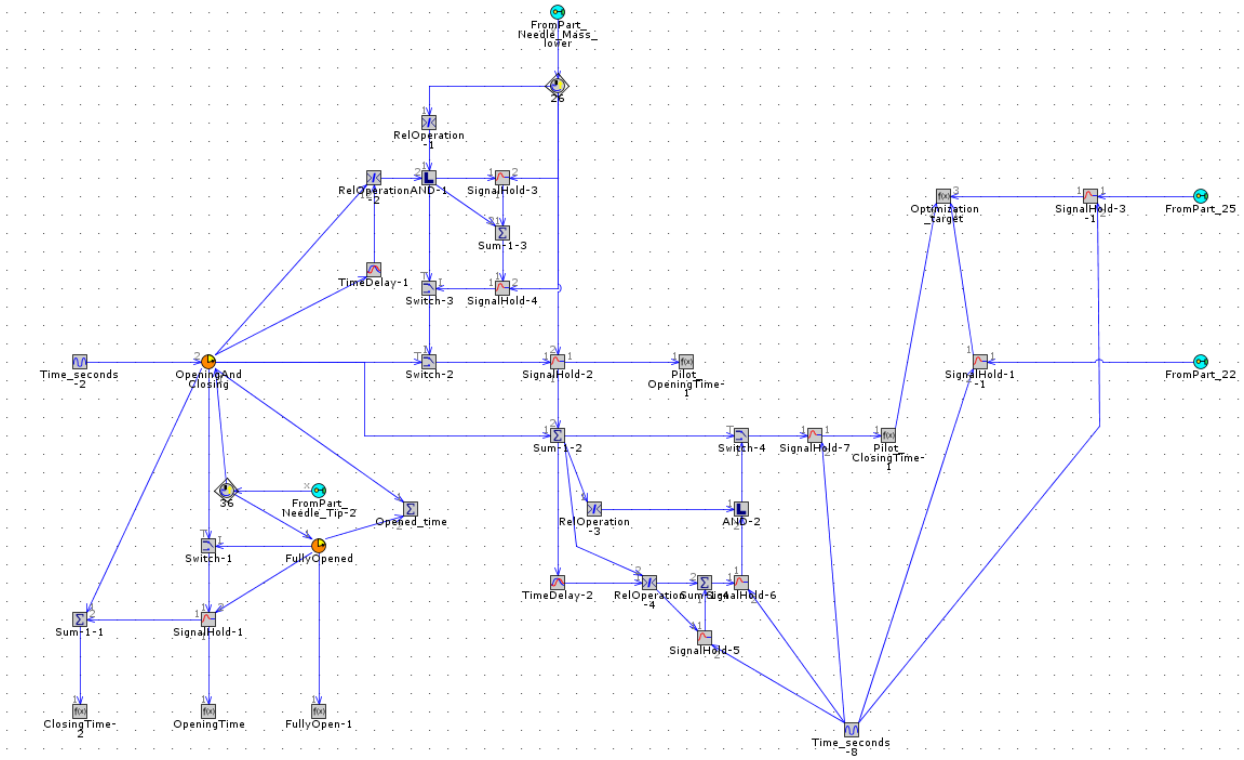

Figure 88. *ScalarPerformance*

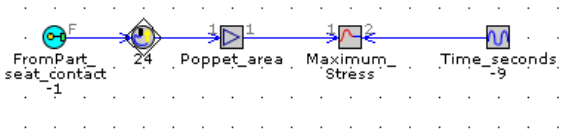

Figure 89. *Maximum stress*

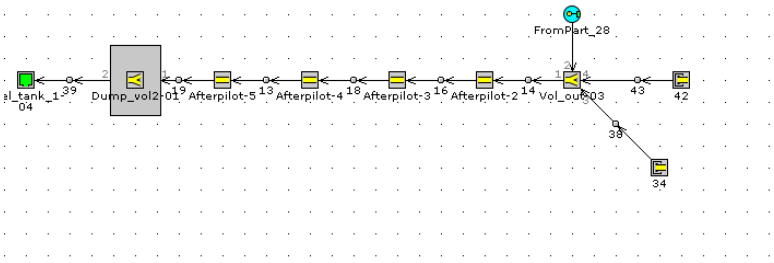

Figure 90. *Drain*